

# Numerical Relativity Initial Data for Neutron Star Binaries and the Hyperbolic Relaxation Method

Dissertation

zur Erlangung des akademischen Grades  
*doctor rerum naturalium* (Dr. rer. nat.)



**FRIEDRICH-SCHILLER-  
UNIVERSITÄT  
JENA**

vorgelegt dem Rat der Physikalisch-Astronomischen Fakultät  
der Friedrich-Schiller-Universität

von Hannes Rüter  
geboren am 18.08.1989 in Wismar

## **Gutachter**

1. Prof. Dr. Bernd Brügmann  
Theoretisch-Physikalisches Institut  
Friedrich-Schiller-Universität Jena
2. PD Dr. Thomas Baumgarte  
Department of Physics and Astronomy  
Bowdoin College, Brunswick, USA
3. Prof. Dr. Gerhard Zumbusch  
Institut für Angewandte Mathematik  
Friedrich-Schiller-Universität Jena

Tag der Disputation: 31.01.2019

“

Begriffe, welche sich bei der Ordnung der Dinge als nützlich erwiesen haben, erlangen über uns leicht eine solche Autorität, dass wir ihres irdischen Ursprungs vergessen und sie als unabänderliche Gegebenheiten hinnehmen. Sie werden dann zu 'Denknotwendigkeiten', 'Gegebenen a priori' usw. gestempelt. Der Weg des wissenschaftlichen Fortschritts wird durch solche Irrtümer oft für längere Zeit ungangbar gemacht. Es ist deshalb durchaus keine müßige Spielerei, wenn wir darin geübt werden, die längst geläufigen Begriffe zu analysieren und zu zeigen, von welchen Umständen ihre Berechtigung und Brauchbarkeit abhängt, wie sie im einzelnen aus den Gegebenheiten der Erfahrung herausgewachsen sind. Sie werden entfernt, wenn sie sich nicht ordentlich legitimieren können, korrigiert, wenn ihre Zuordnung zu den gegebenen Dingen allzu nachlässig war, durch andere ersetzt, wenn sich ein neues System aufstellen lässt, das wir aus irgendwelchen Gründen vorziehen. ”

*Albert Einstein in einem Nachruf auf Ernst Mach.*

Einstein, A.: Ernst Mach. Phys. Z. 18 (1916) 101 - 104



# Contents

<b>1. Introduction</b>	<b>7</b>
<b>2. The Hyperbolic Relaxation Method</b>	<b>11</b>
2.1. Solution of Elliptic Equations Through Hyperbolic Relaxation . . .	11
2.1.1. Basic Concepts and Ideas of the Hyperbolic Relaxation Method	11
2.1.2. Evolution System . . . . .	16
2.1.3. Residual Evolution . . . . .	19
2.1.4. Mode Analysis . . . . .	20
2.1.5. Hyperbolicity Analysis . . . . .	23
2.1.6. Boundary Conditions . . . . .	26
2.2. Hyperbolic Relaxation Method for Elliptic Equations in Divergence Form . . . . .	29
2.2.1. Evolution System . . . . .	29
2.2.2. Comparison with Standard Hyperbolic Relaxation . . . . .	32
2.2.3. Hyperbolicity Analysis . . . . .	33
2.2.4. Boundary Conditions . . . . .	34
<b>3. Numerical Implementation and Test Cases</b>	<b>35</b>
3.1. Numerical Setup . . . . .	35
3.1.1. Grid Setup . . . . .	35
3.1.2. Integration Method . . . . .	36
3.1.3. Initial Guesses . . . . .	37

3.1.4.	Refinement Strategy . . . . .	38
3.2.	Application to Test Cases . . . . .	39
3.2.1.	Poisson Equation – Finite Differencing . . . . .	39
3.2.2.	Poisson Equation – Pseudospectral Method . . . . .	45
<b>4.</b>	<b>Initial Data for General Relativistic Neutron Star Binary Simulations</b>	<b>49</b>
4.1.	Numerical Solution of the Constraint Equations of General Relativity	49
4.1.1.	Conventions and Fundamental Concepts of Numerical Relativity	49
4.1.2.	The Extended Conformal Thin-Sandwich Equations . . . . .	51
4.2.	Numerical Solution of the Hydrodynamical Constraint Equations . .	53
4.2.1.	Review and Critique of the Current Construction Methods for Binary Neutron Star Initial Data . . . . .	53
4.2.2.	Constraints from the Euler Equations on the Rotational Part	62
4.2.3.	Exact Integration of the Euler Equations . . . . .	69
4.2.4.	Extension of the Continuity Equation to Vacuum . . . . .	70
4.3.	Numerical Results . . . . .	74
4.3.1.	Implementation Details . . . . .	74
4.3.2.	Initial Data through Hyperbolic Relaxation . . . . .	77
4.3.3.	Fulfillment of the Regularity Condition . . . . .	78
4.3.4.	Convergence of the Solution . . . . .	78
4.3.5.	Influence of the New Rotational Velocity Choice . . . . .	80
4.4.	Sketch of an Improved Approach to Initial Data for Neutron Star Binaries with Spin . . . . .	86
4.4.1.	Identification of the Problems in the Previous Approach . .	86
4.4.2.	Split Into Irrotational and Rotational Part . . . . .	87
4.4.3.	Choice of the Time Derivatives . . . . .	90
<b>5.</b>	<b>Conclusion</b>	<b>93</b>
<b>6.</b>	<b>Bibliography</b>	<b>97</b>

<b>A. Ehrenwörtliche Erklärung</b>	<b>109</b>
------------------------------------	------------





# 1. Introduction

This thesis is based in parts on the article [1].

Considerations of astrophysical spinning fluid bodies have a long tradition in the history of relativity. Already in “Die Grundlage der allgemeinen Relativitätstheorie” [2] (The Foundation of the General Theory of Relativity [3]) Einstein justifies the necessity of a generalization of relativity by considering two far apart equal sized fluid bodies which are spinning in a rigid motion around an axis given by the imaginary line connecting the bodies. For an observer at rest on one of the bodies the other body appears rotating. If now the surfaces of the bodies are measured by observers that are at rest relative to the body and one of the bodies is found to be a perfect sphere it follows that the other body must be a rotational ellipsoid (due to “centrifugal forces”). It were these kinds of considerations that led Newton to the introduction of a preferred “absolute space”, which was in conflict with Einsteins special relativity. Dropping the assumption of a preferred “absolute space” there is then no longer a storable cause for the different shapes of the stars within the system itself. Einstein concluded that the cause must then lie outside of the system and is given by the far away masses of the “fixed stars sky” and that a generalized theory of relativity must include this effect. Indeed it can be shown that within general relativity a rotating mass shell induces a centrifugal force on the bodies inside it [4].

The first non-trivial exact solution was published by Schwarzschild [5] in 1916.

## 1. Introduction

His solution included black holes, objects with singularities and event horizons, which have been controversially discussed at that time. Almost exactly one hundred years after Einsteins presentation of his final field equations of gravity [6] and Schwarzschild prediction of black holes the Laser Interferometer Gravitational-Wave Observatory (LIGO) observed the first gravitational wave signal (GW150914) of two merging black holes [7]. This achievement has been awarded with the Nobel prize in physics and opened up a new channel for astrophysical observation. This observation was also another important confirmation for the existence of gravitational waves which are predicted by general relativity [8]. Another hint on the existence of gravitational waves was already given by observations of the Hulse-Taylor pulsar (PSR 1913+16) [9, 10], which is a binary system of two neutron stars orbiting around each other and of which one of them is highly magnetized and rapidly rotating around its own axis causing an emission of a beam of radiation that can be detected on earth. The change of the system orbital period can be explained to great accuracy by the emission of gravitational waves and it has been computed that the stars will merge in about 300 million years. Such a merger has been detected only recently in 2017 for the first time through gravitational wave observations (GW170817) [11] by the LIGO-Virgo collaboration. A lot of properties of the merging neutron stars can be deduced from the wave form, but alas some properties, like the spin, can not be constrained by current detectors, because to leading order of the post-Newtonian expansion the wave form is degenerate for example in the spin and the mass ratio. All the more the study of spinning binaries remains an import branch of numerical relativity, since it provides as of now the only way to study the physics of these systems under sufficiently known conditions.

In theory neutron stars are usually described as perfect fluid bodies under extreme pressure due to their own gravitation. The physical state in the core of these stars is still unknown, but it is the hope that one day gravitational wave observations will help to reveal the true nature of the neutron stars interior. It is predicted that especially the merger and post-merger phase would reveal a lot of insights

on the neutron stars equation of state. GW170817 gives already some constraints, but alas the merger parts frequency was too high to be detected. For the interpretation of the merger and post-merger signal numerical simulations of neutron star binary mergers will be important to interpret the signal, since post-Newtonian and effective-one-body calculations are not accurate enough in this regime. Furthermore these simulations are highly relevant to learn about the yet unobservable processes that occur in neutron star collisions. A variety on different numerical relativity codes exists for this purpose such as the `Einstein Toolkit` [12], `SpEC` [13], `BAM` [14, 15] and `bamps` [16, 17], to name just some of them.

This work investigates methods to construct initial data for numerical simulations of binary neutron star mergers. This requires the solution of elliptic equations which will be found numerically by application of the hyperbolic relaxation method [1] that has been recently developed by the author. In Ch. 2 the important findings of the method will be presented. In Ch. 3 the numerical implementation of the method in the numerical relativity code `bamps` is discussed and investigated in some test cases. After that in Ch. 4 the discussion returns to rotating perfect fluids, where the current methods for the construction of neutron star binary initial data will be reviewed and improvements towards physically more correct data are proposed. As it turns out there are additional constraints on the rotational fluid velocity, which have been neglected in previous works. Further problems in the current initial data formalism are pointed out and possible solutions are proposed. Furthermore a new approach is developed, in which the hydrodynamic constraint equations for neutron star initial data are solved avoiding surface fitted coordinates by extending the matter variables to the vacuum region.



## 2. The Hyperbolic Relaxation Method

### 2.1. Solution of Elliptic Equations Through Hyperbolic Relaxation

#### 2.1.1. Basic Concepts and Ideas of the Hyperbolic Relaxation Method

The solution of elliptic partial differential equations (elliptic PDEs) is an important problem in many areas of physics. Correspondingly large is the variety of analytic and numerical methods dealing with the solution of elliptic PDEs. The starting point for many methods is a discretization and (if required) a linearization, which for typical problems arising in physics leads to a sparse system of linear equations for a large but finite number of degrees of freedom. A key role in the solution of linear systems is played by iterative methods, e.g. [18, 19]. Among the basic iterative methods are relaxation methods, in particular Gauss-Seidel and Jacobi relaxation methods, and the family of Krylov subspace methods. Closely connected are strategies to accelerate these methods, such as preconditioners and multigrid methods.

## 2. The Hyperbolic Relaxation Method

Motivated by the need to solve elliptic systems as initial data within a time evolution code hyperbolic equations, the starting point is to study a modification of the classic Jacobi method, which is closely linked to physical relaxation problems. For concreteness, consider as a minimal example the Laplace equation,

$$\Delta\phi = 0, \tag{2.1}$$

for a function  $\phi(x, y, z)$  on a regular subset of  $\mathbb{R}^3$  together with appropriate boundary conditions. The Jacobi relaxation scheme can be obtained by introducing a pseudo time parameter  $t$  and considering instead of (2.1) the parabolic diffusion equation [20]

$$\partial_t\phi = \Delta\phi. \tag{2.2}$$

As time approaches infinity, any initial data for  $\phi$  “relaxes” to a stationary state, where  $\partial_t\phi = 0$  and hence Eq. (2.1) is satisfied as well. The Jacobi iteration method is obtained by discretizing the diffusion equation (2.2). In essence, a pseudo time dependence is introduced, which is not part of the original problem, and the solution to the time-independent problem is obtained by means of a fixed point iteration.

A similar strategy is followed in this work. Instead of embedding the elliptic equation (2.1) in a parabolic equation (2.2), a *hyperbolic* wave equation with damping is considered,

$$\partial_t^2\phi + \partial_t\phi = \Delta\phi. \tag{2.3}$$

The relationship between hyperbolic equations and parabolic diffusion equations has already been investigated in some special cases [21–23]. In particular it can be shown that for large times  $t$  the solution of the hyperbolic equation (2.3) will tend towards the solution of the parabolic PDE, (2.2). The hyperbolic equation can be cast in first order form by introducing the reduction variables  $\psi = \partial_t\phi + \phi$  and

## 2.1. Solution of Elliptic Equations Through Hyperbolic Relaxation

$r_i = \partial_i \phi$ , yielding the system

$$\partial_t \phi = \psi - \phi, \quad (2.4)$$

$$\partial_t \psi = \delta^{ij} \partial_i r_j, \quad (2.5)$$

$$\partial_t r_i = \partial_i \psi - r_i. \quad (2.6)$$

The first of these equations is an ordinary differential equation, and it is directly evident that  $\phi$  will tend towards  $\psi$  exponentially. Thus one can eliminate (2.4) and obtain the solution directly from  $\psi$ .

Combining time derivatives as in (2.3) adds strong damping to the pure wave equation while maintaining the hyperbolic character of the PDE. The idea is that deviations from the stationary state satisfying  $\Delta \phi = 0$  are damped to zero or are propagated away, and furthermore it can be advantageous to perform hyperbolic as opposed to parabolic evolutions.

In the limit of vanishing damping one obtains the plain wave equation. If a stationary state is reached, we again have solved (2.1). This undamped approach has, for example, been used to solve the Poisson equation in the context of self-gravity [24]. Experimenting with (2.3) however, it has been found that the damping is the main desirable feature, while propagation of waves off the grid is far less relevant for the reduction of the residual of Eq. (2.1).

In [25] the authors analyzed a specific hyperbolized version of the Navier-Stokes equations, that exhibits hyperbolic relaxation. Although the type of equations that are considered are similar, the perspective in this work is different. Here the elliptic equation is the fundamental problem and it is embedded in hyperbolic equation with damping to obtain an iterative scheme for the solution of the elliptic equation. Since there does not seem to be an established name for this idea, the method is referred to as *hyperbolic relaxation for elliptic equations* (HypRelax), as opposed to parabolic relaxation that is at the heart of the Jacobi method.

## 2. The Hyperbolic Relaxation Method

With regard to previous literature on hyperbolic relaxation for elliptic equations, some aspects have been explored in [26] in the context of “gauge drivers” for numerical relativity. In particular, [26] introduced one of the most used gauge conditions for certain black hole evolutions, the Gamma-driver for the shift vector, which employs a hyperbolic equation related to the elliptic equation for a minimal distortion shift. They likewise discussed a similar approach to the lapse in which the associated elliptic equation corresponds to maximal slicing. Also see [27] on gauge drivers, where however only parabolic relaxation is considered.

The goal of the present chapter is to develop hyperbolic relaxation given by the prototype in (2.3) into a method to solve a general class of systems of second order, non-linear elliptic equations. The problem of immediate interest are the constraint equations of general relativity together with the constraint equations in relativistic hydrodynamics, that originate from particle number conservation and energy-momentum conservation. In Ch. 4 they are solved as a system of non-linear elliptic equations to obtain initial data for evolution in numerical relativity. However, the formalism is quite independent of this particular problem.

Considering (2.3), let us collect some basic observations here in order to introduce the main questions we want to address. First of all, we have to address the well-posedness of the hyperbolic PDEs. Given a self-adjoint, elliptic operator, the hyperbolicity of equations of type (2.3) should be clear. There exists a rich theoretical background regarding well-posedness and numerical stability for hyperbolic PDEs [28–30], which helps to find relaxation schemes that are well suited for numerical applications.

Second, in addition to the boundary conditions of the original elliptic equation boundary conditions for the hyperbolic equations must be chosen such that they are compatible with the asymptotic elliptic problem. This choice is not unique, but of great importance to obtain successful relaxations. In particular, maximally dissipative boundary conditions are considered.



## 2.1. Solution of Elliptic Equations Through Hyperbolic Relaxation

Third, assuming feasibility and stability of hyperbolic relaxation, a key question concerns the efficiency of the method. In both parabolic and hyperbolic relaxation methods the time parameter is unrelated to the elliptic equation, i.e. the time evolution is of no interest as long as the stationary state is reached efficiently. This is the basis for different acceleration strategies. For hyperbolic relaxation, there is a finite propagation speed, and in contrast to the diffusion equation it is not clear how to by-pass that speed to accelerate the method.

As it stands, there are pragmatic considerations that can make hyperbolic relaxation methods interesting, in particular when solving elliptic equations as part of a larger project. For example, elliptic PDEs are often solved to provide initial data for evolution systems that are subject to certain constraint equations, e.g. the Maxwell equations or the Einstein equations. However, the main work load is the actual evolution of the data by integrating a hyperbolic PDE. In such a case the hyperbolic relaxation method does not have to compete with optimized standard methods in terms of efficiency as long as solving the elliptic equation is only a small part of the entire work load. On the other hand, a hyperbolic relaxation method may be easy to implement using the existing infrastructure of a numerical evolution code, avoiding the need for and the complications of an external elliptic solver. Using the same infrastructure also has the advantage that interpolation errors can be avoided by using the same grid discretization. Considering our research in numerical relativity, a sophisticated infrastructure for evolutions is indeed available, but we were looking for alternative elliptic solvers. Hence hyperbolic relaxation is implemented in the pseudospectral hyperbolic evolution code `bamps` [16, 31], which only required minor modifications once the formalism itself was established.

Throughout the thesis the Einstein summation convention is used, i.e. it is summed over indices that occur once as an upper index and once as a lower index, e.g.  $s^i t_i = \sum_i s^i t_i$ . Latin letters  $i, j, k, \dots$  denote coordinate components and they are lowered and raised by an arbitrary metric with positive signature. An index  $s$

## 2. The Hyperbolic Relaxation Method

denotes a contraction with a vector  $s_i$ , in particular  $\partial_s = s^i \partial_i = s^i \frac{\partial}{\partial x^i}$ . Greek letter indices  $\alpha, \beta, \gamma$  denote components of a field and they are lowered and raised by the Euclidean metric  $\delta_{\alpha\beta}$ . Note that later in Ch. 4, conforming with the conventional notation, Greek letters will denote four dimensional spacetime indices and Latin lower case letters will denote only spatial coordinate components.

### 2.1.2. Evolution System

In the following the principal ideas of the hyperbolic relaxation method will be presented and the equations that follow for the iteration scheme will be derived. Although it is possible to write down hyperbolic relaxation schemes in second order form like Eq. (2.3), the focus will be on a first order formulation. This is primarily done because the used evolution code `bamps` only handles first derivatives, but the the reduction to first order also allows considerable freedom in the problem setup.

In this chapter the systems of elliptic equations under consideration are given in second order form, i.e.

$$(L\psi)_\alpha = a(x^k)^{ij\beta}_\alpha \partial_i \partial_j \psi_\beta + F_\alpha(x^k, \psi_\beta, \partial_i \psi_\beta) = 0, \quad (2.7)$$

where the  $\psi_\alpha$  are the  $N$  unknown solution variables and  $F$  is a continuous function of the solution variables, their derivatives and the  $D$  coordinates  $x^k$ . In the following  $a^{ij\beta}_\alpha$  is taken to be a smooth function of the coordinates and this dependence will be suppressed in the notation. Every elliptic system will be accompanied by a set of boundary conditions on the variables  $\psi_\alpha$  and we discuss their treatment in section 2.1.6. In the following we consider *classically elliptic* systems [32] only, i.e. systems with

$$\det(a^{ij\beta}_\alpha s_i s_j) \neq 0 \quad \forall s \in \mathbb{R}^D \setminus \{0\}, \quad (2.8)$$

where the determinant is understood to be taken on the indices  $\alpha$  and  $\beta$ .

## 2.1. Solution of Elliptic Equations Through Hyperbolic Relaxation

To solve the second order equation (2.7) one could employ the Jacobi method, which can be motivated by evolving the parabolic partial differential equation:

$$\partial_t \psi_\alpha = (L\psi)_\alpha, \quad (2.9)$$

where  $t$  is some parameter that plays the role of time.

For a classically elliptic system with constant coefficients the Jacobi method can only converge if  $a^{ji\beta}_\alpha$  is positive definite on the whole domain, i.e. there exists an  $\epsilon > 0$

$$a^{ji\beta}_\alpha t_{j\beta} t_i^\alpha \geq \epsilon t^{i\alpha} t_{i\alpha} \quad \forall t \in \mathbb{R}^{D \times N} \setminus \{0\}, \quad (2.10)$$

which will be assumed in the rest of this chapter. This condition corresponds to the notion of *strong ellipticity*, which defines an important subclass of classically elliptic systems [32]. Note that we have the freedom to multiply the elliptic equation with an invertible matrix  $d^\beta_\alpha$ , yielding  $(\tilde{L}\psi)_\alpha = d^\beta_\alpha (L\psi)_\beta = 0$ , which has the same solutions as the original equation. This freedom allows the transformation of some systems that are classically but not strongly elliptic into strongly elliptic form.

To construct the hyperbolic relaxation equations one can reduce the second order elliptic system to first order by introducing the *reduction variables*  $r_{i\alpha}$ :

$$0 = a^{ij\beta}_\alpha \partial_i r_{j\beta} + F_\alpha(\psi_\beta, r_{i\beta}), \quad (2.11)$$

$$0 = \partial_i \psi_\alpha - r_{i\alpha}. \quad (2.12)$$

In analogy to the Jacobi method (2.9)  $\psi_\alpha$  is evolved by taking Eq. (2.11) as the right-hand side, yielding

$$\partial_t \psi_\alpha = a^{ij\beta}_\alpha \partial_i r_{j\beta} + F_\alpha(x^i, \psi_\beta, r_{i\beta}) \quad (2.13)$$

and one proceeds similarly with the equations for the reduction variables  $r_i$ :

$$\partial_t r_{i\alpha} = b^j_{i\alpha} (\partial_j \psi_\beta - r_{j\beta}), \quad (2.14)$$

## 2. The Hyperbolic Relaxation Method

where  $b_i^{j\beta}$  is arbitrary under the requirement of positive definiteness, meaning in analogy to Eq. (2.10)

$$b_i^{j\beta} t_{j\beta} t^{i\alpha} > \epsilon t_{i\alpha} t^{i\alpha} \quad \forall t \in \mathbb{R}^{D \times N} \setminus \{0\}. \quad (2.15)$$

The system of Eqs. (2.13) and (2.14) forms a first order hyperbolic differential equation which will be referred to as the the *hyperbolic relaxation system*. Clearly the reduction constraint Eq. (2.12) is not enforced at all times and will indeed be violated during the relaxation process, however we are only interested in the steady state, which fulfills the reduction constraint, because Eq. (2.14) drives the reduction variable  $r_i$  towards  $\partial_i \psi$ . This *driver* concept is a general idea of the method that will also be used in a generalized approach in Sec. 2.2. To get an idea how this driver works, let us assume for arguments sake that  $\partial_t \partial_i \psi_\alpha = 0$ , which is reasonable close to the steady state. The solution for  $r_{i\alpha}$  then has the form

$$r_{i\alpha}(t) = \sum_{l=1}^n e^{-\lambda_l t} \sum_{k_l=0}^{m_l} x^{k_l} h_{k_l i\alpha} + \partial_i \psi_\alpha, \quad (2.16)$$

where  $h$  is constant and the  $\lambda_l$  are the  $n$  eigenvalues defined by the eigenvalue equation  $b_i^{j\beta} t_l^{i\alpha} = \lambda_l t_l^{j\beta}$  and  $m_l$  depends on the geometric multiplicity of  $\lambda_l$ . From the positive definiteness of  $b$  we know that all the eigenvalues have positive real part and it follows immediately that  $r_{i\alpha}$  approaches  $\partial_i \psi_\alpha$  exponentially. Indeed in Sec. 2.1.4 it will be shown for a simple case that the modes of the system are always damped even for  $\partial_t \partial_i \psi_\alpha \neq 0$ . It is emphasized however that in some cases, e.g. if the elliptic system has no solution,  $\partial_i \psi_\alpha$  can grow faster than  $r_{i\alpha}$  and thus the reduction constraints cannot be satisfied asymptotically in time.

It is obvious that if the hyperbolic relaxation system reaches a steady state we must have obtained a solution to the first order elliptic system Eqs. (2.11) and (2.12), and hence also of the original elliptic equation (2.7).

A small variation of the relaxation equations can be obtained by a different choice of the reduction variable. For example the reduction variable could be chosen as

follows

$$\partial_i \psi_\alpha - c_i^j r_{j\alpha}, \quad (2.17)$$

where  $c_i^j$  is some positive definite matrix. It can then be shown that the evolution equation

$$\partial_t r_{i\alpha} = b_i^{j\beta} (\partial_j \psi_\beta - c_j^k r_{k\beta}), \quad (2.18)$$

will drive  $r_{j\alpha}$  towards  $(c^{-1})_j^i \partial_i \psi_\alpha$ . An application for this can be found for example in numerical relativity applications where it is sometimes advantageous to use a derivative that has been raised by the spatial metric as reduction variable. This variant is however not further considered in the course of this thesis.

It is natural to ask here why derivation has been restricted to second order elliptic systems rather than including also first order systems. The reason is that only for this class of operators it is possible to identify a hyperbolic relaxation scheme which can be expected to efficiently settle down to a steady state. The next natural query is what, if anything, is gained by insisting on taking the relaxation scheme in first order form, beyond the practical requirement that the scheme can be implemented within the used evolution code. As we have seen, the reduction allows a variety of choices for  $b_i^{j\beta}$ , which is not directly evident in the second order form. In fact it is not clear whether a similar second order form relaxation equation like Eq. (2.3) can be found for generic  $b_i^{j\beta}$ . As will be seen in Sec. 3.1.4 the first order formulation also provides a method to define a refinement criterion.

### 2.1.3. Residual Evolution

The residuals of the first order system, Eqs. (2.11),(2.12), are given by

$$R_\alpha = a^{ij\beta} \partial_i r_{j\beta} + F_\alpha(x^i, \psi_\beta, r_{i\beta}), \quad (2.19)$$

$$R_{i\alpha} = b_i^{j\beta} (\partial_j \psi_\beta - r_{j\beta}). \quad (2.20)$$

## 2. The Hyperbolic Relaxation Method

A simple calculation shows that the residuals will evolve according to

$$\partial_t R_\alpha = a^{ij\beta}{}_\alpha \partial_i R_{j\beta} + \frac{\partial F_\alpha}{\partial \psi_\beta} R_\beta + \frac{\partial F_\alpha}{\partial r_{i\beta}} R_{i\beta}, \quad (2.21)$$

$$\partial_t R_{i\alpha} = b^j{}_{i\alpha}{}^\beta (\partial_j R_\beta - R_{j\beta}). \quad (2.22)$$

For a working relaxation scheme, we want the residual evolution system to be stable, i.e. the first order residuals should converge to zero for  $t \rightarrow \infty$ , for residuals that are sufficiently close to zero. Systems of this type and stability conditions are discussed in detail in [33] and [34]. It is not possible for us to give general results on the stability of the hyperbolic relaxation scheme, as the multitude of possible systems is too large to be covered in a closed form, especially for elliptic systems with more than one variable. A stability analysis must therefore be done individually for the concrete problem.

### 2.1.4. Mode Analysis

To shed some light on the behavior of solutions to the hyperbolic relaxation, a simple mode analysis is performed ignoring the issue of boundary conditions for a generalization of equation (2.3)

$$\epsilon \partial_t^2 \phi + \eta \partial_t \phi = \Delta \phi, \quad (2.23)$$

where  $\epsilon$  and  $\eta$  are real, non-negative constants. A third constant in front of  $\Delta \phi$  has been rescaled to one without loss of generality. With  $\epsilon = \eta = 1$  as in Eq. (2.3) the unit of time is fixed to be dimensionless (unity since  $[T^2] = [T]$ ).

Inserting the plane-wave ansatz

$$\phi_{\text{pw}}(t, x) = e^{i(kx - \omega t)}, \quad (2.24)$$

with constants  $k$  and  $\omega$ , into the hyperbolic relaxation equation (2.3) we obtain

$$\epsilon \omega^2 + i\eta \omega = k^2, \quad (2.25)$$

$$\omega_\pm(k) = -\frac{1}{2\epsilon} (\eta i \pm \sqrt{4\epsilon k^2 - \eta^2}). \quad (2.26)$$

## 2.1. Solution of Elliptic Equations Through Hyperbolic Relaxation

The wavenumber  $k$  is a real number related to the wave length,  $k = 2\pi/\lambda$ , while  $\omega$  may be a complex number. Recall that for the wave equation  $\omega_{\pm}(k) = \pm k$ , while for the heat equation  $\omega(k) = -ik^2$ . For hyperbolic relaxation, there is a further case distinction for the sign under the square root  $\sqrt{4\epsilon k^2 - \eta^2}$ . The existence of a transition at a specific length scale  $\lambda_{\text{crit}} = \frac{2\pi}{k_{\text{crit}}} = \frac{4\pi\sqrt{\epsilon}}{\eta}$  signals that the chosen hyperbolic relaxation equation has fixed a scale, that can be adjusted by changing the parameters  $\eta$  and  $\epsilon$ .

For sufficiently large wavenumber,

$$\phi_{\text{pw}} = e^{-\frac{\eta}{2\epsilon}t} e^{i(kx \pm \frac{1}{2\epsilon}\sqrt{4\epsilon k^2 - \eta^2}t)}, \quad k \geq \frac{\eta}{2\sqrt{\epsilon}}, \quad (2.27)$$

which is a damped wave with phase velocity  $v(k) = \frac{1}{\epsilon}\sqrt{\epsilon - \frac{\eta^2}{4k^2}}$ . The damping is independent of  $k$  (as opposed to the heat equation with  $e^{-k^2t}$ ). The phase velocity approaches  $v = 1/\sqrt{\epsilon}$  for large  $k$ , but for  $k$  approaching the critical value  $\frac{\eta}{2\sqrt{\epsilon}}$  from above the phase velocity tends towards  $v = 0$ . This has the consequence that the maximal possible time step scales like  $\Delta t \sim \sqrt{\epsilon}\Delta x$  for large  $k$  (high resolution), but has a finite upper bound for small  $k$ . Increasing the parameter  $\epsilon$  might appear to be a good idea at first, since it allows one to use larger time steps, but at the same time it reduces the damping by the same factor.

For sufficiently small wavenumber,

$$\phi_{\text{pw}} = e^{-\frac{1}{2\epsilon}(\eta \pm \sqrt{\eta^2 - 4\epsilon k^2})t} e^{ikx}, \quad 0 \leq k \leq \frac{\eta}{2\sqrt{\epsilon}}, \quad (2.28)$$

which is a non-moving wave profile  $e^{ikx}$  times a  $k$ -dependent damping factor. For  $k = \frac{\eta}{2\sqrt{\epsilon}}$ , the damping is  $e^{-\frac{\eta}{2\epsilon}t}$ , while for  $k$  equal to zero there are two cases,  $e^0$  or  $e^{-\frac{\eta}{\epsilon}t}$ . For small  $k$ , the worse (more weakly) damped case is  $\exp(-\frac{1}{2\epsilon}(\eta - \sqrt{\eta^2 - 4\epsilon k^2})t) \approx \exp(-\frac{1}{\eta}k^2t)$ , which is the same damping as for the basic heat equation, when we choose  $\eta = 1$ .

Summarizing, the plane-wave mode analysis suggests that solutions to the hyperbolic relaxation equation exhibit a mixture of relaxation and wave propagation

## 2. The Hyperbolic Relaxation Method

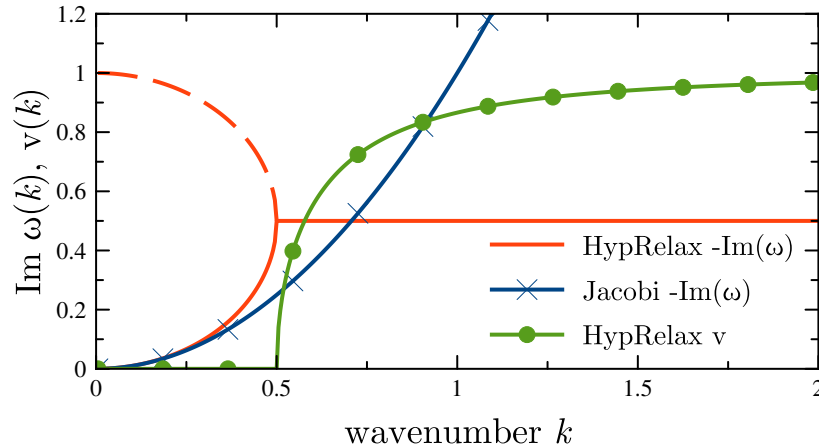


Figure 2.1.: Damping and propagation speed of basic hyperbolic relaxation with parameters  $\epsilon = 1$  and  $\eta = 1$  compared to parabolic relaxation. There is a transition at  $k_{\text{crit}} = \frac{1}{2}$ , which can be moved to lower values by adjusting  $\eta$ . The overall damping is determined by the slowest damping rate.

phenomena, see Fig. 2.1. For wave numbers larger than a critical value,  $k \geq k_{\text{crit}}$  with  $k_{\text{crit}} = \frac{\eta}{2\sqrt{\epsilon}}$ , there is wave propagation with simultaneous damping. Noteworthy is that the damping is independent of  $k$ ,  $e^{-\frac{\eta}{2\epsilon}t}$ . This is a promising feature compared to parabolic relaxation with  $e^{-k^2t}$  for intermediate values of  $k$ . For large values of  $k$  parabolic relaxation has much stronger damping, but the overall convergence rate is dominated by small  $k$ . For hyperbolic relaxation, there is no wave propagation for  $k \leq k_{\text{crit}}$ , but the damping persists. Interestingly, the damping factor asymptotes towards  $e^{-\frac{1}{\eta}k^2t}$  for  $k \rightarrow 0$ , and is never worse than parabolic relaxation for small  $k$ , when we choose  $\eta = 1$ .

If the first order relaxation equations are mimicked by (2.13) and (2.14) by

$$\partial_t \psi = \frac{1}{\eta} \partial_j r^j, \quad \partial_t r_i = \frac{\eta}{\epsilon} (\partial_i \psi - r_i), \quad (2.29)$$

we recover the modes in (2.26) and  $D - 1$  transverse modes that have  $\psi = 0$  and for which  $\omega(k) = -i\frac{\eta}{\epsilon}$  is purely imaginary.



For the choice of  $\eta$  and  $\epsilon$  we can take our motivation from the gauge driver construction [26] and set  $\epsilon = 1$ ,  $\eta$  an arbitrary non-negative constant, and obtain

$$\omega_{\pm}(k) = -\frac{1}{2}(i\eta \pm \sqrt{4k^2 - \eta^2}). \quad (2.30)$$

A uniform scaling of time, i.e.  $\epsilon = \eta^2$  with arbitrary  $\eta$ , has also been considered.

To avoid small  $k$  that drop below (or too far below)  $k_{\text{crit}}$ , we can adjust  $\epsilon$  or  $\eta$  such that the length scale of  $k$  corresponds to the physical size  $L$  of the domain, say  $\lambda_{\text{crit}} = 2L$ . This will decrease the damping for large  $k$ , but will also avoid the severe slow down when the damping approaches that of parabolic relaxation. One could also think of varying  $\eta$  from one iteration step to another, maybe even adaptively. This however is beyond the scope of this thesis.

### 2.1.5. Hyperbolicity Analysis

Before starting the hyperbolicity analysis of the HypRelax system it is convenient to introduce the following notation for inverse tensors. Whenever an inverse tensor appears it has to be understood as the inverse of matrices with respect to the field indices. For example the inverse of the tensor  $c^{\beta}_{\alpha}$  is  $(c^{-1})^{\alpha}_{\gamma}$  and we have

$$c^{\beta}_{\alpha}(c^{-1})^{\alpha}_{\gamma} = \delta^{\beta}_{\gamma}. \quad (2.31)$$

For the hyperbolicity analysis the hyperbolic relaxation system is first written in matrix form

$$\partial_t \mathbf{u} = \mathbf{P}^k \partial_k \mathbf{u} + h(x^i, \mathbf{u}) \quad (2.32)$$

with

$$\mathbf{P}^k = \begin{pmatrix} 0 & a^{ki\beta}_{\alpha} \\ b^k_{i\alpha} & 0 \end{pmatrix}, \quad \mathbf{u} = \begin{pmatrix} \psi_{\alpha} \\ r_{i\alpha} \end{pmatrix}. \quad (2.33)$$

## 2. The Hyperbolic Relaxation Method

The principal symbol of this system is then given by

$$\mathbf{P}^s = \mathbf{P}^k s_k = \begin{pmatrix} 0 & a^{s_i \beta} \alpha \\ b^{s_i \beta} \alpha & 0 \end{pmatrix}, \quad (2.34)$$

where  $s_i$  is an arbitrary unit vector,  $s^i s_i = 1$ . Suppose  $c^\beta_\alpha = a^{s_i \epsilon} b^{s_i \beta}_\epsilon$  has a complete set of eigenvectors  $w_\gamma^\alpha$  with  $c^\beta_\alpha w_\gamma^\alpha = \sigma_\gamma^\alpha w_\alpha^\beta$ , where  $\sigma_\gamma^\alpha$  is diagonal. If furthermore all the eigenvalues, i.e. the diagonal elements of  $\sigma_\gamma^\alpha$ , are positive then  $\mathbf{P}^s$  has the following left eigenvectors

$$\mathbf{v}_{j\gamma}^0 = (0, \delta_\gamma^\alpha \delta_j^i - b^{s_j \epsilon} (b^{s_s -1})^\alpha_\epsilon s^i), \quad (2.35)$$

$$\mathbf{v}_\gamma^\pm = (w_\gamma^\alpha, \pm (\rho^{-1})_\gamma^\delta w_\delta^\epsilon a^{s_i \alpha}_\epsilon), \quad (2.36)$$

where  $\rho_\gamma^\beta$  is the root of  $\sigma_\gamma^\beta$ , i.e. it is a positive diagonal tensor with  $\rho_\gamma^\alpha \rho_\alpha^\beta = \sigma_\gamma^\beta$ . Note that of the eigenvectors  $\mathbf{v}_{j\gamma}^0$  only  $(D-1)N$  are linearly independent, while the  $\mathbf{v}_\gamma^\pm$  are  $2N$  independent vectors. If there exists a constant  $K$ , independent of  $s^i$ , such that  $\|\mathbf{V}\|_2 + \|\mathbf{V}^{-1}\|_2 < K$ , where  $\mathbf{V}$  is an, in general  $s^i$ -dependent, square matrix constructed from a linearly independent set of the eigenvectors  $\mathbf{v}$ , then the system is strongly hyperbolic [28–30]. The characteristic variables  $\hat{u}$  and their characteristic speeds  $\lambda$  are thus

$$\hat{u}_{j\gamma}^0 = r_{j\gamma} - b^{s_j \epsilon} (b^{s_s -1})^\alpha_\epsilon s^i r_{i\alpha}, \quad \lambda_{i\gamma}^0 = 0, \quad (2.37)$$

$$\hat{u}_\gamma^\pm = w_\gamma^\alpha \psi_\alpha \pm (\rho^{-1})_\gamma^\delta w_\delta^\epsilon a^{s_i \alpha}_\epsilon r_{i\alpha}, \quad \lambda_\gamma^\pm = \pm \rho_\gamma^\alpha e_\alpha, \quad (2.38)$$

where  $e_\alpha$  denote the Cartesian basis vectors. From this we can recover the evolved variables in terms of the characteristics:

$$\psi_\alpha = \frac{1}{2} (w^{-1})_\alpha^\gamma (\hat{u}_\gamma^+ + \hat{u}_\gamma^-), \quad (2.39)$$

$$r_{i\alpha} = \hat{u}_{i\alpha}^0 + b^{s_i \epsilon} (c^{-1})^\beta_\epsilon \left( (w^{-1})_\beta^\delta \rho_\delta^\gamma \frac{\hat{u}_\gamma^+ - \hat{u}_\gamma^-}{2} - a^{s_j \gamma} \beta \hat{u}_{j\gamma}^0 \right). \quad (2.40)$$

The freedom in the choice of  $b^{j\beta}_i \alpha$  can be used to impose certain properties on the hyperbolic relaxation system. In the following some interesting choices will be

## 2.1. Solution of Elliptic Equations Through Hyperbolic Relaxation

discussed, that fulfill the restriction of positive definiteness (2.15) that has been set for  $b$ .

1. *b is the identity.* A very easy and natural choice is  $b^j_{i\alpha} = \delta_i^j \delta_\alpha^\beta$ . With this choice we have  $c^\beta_\alpha = a^{ss\beta}_\alpha$ , which has only eigenvalues with positive real part due to (2.10). The imaginary part however can be non-vanishing. If however  $a^{ss\alpha}_\gamma = a^{ss}_\gamma{}^\alpha$ , then  $c$  is guaranteed to have a complete set of eigenvectors with purely real eigenvalues and thus system is strongly hyperbolic. If we have  $a^{ij\alpha}_\gamma = a^{ij}_\gamma{}^\alpha$ , then the system is even symmetric hyperbolic with symmetrizer:

$$\mathbf{H} = \begin{pmatrix} \delta_\gamma^\alpha & 0 \\ 0 & a^{ij\alpha}_\gamma \delta_{jl} \end{pmatrix}. \quad (2.41)$$

2. *b is the transpose of a.* One can also make the system trivially symmetric hyperbolic by choosing  $b^j_{i\alpha} = a^j_{i\alpha}{}^\beta$ . The principal symbol of this system is symmetric and thus the system is symmetric hyperbolic.

3. *b is the inverse of a.* We can choose  $b$  to be the inverse of  $a$  in the sense that  $b$  fulfills  $a_k{}^{i\alpha}_\gamma b^j_{i\alpha} = \delta_k^j \delta_\gamma^\beta$ . This choice is particularly interesting, because we then have  $c^\beta_\alpha = \delta_\alpha^\beta$  and thus all the non-zero characteristic speeds have values  $\pm 1$ . Furthermore the eigenvectors of  $c$  become trivial:  $w_\gamma{}^\alpha = \delta_\gamma^\alpha$ . A symmetrizer for this system is

$$\mathbf{H} = \begin{pmatrix} \delta_\gamma^\alpha & 0 \\ 0 & a_m{}^{i\alpha}_\omega a^m{}_{l\gamma}{}^\omega \end{pmatrix}. \quad (2.42)$$

The characteristic speeds determine (among other factors) the maximum allowed time step and therefore it is usually preferable to have all the traveling characteristic variables propagating with the same speeds, such that all variables are damped with the maximum rate. Therefore this choice for  $b^j_{i\alpha}$  can be considered optimal for typical cases. A straightforward generalization of this choice allows  $b^j_{i\alpha}$  to be scaled by a constant factor, which will also uniformly scale the characteristic speeds.

### 2.1.6. Boundary Conditions

The basic idea to impose boundary conditions in the `bamps` code is to modify the right hand side of the hyperbolic relaxation system. The outward pointing unit normal covector  $s_i$  to the boundary surface is naturally defined by taking the gradient of a scalar field which is increasing across, but constant in the boundary, and then normalizing this gradient to unit magnitude using our arbitrary but fixed metric. This metric is subsequently used to raise the index and form the outward pointing vector  $s^i$ . Restricting the discussion to strongly hyperbolic systems it is made sure that a regular ( $s^i$ -dependent) similarity transformation matrix  $\mathbf{T}_s$  exists which transforms between the evolved variables  $\mathbf{u}$  and a linearly independent set of the characteristic variables  $\hat{\mathbf{u}}$  given in Eq. (2.37) and (2.38)

$$\mathbf{u} = \mathbf{T}_s \hat{\mathbf{u}}. \quad (2.43)$$

One can then decompose the evolution equations (2.32) as

$$\partial_t \mathbf{u} = \mathbf{P}^s \partial_s \mathbf{u} + \mathbf{P}^k q_k^i \partial_i \mathbf{u} + h(x^i, \mathbf{u}), \quad (2.44)$$

where  $q_k^i = \delta_k^i - s_k s^i$  is the projector onto the boundary surface. Multiplying by  $\mathbf{T}_s^{-1}$  and one obtains

$$\begin{aligned} d_t \hat{\mathbf{u}} &= \mathbf{T}_s^{-1} \mathbf{P}^s \partial_s \mathbf{u} + \mathbf{T}_s^{-1} (\mathbf{P}^k q_k^i \partial_i \mathbf{u} + h(x^i, \mathbf{u})) \\ &= \mathbf{T}_s^{-1} \mathbf{P}^s \mathbf{T}_s \mathbf{T}_s^{-1} \partial_s \mathbf{u} + \mathbf{T}_s^{-1} (\mathbf{P}^k q_k^i \partial_i \mathbf{u} + h(x^i, \mathbf{u})) \\ &= \mathbf{\Lambda}^s d_s \hat{\mathbf{u}} + \mathbf{T}_s^{-1} (\mathbf{P}^k q_k^i \partial_i \mathbf{u} + h(x^i, \mathbf{u})). \end{aligned} \quad (2.45)$$

Here the straight derivative symbol  $d$  denotes that the transformation matrix stands outside of the derivative, i.e.  $d_t \hat{\mathbf{u}} \equiv \mathbf{T}_s^{-1} \partial_t \mathbf{u}$ , and  $\mathbf{\Lambda}^s$  is a diagonal matrix containing the characteristic speeds. Boundary conditions on the incoming variables, i.e. those with positive characteristic speeds, can now be imposed by modifying their right hand sides. After the right hand sides have been modified the system is then transformed back by multiplying with  $\mathbf{T}_s$ .

### Penalty Method

In the penalty method [35–37] the boundary conditions are *weakly imposed* by modifying the right hand sides of the incoming characteristic variables  $\hat{u}_\gamma^+$  in the following way

$$d_t \hat{u}_\gamma^+ \hat{=} D_t \hat{u}_\gamma^+ + p(\hat{u}_\gamma^{+BC} - \hat{u}_\gamma^+), \quad (2.46)$$

where  $p$  is the penalty parameter,  $u_\gamma^{+BC}$  is some given boundary data that we want  $\hat{u}_\gamma^+$  to approach,  $D_t \hat{u}_\gamma^+$  is the unmodified right hand side and  $\hat{=}$  denotes equality at the boundary. The penalty parameter can not be chosen arbitrarily, but must be carefully chosen. A detailed derivation of the penalty parameters used in `bamps` can be found in [16].

### Maximally Dissipative Boundary Conditions

Maximally dissipative boundary conditions [28–30, 38] allow to set boundary conditions of the form

$$s^i \partial_i \psi_\alpha |_{\partial\Omega} = \phi_\alpha(\psi_\beta, \partial_i \psi_\beta, q_j^i \partial_i \partial_k \psi_\beta), \quad (2.47)$$

where  $\phi$  is a function that is allowed to depend on the coordinates  $x^i$ , the fields  $\psi_\alpha$ , their derivatives and the transverse projections ( $q_j^i = \delta_j^i - s^i s_j$ ) of their second derivatives. For clarity and brevity dependence on all the arguments is suppressed in the following.

Enforcing the boundary conditions (2.47) would cause undesirable reflections from the outer boundary during the relaxation process. It is possible however to construct maximally dissipative boundary conditions such that (2.47) is fulfilled in the steady state. Maximally dissipative boundary conditions are imposed by requiring

$$(\rho^{-1})_\gamma^\beta w_\beta^\alpha \partial_t \psi_\alpha + w_\gamma^\alpha \partial_s \psi_\alpha = w_\gamma^\alpha \phi_\alpha. \quad (2.48)$$

This boundary condition is actually different from Eq. (2.47) during the relaxation process. However, again we are only interested in the steady state at the end of the

## 2. The Hyperbolic Relaxation Method

evolution, where  $\partial_t \psi_\alpha = 0$  and thus the correct boundary condition will be imposed. For numerical stability the functions  $\phi_\alpha$  must not depend on normal derivatives of the evolved variables. Therefore in (2.47) in the arguments of  $\phi_\alpha$  the replacements  $\partial_i \psi_\beta \rightarrow r_{i\beta}$  and  $q_j^i \partial_i \partial_k \psi_\beta \rightarrow q_j^i \partial_i r_{k\beta}$  have to be made.

For the normal derivatives of the incoming characteristic one obtains the relation

$$d_s \hat{u}_\gamma^+ = w_\gamma^\alpha \partial_s \psi_\alpha + (\rho^{-1})_\gamma^\delta w_\delta^\epsilon a^{s i \alpha} \partial_s r_{i\alpha} \quad (2.49)$$

$$= w_\gamma^\alpha \phi_\alpha - (\rho^{-1})_\gamma^\delta w_\delta^\alpha (\partial_t \psi_\alpha - a^{s j \epsilon} \partial_s r_{j\epsilon}), \quad (2.50)$$

where in the actual implementation  $\partial_t \psi_\alpha$  is to be replaced by Eq. (2.13). This equation is now used to impose the boundary condition by replacing the  $d_s \hat{u}_\gamma^+$  terms in Eq. (2.45), yielding the modified right hand side

$$d_t \hat{u}_\gamma^+ \hat{=} D_t \hat{u}_\gamma^+ - \rho_\gamma^\beta (w_\beta^\alpha \partial_s \psi_\alpha + (\rho^{-1})_\beta^\delta w_\delta^\alpha \partial_t \psi_\alpha - w_\beta^\alpha \phi_\alpha). \quad (2.51)$$

With the general expression at hand, it is now possible to discuss choices for  $\phi_\alpha$  that lead in the steady state to standard boundary conditions for elliptic equations.

*1. Dirichlet conditions.* Dirichlet conditions are of the form  $\psi_\alpha|_{\partial\Omega} = g_\alpha$ , where the  $g_\alpha$  are some function defined on the domain boundary  $\partial\Omega$ . To achieve such a boundary condition in the steady state,  $\phi_\alpha$  has to take the form

$$\phi_\alpha = s^i r_{i\alpha} + e^\beta_\alpha (g_\beta - \psi_\beta), \quad (2.52)$$

where  $e$  is positive definite, i.e.  $e^\beta_\alpha t_\beta t^\alpha > 0$ . In the steady state we have  $\partial_i \psi_\alpha = r_{i\alpha}$  and thus Eq. (2.48) becomes  $0 = e^\beta_\alpha (g_\beta - \psi_\beta)$ , which is only fulfilled for the requested boundary condition. The positive definiteness of  $e$  is important to guarantee stability at the boundary. Suppose we have  $\partial_i \psi_\alpha = r_{i\alpha}$  fixed, then Eq. (2.48) has the form

$$(\rho^{-1})_\gamma^\beta w_\beta^\alpha \partial_t \psi_\alpha = w_\gamma^\alpha e^\beta_\alpha (g_\beta - \psi_\beta), \quad (2.53)$$

which would have solutions not asymptoting to  $g_\alpha$  if  $e$  was not positive definite. Besides positive definiteness there are no further restrictions apparent on  $e$  and

## 2.2. Hyperbolic Relaxation Method for Elliptic Equations in Divergence Form

therefore, it can be chosen to be the identity  $e^\beta_\alpha = \delta^\beta_\alpha$ , which is the choice used in all the investigations presented this work.

2. *Neumann conditions.* Neumann boundary conditions are of the form  $s^i \partial_i \psi_\alpha|_{\partial\Omega} = g_\alpha$ . They are straightforwardly implemented by setting  $\phi_\alpha = g_\alpha$ .

3. *Robin conditions.* Robin boundary conditions are a mixture of Dirichlet and Neumann boundary conditions and can be written as  $s^i \partial_i \psi_\alpha|_{\partial\Omega} = g_\alpha + f^\beta_\alpha \psi_\beta$ , where the  $f^\beta_\alpha$  are functions defined on the domain boundary. Their implementation is also straight forward choosing  $\phi_\alpha = g_\alpha + f^\beta_\alpha \psi_\beta$ .

## 2.2. Hyperbolic Relaxation Method for Elliptic Equations in Divergence Form

### 2.2.1. Evolution System

In some cases elliptic equations are better expressed in divergence form, i.e. they are given by

$$(L\phi)_\alpha = \partial_i (A^i_\alpha(x^k, \psi_\beta, \partial_k \psi_\beta)) + B_\alpha(x^k, \psi_\beta, \partial_k \psi_\beta) = 0, \quad (2.54)$$

where it is always assumed that the functions  $B_\alpha$  and  $A^i_\alpha$  are continuous and continuous differentiable respectively. Of course these equations could always be expressed in the standard form of Eq. (2.7), but possibly with a lot of terms depending on the complexity of  $A^i_\alpha$  and  $B_\alpha$ . In particular the equation might be only quasilinear, posing a challenge to the characteristic analysis of the HypRelax method and subsequently the construction of boundary conditions.

Given an equation of the form (2.54) the question might arise whether its type is actually elliptic or not. To prove this it is necessary to reduce the equation to the

## 2. The Hyperbolic Relaxation Method

standard form (2.7) and investigate its principal part given in terms of  $A^i_\alpha$  by

$$a^{ij\beta}_\alpha = \frac{\partial}{\partial(\partial_j\psi_\beta)} A^i_\alpha(x^k, \psi_\beta, \partial_k\psi_\beta). \quad (2.55)$$

There are some theorems on solutions to elliptic equations that hold specifically for elliptic equations in divergence form, see e.g. [39]. Usually they exploit the simple applicability of the Gauss theorem. For example for vanishing  $B_\alpha$  it follows easily that solutions only exist if all closed surface integrals over  $s_i A^i_\alpha$ ,  $s_i$  being the normal vector to the surface, vanish. In the construction of the hyperbolic relaxation scheme for divergence form equations we will not rely particularly on these special properties. Instead we will exploit that this form admits the construction of a relaxation scheme with an easy to analyze principal part, where the standard method of Chap. 2 would only allow schemes with probably non-linear, variable principal part coefficients. This new type of hyperbolic relaxation scheme will find its application in the computation of initial data as will be outlined in Chap. 4. I will refer to this method with the abbreviation HypRelaxDiv, distinguishing it from the HypRelax method of the previous chapter.

The construction of the HypRelaxDiv scheme goes along the same lines as the standard HypRelax method, i.e. we start by introducing reduction variables  $r_{i\alpha}$  for the first derivatives of  $\psi_\alpha$  yielding the first order system

$$0 = \partial_i(A^i_\alpha(x^k, \psi_\beta, r_{k\beta})) + B_\alpha(x^k, \psi_\beta, r_{k\beta}) \quad (2.56)$$

$$0 = \partial_i\psi_\alpha - r_{i\alpha}. \quad (2.57)$$

To evaluate the derivative in the first of these equations another variable  $F^i_\alpha$  is introduced to write the system in the form

$$0 = \partial_i(F^i_\alpha) + B_\alpha(x^k, \psi_\beta, r_{k\beta}) \quad (2.58)$$

$$0 = \partial_i\psi_\alpha - r_{i\alpha} \quad (2.59)$$

$$0 = A^i_\alpha(x^k, \psi_\beta, r_{k\beta}) - F^i_\alpha. \quad (2.60)$$



## 2.2. Hyperbolic Relaxation Method for Elliptic Equations in Divergence Form

For clarity the dependence on the arguments of  $A^i_\alpha$  and  $B_\alpha$  is suppressed in the rest of the thesis and it is understood that they do not depend on derivatives of our variables. The relaxation scheme is obtained if we add pseudo-time derivatives on the right hand side and obtain

$$\partial_t \psi_\alpha = \partial_i (F^i_\alpha) + B_\alpha \quad (2.61)$$

$$\partial_t r_{i\alpha} = b^j_{i\alpha} (\partial_j \psi_\beta - r_{j\beta}) \quad (2.62)$$

$$\partial_t F^i_\alpha = c^i_{j\alpha} (A^j_\beta - F^j_\beta) + d^i_{j\alpha} (\partial^j \psi_\beta - r^j_\beta), \quad (2.63)$$

where the functions  $b^j_{i\alpha}$ ,  $c^i_{j\alpha}$  and  $d^i_{j\alpha}$  have been introduced to generalize the scheme. They are analogous to the function  $b^j_{i\alpha}$  in the standard HypRelax scheme and have to fulfill the positive condition (2.15). Eq. (2.61) and (2.62) can be discussed in complete analogy to the standard HypRelax method. The new equation (2.63) works as a driver letting  $F^i_\alpha$  approach  $A^i_\alpha$  exponentially, exactly in the same way as  $r_{i\alpha}$  approaches  $\partial_i \psi_\alpha$ . In Eq. (2.63) the reduction constraint (2.59) has been added to make the system strongly hyperbolic. Without this term the system would only be weakly hyperbolic.

From the flexibility in the choice of  $b^j_{i\alpha}$ ,  $c^i_{j\alpha}$  and  $d^i_{j\alpha}$  it is directly evident that we have strong control over the principal part of this relaxation scheme, which is helpful for the construction of stable relaxation schemes and in particular for the implementation of boundary conditions.

There are possible variations to the scheme proposed above. For example one could add the term  $\partial_i r^i_\alpha$  to (2.61) and subtract  $d^i_{j\alpha} r^j_\beta$  from (2.63) making the system symmetric in the principal part for appropriate choice of the coefficients. Another variation would multiply the right-hand side of Eq. (2.61) which allows to control the rate of change in certain regions on the grid and thus might be a way to stabilize the relaxation.

Given the equations in divergence form it is also possible to construct a relaxation scheme in flux-balance form without introducing the new variable  $F^i_\alpha$ , e.g.

## 2. The Hyperbolic Relaxation Method

by Galerkin methods. For test purposes a Discontinuous Galerkin method has been implemented solving the Poisson equation, but it still lacks an application since this method is relative expensive and provides no direct advantage. Another variation is found modifying the driver in the same way discussed for Eq. (2.18). In some special cases it is also possible to construct methods completely without the reduction variables  $r_{i\alpha}$ .

### 2.2.2. Comparison with Standard Hyperbolic Relaxation

Having analyzed the general properties of both the standard HypRelax scheme and the one for divergence equations both will now be discussed comparatively. In Sec. 2.2.1 it has already been discussed, that the divergence form can be algebraically simpler and thus reduce the computational costs. Furthermore the principal part can be chosen in inherently simple enabling one to construct viable boundary conditions. Those two points should be the main motivation to chose the divergence form version. The advantage of the standard method are its lower storage costs, as it only requires  $(D+1)N$  variables instead of  $(2D+1)N$ . Furthermore one has to consider the number of derivatives that are needed. For a spectral method computing derivatives becomes the most costly part for high spectral resolutions. Luckily the proposed relaxation scheme for divergence equations requires only derivatives of  $\psi_\alpha$  and  $F_\alpha^i$ , but not  $r_\alpha^i$  and therefore the computational costs due to derivatives is the same. One has to note however that one of the main aims of the HypRelax method is to reutilize existing infrastructure, which is often not designed to exclude certain evolved variables from the derivative computation. So there is a small initial coding effort necessary to make the method for divergence equations equally efficient.

### 2.2.3. Hyperbolicity Analysis

The characteristic variables of the HypRelaxDiv system are very similar to the characteristic variables of the HypRelax system discussed in Sec. 2.1.5. Therefore the analysis here will be presented in a condensed form.

The principal symbol of the HypRelaxDiv system is

$$\mathbf{P}^s = \mathbf{P}^k s_k = \begin{pmatrix} 0 & 0 & s_i \delta_\alpha^\beta \\ b_{i\alpha}^{s\beta} & 0 & 0 \\ d^{is\beta}_\alpha & 0 & 0 \end{pmatrix}. \quad (2.64)$$

In contrast to the HypRelax system the matrix  $c_\alpha^\beta$  is now given by  $c_\alpha^\beta = d^{ss\beta}_\alpha$  and as for the HypRelax system it is assumed that it has a complete set of eigenvectors  $w_\gamma^\alpha$  with  $c_\alpha^\beta w_\gamma^\alpha = \sigma_\gamma^\alpha w_\alpha^\beta$ , where  $\sigma_\gamma^\alpha$  is a positive definite diagonal matrix. The left eigenvectors of  $\mathbf{P}^s$  are then given by

$$\mathbf{v}_\gamma^\pm = (w_\gamma^\alpha, 0, \pm(\rho^{-1})_\gamma^\delta w_\delta^\alpha s_i), \quad (2.65)$$

$$\mathbf{v}^{(F)j}_\gamma = (0, 0, \delta_\gamma^\alpha \delta_j^i - d^{js\epsilon}_\gamma (d^{ss-1})_\epsilon^\alpha s_i), \quad (2.66)$$

$$\mathbf{v}_{j\gamma}^{(r)} = (0, \delta_\gamma^\alpha \delta_j^i - b_{j\gamma}^{s\epsilon} (b_s^{-1})_\epsilon^\alpha s^i, 0), \quad (2.67)$$

$$\mathbf{v}_\gamma^\times = (0, (b_s^{-1})_\gamma^\alpha s^i, -(d^{ss-1})_\gamma^\alpha s_i), \quad (2.68)$$

where the matrix  $\rho_\gamma^\beta$  is the root of  $\sigma_\gamma^\beta$ . The characteristic variables  $\hat{u}$  and their characteristic speeds  $\lambda$  are thus

$$\hat{u}_\gamma^\pm = w_\gamma^\alpha \psi_\alpha \pm (\rho^{-1})_\gamma^\delta w_\delta^\alpha s_i F_\alpha^i, \quad \lambda_\gamma^\pm = \pm \rho_\gamma^\alpha e_\alpha, \quad (2.69)$$

$$\hat{u}^{(F)j}_\gamma = F_\gamma^j - d^{js\epsilon}_\gamma (d^{ss-1})_\epsilon^\alpha s_i F_\alpha^i, \quad \lambda^{(F)j}_\gamma = 0, \quad (2.70)$$

$$\hat{u}_{j\gamma}^{(r)} = r_{j\gamma} - b_{j\gamma}^{s\epsilon} (b_s^{-1})_\epsilon^\alpha s^i r_{i\alpha}, \quad \lambda_{i\gamma}^{(r)} = 0, \quad (2.71)$$

$$\hat{u}_\gamma^\times = (b_s^{-1})_\gamma^\alpha s^i r_{i\alpha} - (d^{ss-1})_\gamma^\alpha s_i F_\alpha^i, \quad \lambda_\gamma^\times = 0. \quad (2.72)$$

## 2. The Hyperbolic Relaxation Method

From this the evolved variables can be recovered from the characteristics by:

$$\psi_\alpha = \frac{1}{2}(w^{-1})_\alpha^\gamma (\hat{u}_\gamma^+ + \hat{u}_\gamma^-), \quad (2.73)$$

$$F_\alpha^i = \hat{u}_\alpha^{(F)i} + d_\alpha^{is\epsilon} (\rho^{-1})_\epsilon^\gamma \frac{\hat{u}_\gamma^+ - \hat{u}_\gamma^-}{2} \quad (2.74)$$

$$r_{i\alpha} = \hat{u}_{i\alpha}^{(r)} + b_{i\alpha}^{s\epsilon} \left( \hat{u}_\epsilon^\times + (d^{ss-1})_\epsilon^\gamma s_j \hat{u}_\gamma^{(F)j} + (\rho^{-1})_\epsilon^\gamma \frac{\hat{u}_\gamma^+ - \hat{u}_\gamma^-}{2} \right). \quad (2.75)$$

The most natural choice for  $d_j^{i\beta}{}_\alpha$  is  $d_j^{i\beta}{}_\alpha = \delta_j^i \delta_\alpha^\beta$  for which the characteristic speeds become  $\pm 1$  and the eigenvectors of  $c$  become trivial:  $w_\gamma^\alpha = \delta_\gamma^\alpha$ .

### 2.2.4. Boundary Conditions

The boundary conditions of the HypRelaxDiv system can be discussed in exactly the same way as for the HypRelax system. In fact for the outer boundary conditions one obtains exactly the same expression for the modification of the characteristic variable right-hand sides, Eq. (2.51). The only difference is that  $w_\gamma^\alpha$  and  $\rho_\gamma^\beta$  are now computed for  $c_\alpha^\beta = d^{ss\beta}{}_\alpha$ , as it has already been defined in the hyperbolicity analysis above.

# 3. Numerical Implementation and Test Cases

## 3.1. Numerical Setup

### 3.1.1. Grid Setup

The HypRelax method is implemented in the pseudospectral hyperbolic evolution code `bamps` and the reader is referred to [16], for a detailed description of the grid setup. Here only a short summary of the basic grid setup and numerical method is given. The grid consists of different coordinate patches, a cube patch in the center, transition shell patches and outer shell patches. On each patch there is a mapping between local Cartesian coordinates to global Cartesian coordinates, where on shell patches we employ the “cubed sphere” construction [40]. The patches themselves can consist of smaller subpatches, which are the smallest units used for the parallelization scheme. For a visual impression of the grid see Fig. 4.1, which depicts the grid in the  $xy$ -plane.

On each subpatch the fields are approximated by a Chebyshev pseudospectral method, i.e. the subpatches are discretized in every direction by the Gauss-Lobatto collocation points. It is then possible to reconstruct the Chebyshev coefficients from the fields values at the collocation points. The `bamps` code is

### 3. Numerical Implementation and Test Cases

adapted to evolutions in three dimensions. For axisymmetric and spherically symmetric problems the cartoon method is used to reduce the computational domain to two or one dimensions respectively [16].

#### 3.1.2. Integration Method

The time integration for relaxation methods does not require a high order of error convergence, since we are only interested in the steady state at the end of the evolution. More important are the efficiency and stability of the integration algorithm. For the time integration the method of lines is used. It is known that for linear hyperbolic equations the simple forward Euler-method and also explicit second-order Runge-Kutta methods are, at least without artificial dissipation, unstable (see for example chapter 6.7 of [28]) and thus are not suited for the integration of the hyperbolic relaxation equations.

In the applications presented in this work the popular fourth-order Runge-Kutta scheme (RK4) is employed, which is stable for hyperbolic equations. This method needs four evaluations of the right-hand side per time step, which appears to be not very efficient. After all, it is not really necessary to use very accurate integrator, since we are only interested in approaching the stationary state. Therefore it is worthwhile to investigate other classes of integrators, e.g. multistep methods like the third- or fourth-order Adams schemes [41], which effectively only require one or two evaluations per time step and are usually also stable for hyperbolic PDEs. Some simple experiments with the Poisson equation indicated, however, that RK4 is more efficient than RK3 or a fourth order Adams scheme since RK4 allows comparatively large time steps.

Contrary to what is described in [16], it is not necessary to use a filter to assure stability stability in the hyperbolic relaxation method, since the system usually

tends towards a stable static or stationary solution automatically. Consequently the filter in `bamps` is switched of to exploit the full spectral resolution.

In the `bamps` code there are two types of boundaries. On the one hand boundaries between different subpatches, and on the other hand the boundaries of the computational domain, in particular the outer boundaries. To treat boundaries between subpatches the penalty method described in Sec. 2.1.6 is employed setting the boundary data to be the outgoing characteristic of the neighboring subpatch.

To treat the outer boundary with this method one has to provide a function  $g_\gamma$  equaling  $u_\gamma^{+BC}$  at the boundary, i.e.

$$\hat{u}_\gamma^{+BC} = w_\gamma^\alpha \psi_\alpha + (\rho^{-1})_\gamma^\delta w_\delta^\epsilon a^{si\alpha} r_{i\alpha} = g_\gamma. \quad (3.1)$$

Here the given data could be generalized to include combinations of the outgoing characteristic variables at outer boundary. This strategy could be used to implement a desired boundary condition from the original elliptic PDE, but has the undesirable side-effect of reflection from the boundary, which may serve as an obstruction to decay of the residual. On the other hand, a boundary condition of the direct form (3.1) would be unusual in practice for elliptic equations, as the characteristic fields of the relaxation scheme have no special meaning in the original system. Therefore the penalty method is not best suited for the treatment of the outer boundaries. Instead, as described in Sec. 2.1.6, the desired boundary conditions for the elliptic system are embedded inside boundary conditions for the relaxation scheme that are more likely to absorb outgoing waves.

### 3.1.3. Initial Guesses

To start the hyperbolic relaxation one has to provide an initial guess to the solution. A suitable initial guess will always depend on the specific form of the problem, in particular it should be chosen such that in the course of the relaxation the

### 3. Numerical Implementation and Test Cases

variables do not have to cross any points where the equations (e.g. terms in the non-principal part) become singular. Tests have shown that the solver is particularly well behaved when starting with a guess that is stationary in the interior, but not at the boundary. The whole solution then starts to relax from the boundary to the inside. For applications to numerical relativity initial data this means taking the flat metric everywhere. This leads indeed to stable relaxations, which demonstrates a remarkably high robustness that can be achieved by the method. For the reduction variables the initial guess is simply the derivative of the initial guess for the solution variables, i.e.  ${}^{(ini)}r_{i\alpha} = \partial_i {}^{(ini)}\psi_\alpha$ .

#### 3.1.4. Refinement Strategy

To speed up the relaxation process a simple scheme of successive refinement is used. It can be assumed that the right-hand side of the solution variables  $\partial_t \psi_\alpha$ , Eq. (2.13), is a good approximation to the residual of the elliptic equation  $(L\psi)_\alpha$ , Eq. (2.7). This however is only true until a discretization limit is reached below which the norm of the residual is no longer decreasing. The norm of the  $\partial_t \psi_\alpha$  will typically continue decreasing until machine precision is reached. Numerical experiments have shown that this continued decrease will only be present if no spectral filter is applied. This observation makes it possible to construct an indicator signaling when the discretization limit is reached and thus relaxation should be continued on a higher resolution grid. In particular the following following criterion has been found to work well in practice,

$$\int \sum_{\alpha=1}^N |\partial_t \psi_\alpha| dV < c \int \sum_{\alpha=1}^N |(L\psi)_\alpha| dV, \quad (3.2)$$

where  $c$  is some constant smaller than one. A choice of  $c = 0.1$  will usually work reasonably well. Depending on the specific problem, in particular if the solution is smooth, also smaller values might be beneficial. The resolution is increased when Eq. (3.2) is true and additionally whenever the error of the elliptic equation reaches



machine precision, i.e. when the norm of  $(L\psi)_\alpha$  is smaller than  $10^{-13}$  times the number of grid points.

The solver starts the relaxation on the coarsest grid and checks every  $n_{\text{check}}$  relaxation steps whether to proceed relaxation on a finer grid based on whether one of the two criteria mentioned above is fulfilled. The final resolution can be determined by an error bound on the residual of the elliptic equation, or by some predetermined resolution, which may be required for the evolution of the data. For the refinement the resolution on every subpatch is increased by two collocation points in every direction, which is equivalent to adding two Chebyshev modes in every direction. The coarse steady state solution is then interpolated to the new subpatches and the procedure is repeated until the desired resolution is reached. For the reduction variables it is advisable to use the interpolated values as well instead of taking the numerical derivative of the solution variables, since the latter introduces new errors, which costs some extra effort to damp.

## 3.2. Application to Test Cases

### 3.2.1. Poisson Equation – Finite Differencing

To provide a reference point independent of the specific pseudospectral methods of `bamps`, first a minimal implementation using a finite difference method is discussed solving the Poisson equation. The following hyperbolic relaxation equation is considered

$$\partial_t^2 \phi + \eta \partial_t \phi = \Delta \phi - \rho, \quad (3.3)$$

which is implemented as a first order in time, second order in space system,

$$\partial_t \phi = \pi - \eta \phi, \quad (3.4)$$

$$\partial_t \pi = \Delta \phi - \rho. \quad (3.5)$$

### 3. Numerical Implementation and Test Cases

The fully first order version of this system is analyzed in Sec. 3.2.2. At the boundaries asymptotic Dirichlet conditions analogous to (2.52),  $\partial_t \phi = g - \phi$  and  $\partial_t \pi = g - \pi$  are used. The parameter  $\epsilon$  that has been introduced in the discussion of Sec.2.1.4 is set to 1, since its dominant effect would be just a rescaling of the iteration step size.

A centered, second order accurate finite differences in space is chosen, and the default time integrator is the classic fourth-order Runge-Kutta method. The numerical domain is an equidistant grid of points in  $[-\frac{L}{2}, \frac{L}{2}]^d$ , dimension  $d = 1, 2$ , or 3, with Cartesian coordinates. There are  $N$  points in each of up to three directions with a total of  $V = N^d$  points.

Let us discuss some results for vanishing source term,  $\rho = 0$ , and vanishing Dirichlet boundary,  $g = 0$ , where the method has to reduce from an initial guess of  $\phi = 1/(1 + x_j x^j)$  and  $\pi = 0$  at  $t = 0$  to the asymptotic, late-time value  $\phi = \pi = 0$ .

Fig. 3.1 shows results for a box of size  $L = 20$ , damping parameter  $\eta = 1$ , varying the number of points and the number of dimensions. The norm is weighted by the grid spacing  $\Delta x$  to represent the integral of the residual,  $|f|_2 = (\sum f^2 \Delta x^d)^{1/2}$ . The faster convergence for higher dimensions is due to the fact, that the relative volume near the boundary increases with dimensionality. The convergence is always exponential in time, with two distinct phases. Inspection of the evolution of  $\phi$  and  $\pi$  shows that the initial phase corresponds to the damping of short wavelengths (in this example until  $t \approx 20$ ), after which long wavelengths dominate and the convergence is slower. The convergence of the (weighted) norm of the residual with time is quite independent of the resolution. In this example the time-step is  $\Delta t = \lambda \Delta x$ , so the number of time steps is proportional to the number  $N$  of grid points in one direction. For efficiency values  $\lambda = 1.4, 1.0, 0.8$  are chosen for 1D, 2D, and 3D, respectively, and obtain stable time-stepping with RK4. The work per right-hand-side evaluation is  $\mathcal{O}(N^d)$ , so the total work to reach a final time  $T$  is  $\mathcal{O}(N^{d+1})$ .

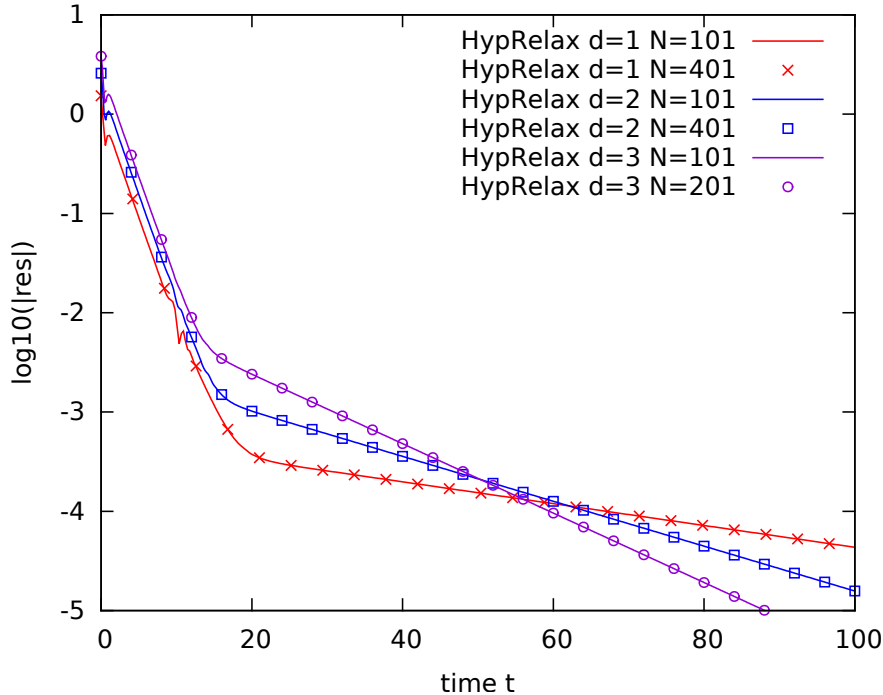


Figure 3.1.: Poisson equation, FD method. Convergence of the residual with time for one, two, and three dimensions. Shown is a solid line for  $N = 101$  and markers for a higher resolution given by  $N = 201$  or  $401$  points. On the scale of the plot, the convergence rate is independent of resolution for any given number of dimensions.

A key question is how efficient hyperbolic relaxation is compared to other methods. Fig. 3.2 shows a comparison of different methods for a two-dimensional example with  $N = 101$  points. The methods considered are hyperbolic relaxation as above, the standard Jacobi iteration [42], and the BiCGSTAB method as an example for a Krylov subspace method [43]. Also included are two additional variants of hyperbolic relaxation. In these examples  $\Delta t = 1.0\Delta x$  for RK4 in 2D.

Referring to Fig. 3.2, the Jacobi method shows the slowest convergence. Reducing the residuum of the 2D Poisson equation by a factor  $10^{-p}$  requires  $n \approx \frac{1}{2}pN^2$  iterations on a  $N \times N$  grid [42]. For a 2D grid with  $V = N^2$  degrees of freedom, the operation count is therefore  $\mathcal{O}(V^2) = \mathcal{O}(N^4)$ , compared to  $\mathcal{O}(N^3)$  for optimal SOR

### 3. Numerical Implementation and Test Cases

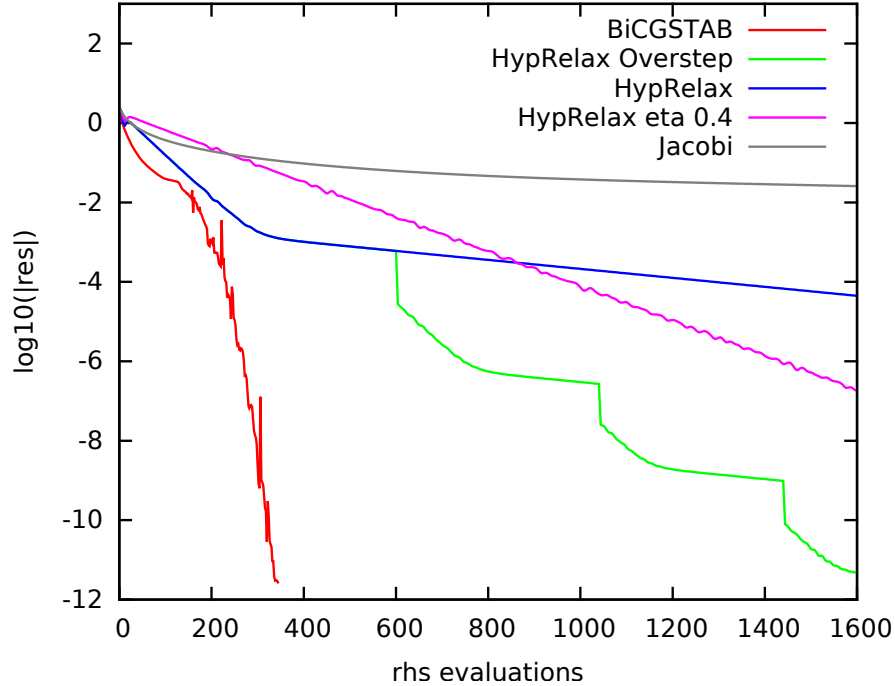


Figure 3.2.: Poisson equation, FD method. Convergence of the residual with the number of right-hand-side evaluations. Shown is a comparison between different methods for  $N = 101$  in two dimensions.

and  $\mathcal{O}(V \log V)$  for multigrid methods. Hyperbolic relaxation with  $\mathcal{O}(V) \times \mathcal{O}(N) = \mathcal{O}(N^3)$ , as demonstrated in Fig. 3.1, is therefore a reasonable candidate for further consideration. In the concrete example, the Jacobi method is significantly slower than hyperbolic relaxation, but the Jacobi method is usually not considered as a stand-alone method.

For this simple comparison, the BiCGSTAB method is used without a preconditioner, but the Laplace operator leads to a sufficiently well conditioned operator such that convergence is fast nevertheless, compared to the other methods considered here. There is an initial phase of relatively slow convergence, but once the trial solution is sufficiently close to the final answer, convergence becomes much faster.

Remarkably, hyperbolic relaxation does about as well as BiCGSTAB during the

first phase. However, convergence slows down after the shorter wavelengths have been damped and errors due to larger wavelength remain. Three ideas have been considered to improve the convergence of hyperbolic relaxation for long wavelengths. Not shown here is the multi-level refinement strategy which is employed in the `bamps` code, see Sec. 3.1.4.

As an immediate application of the mode analysis of Sec. 2.1.4, the damping parameter  $\eta$  is introduced, which for the basic experiments so far was set to  $\eta = 1$ . Also shown in Fig. 3.2 is the result for  $\eta = 0.4$ , which exhibits a constant decay rate that is slower than  $\eta = 1$  initially, but faster for later iterations. This effect depends on  $\eta$  and the size  $L = 20$  of the box. With  $\epsilon = 1$ , for  $\eta = 1$  we have  $\lambda_{crit} = 4\pi < L$ , and for  $\eta = 0.4$  we have  $\lambda_{crit} = 10\pi > L$ . This indicates that for  $\eta = 0.4$  all wavelengths fitting into the box fall into the range  $\lambda < \lambda_{crit}$ , and the expected constant damping rate is  $e^{-\frac{\eta}{2}t}$  for all wavelengths. On the other hand, for  $\eta = 1$  wavelengths both smaller and larger than  $\lambda_{crit}$  are present initially, but damping for  $\lambda < \lambda_{crit}$  is faster than for  $\lambda > \lambda_{crit}$ , so after an initial transient the damping rate slows down when  $\lambda > \lambda_{crit}$  is the dominant contribution. There is a trade-off between reducing  $\eta$  in order to suppress  $\lambda < \lambda_{crit}$  for a given domain size, and increasing  $\eta$  for a stronger damping factor  $e^{-\frac{\eta}{2}t}$ . In the example of Fig. 3.2 HypRelax with  $\eta = 0.4$  overtakes HypRelax with  $\eta = 1$  at about 900 RHS evaluations. It seems possible to construct a dynamically adjusted damping  $\eta(t)$ .

Similar results hold for the parameter  $\epsilon$  in (2.23) as discussed in Sec. 2.1.4. At large  $k$  the velocity of the modes scales with  $1/\sqrt{\epsilon}$  but is independent of  $\eta$ , so for optimal performance the Courant factor has to be adjusted together with  $\epsilon$  but can be kept constant when  $\eta$  is varied.

As a next idea experiments with a “one-step overrelaxation” method (as opposed to successive overrelaxation) have been carried out. This is based on the observation that after the initial propagation/damping phase of hyperbolic relaxation, the second time derivative of  $\phi$  becomes significantly smaller than the first time derivative,

### 3. Numerical Implementation and Test Cases

$\partial_t^2 \phi \ll \partial_t \phi$ . Hence it seems promising to attempt a *linear* extrapolation in time. The curve labeled “overstep” in Fig. 3.2 is obtained by searching every few iterations for the time step  $\Delta T = \lambda \Delta t$  that minimizes the global residual of  $\phi_{new} = \phi + \Delta T F(\phi)$ , where  $F$  is the update suggested by the time stepping algorithm (e.g. RK4). This is similar to various other 1D step-size optimizations. For the example considered here (but also for  $\rho \neq 0$  as below), the late time solution of hyperbolic relaxation is sufficiently regular that indeed an appropriate global  $\Delta T$  can be found. The overstep algorithm only accepts the large step  $\Delta T$  if it decreases the residual by at least a factor  $f$ , say  $f = 10$  (we tried  $f = 2$  to  $f = 1000$ ). The optimal choice of  $f$  depends on different features of the problem, in particular choosing  $f$  too small can make the method less efficient. Each overstep introduces new local error modes (since  $\Delta T$  is a global parameter). As can be seen in Fig. 3.2, the approximate solution is disturbed, but converges again with the typical speed for shorter wavelengths to a new regular state. In the optimal case the overall convergence rate seems to approach that of the fast phase of hyperbolic relaxation. It may be possible to derive a continuous variant of this method analogous to successive overrelaxation, which we leave to future research. With the *scheduled Jacobi method* [44, 45] there has been a similar idea for a parabolic solver, accelerating the Jacobi method considerably by a clever schedule of over- and underrelaxation steps.

The main points regarding the convergence rate of hyperbolic relaxation as shown in Fig. 3.2 are that the method works out-of-the-box and that its performance falls somewhere between Jacobi and BiCGSTAB. There seems to be quite some potential for accelerating the convergence rate of hyperbolic relaxation. From the point of view of solving elliptic equations with a code designed for hyperbolic equations, note that hyperbolic relaxation is “only” slower by a factor of about 5 (to reach a residual of  $10^{-9}$  in this example) than a standard method like BiCGSTAB, which however may not be readily available.

### 3.2.2. Poisson Equation – Pseudospectral Method

To test the hyperbolic relaxation elliptic solver as implemented in `bamps` the Poisson's equation,

$$\Delta\psi - \rho = 0 \quad (3.6)$$

is considered in spherical symmetry, i.e.  $\rho = \rho(r)$ ,  $r = \sqrt{x^i x_i}$ . To solve this equation the following hyperbolic relaxation system is chosen

$$\partial_t \psi = \delta^{ij} \partial_i r_j - \rho, \quad (3.7)$$

$$\partial_t r_i = \partial_i \psi - r_i. \quad (3.8)$$

For a first test  $\rho$  is chosen to be smooth, i.e. it is infinitely often continuously differentiable,

$$\rho = \rho_0 \left( \frac{-6}{R^2} + \frac{4r^2}{R^4} \right) e^{-r^2/R^2}, \quad (3.9)$$

where  $R$  and  $\rho_0$  are non-zero parameters. For this  $\rho$  Poisson's equation has the solution

$$\psi_{analytic} = \rho_0 e^{-r^2/R^2}. \quad (3.10)$$

At the boundary a falloff in  $\psi$  compatible with this solution is obtained by imposing the Robin boundary condition  $\partial_r \psi = s^i \partial_i \psi = -2r\psi/R^2$ .

For the second test a non-smooth  $\rho$  is chosen that corresponds to a homogeneously charged sphere, which is like a toy model for stars. The density  $\rho$  is then given by

$$\rho = \begin{cases} \rho_0 & \text{if } r \leq R \\ 0 & \text{if } r > R, \end{cases} \quad (3.11)$$

for which the Poisson equation has the solution

$$\psi_{analytic} = \rho_0 \begin{cases} \frac{r^2}{6} - \frac{R^2}{2} & \text{if } r \leq R \\ -\frac{R^3}{3r} & \text{if } r > R. \end{cases} \quad (3.12)$$

Again Robin boundary conditions are imposed according to the falloff of this solution, i.e.  $\partial_r \psi = s^i \partial_i \psi = -\psi/r$ .

### 3. Numerical Implementation and Test Cases

The outer boundary is placed at a radius of 10 and the grid is divided into a total of eight subpatches, where the inner five extend over the interval  $[0, 5]$  and the outer three, having a coarser resolution, extend over  $[5, 10]$ . The parameters determining  $\rho$  are chosen to be  $R = 5$  and  $\rho_0 = 1$ . For the non-smooth case special care has to be taken to ensure convergence. In particular the grid is chosen such that the discontinuity lies at a boundary of subpatch, ensuring second order convergence. In both test cases the relaxed solution converges with the number of grid points to the analytical solution. To investigate the convergence it must be made sure that the solution is completely relaxed on every resolution. This is achieved by choosing in Eq. (3.2)  $c = 0.0001$ . In Fig. 3.3 the absolute difference between the analytical and numerical solution integrated over the outermost subpatch is reported. It is noted however that the convergence behavior is the same on all other subpatches. As expected the error of the numerical solution is found to decrease exponentially with the number of points for the smooth  $\rho$  from Eq. (3.9). For the non-smooth  $\rho$  of Eq. (3.11) it is well known that convergence can only be polynomial and indeed the convergence is approximately of order two, which is the expected convergence order for discontinuous  $\rho$  [41]. Of course this is not very efficient for a spectral method. In non-smooth regions it is therefore often preferable to increase the number of subpatches (h-refinement) instead of the number of collocation points per subpatch. In numerical applications one often uses spectral methods even for non-smooth problems, i.e. in (general relativistic) hydrodynamics, and thus it is still interesting to investigate the behaviour of the method on grids suited for these simulations.

In Fig. 3.4 the progression of the L1-norm is investigated for different quantities that can be used to approximate the error. The first observation is that the difference to the analytical solution decreases even when the computed residual, given by left-hand side of Eq. (3.6), is already leveling off. This is especially remarkable for the non-smooth case, where the residual itself is not converging at all. For the smooth case one secondly observes that after refining the grid the norm of right-hand side of Eq. (3.7) practically continues at the same level as before. The norm of the residual



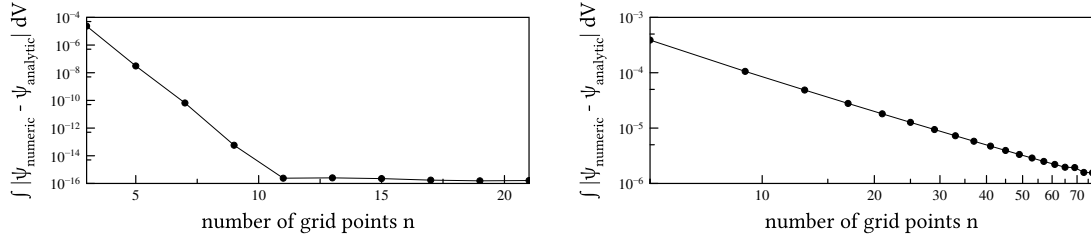


Figure 3.3.: Convergence of the L1-norm of the difference between the analytical and the numerical solution. Left plot: smooth  $\rho$  (Eq. (3.9)). Right plot: non-smooth  $\rho$  (Eq. (3.11)). Note that in the left plot only the error axis is logarithmic, while in the lower plot both axes are logarithmic.

on the other hand drops quickly after refining, reaching the right-hand sides level until again the discretization limit is reached. These observations suggest that for problems with smooth solutions it is preferable to relax for longer on the coarse grid. For problems with non-smooth solutions, however, new error develops during each refinement and thus refining for longer on the coarse grid is not paying off. Furthermore, it is preferable to increase the grid resolution faster.

As a last simple test, the behavior is tested in the case of non-unique solutions. For this the smooth  $\rho$  from Eq. (3.9) has been considered together with the Neumann boundary condition  $\partial_r \psi = 0$ , for which multiple solutions differing only by an additive constant exist. the result is that after some relaxation the right hand side of Eq. (3.7) becomes approximately constant in space. From this point on the solution is no longer improving, since only constant terms, which do not improve the residual of Eq. (3.6), are added.

### 3. Numerical Implementation and Test Cases

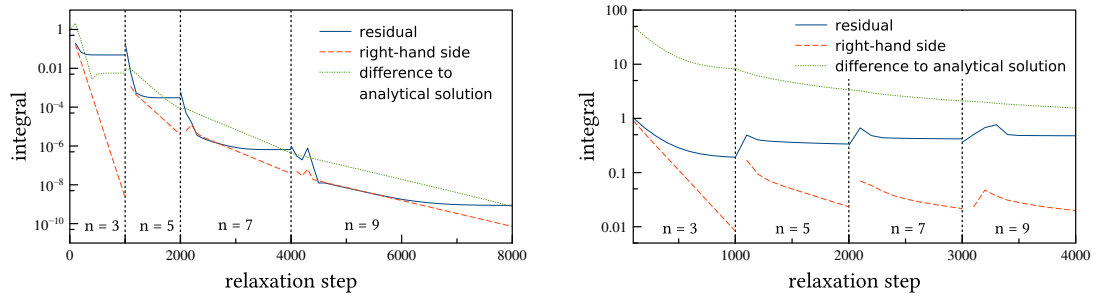


Figure 3.4.: Progression of the L1-norm of different error quantities during the relaxation process for the Poisson equation. Vertical dashed lines indicate transitions to a finer grid. The respective error quantities are: blue solid line: residual, defined as left-hand side of Eq. (3.6), orange dashed line: right-hand side of Eq. (3.7), green dotted line: difference to the analytical solution. Left plot: for smooth  $\rho$  (Eq. (3.9)). Right plot: for non-smooth  $\rho$  (Eq. (3.11)).

# 4. Initial Data for General Relativistic Neutron Star Binary Simulations

## 4.1. Numerical Solution of the Constraint Equations of General Relativity

### 4.1.1. Conventions and Fundamental Concepts of Numerical Relativity

Throughout this chapter the following conventions will be used. All equations are given in geometric units, i.e. the gravitational constant  $G = 1$  and the speed of light  $c = 1$ . Furthermore indices with lower-case Greek letters denote spacetime indices  $0, 1, 2, 3$  and indices with lower-case Latin letters denote spatial indices  $1, 2, 3$ .

The subject of numerical relativity is that of finding a numerical solution to the Einstein field equations [6]

$$R_{\mu\nu} - \frac{1}{2}g_{\mu\nu}R = 8\pi T_{\mu\nu}, \quad (4.1)$$

#### 4. Initial Data for General Relativistic Neutron Star Binary Simulations

which form a system of coupled second order partial differential equations for the spacetime metric  $g_{\mu\nu}$ . The Ricci tensor  $R_{\mu\nu}$  and the Ricci scalar  $R$  are given as contractions of the Riemann tensor  $R_{\mu\lambda\sigma}$ :

$$R^\mu{}_{\nu\lambda\sigma} = \partial_\lambda \Gamma^\mu{}_{\nu\sigma} - \partial_\sigma \Gamma^\mu{}_{\nu\lambda} + \Gamma^\mu{}_{\rho\lambda} \Gamma^\rho{}_{\nu\sigma} - \Gamma^\mu{}_{\rho\sigma} \Gamma^\rho{}_{\nu\lambda}, \quad (4.2)$$

$$R_{\mu\nu} = R^\sigma{}_{\mu\sigma\nu} \quad R = R^\mu{}_\mu, \quad (4.3)$$

where  $\Gamma^\mu{}_{\nu\sigma}$  is the Christoffel symbol

$$\Gamma^\mu{}_{\nu\sigma} = \frac{1}{2} g^{\mu\alpha} (\partial_\sigma g_{\alpha\nu} + \partial_\nu g_{\alpha\sigma} - \partial_\alpha g_{\nu\sigma}). \quad (4.4)$$

To solve the Einstein field equations numerically they are usually reformulated in first order in time form, so that they can be integrated numerically using the method of lines. Such a reformulation can be found by foliating the spacetime into spatial hypersurfaces and expressing the metric in the 3+1 decomposed form

$$ds^2 = -\alpha^2 dt^2 + \gamma_{ij} (dx^i + \beta^i dt)(dx^j + \beta^j dt), \quad (4.5)$$

where the quantities  $\alpha$  and  $\beta^i$  are called lapse and shift and  $\gamma_{ij}$  is the induced metric on the spatial hypersurface. There is a unit timelike normal vector  $n^\mu$  orthogonal to the spatial hypersurface, which can be expressed in terms of the lapse and shift by

$$n^\mu = \begin{pmatrix} 1/\alpha \\ -\beta^i/\alpha \end{pmatrix} \quad n_\mu = \begin{pmatrix} -\alpha \\ 0 \end{pmatrix}. \quad (4.6)$$

The projection of a tensor onto a spatial hypersurface is accomplished by contracting every index with the projection operator

$$\gamma^\mu{}_\nu := \delta^\mu{}_\nu + n^\mu n_\nu. \quad (4.7)$$

This allows in particular the introduction of the spatial derivative operator  $D$  defined by

$$D_\alpha A^{\mu_1 \dots \mu_n}{}_{\nu_1 \dots \nu_n} := \gamma^{\tilde{\alpha}}{}_\alpha \gamma^{\mu_1}{}_{\tilde{\mu}_1} \dots \gamma^{\mu_n}{}_{\tilde{\mu}_n} \gamma^{\tilde{\nu}_1}{}_{\nu_1} \dots \gamma^{\tilde{\nu}_n}{}_{\nu_n} \nabla_{\tilde{\alpha}} A^{\tilde{\mu}_1 \dots \tilde{\mu}_n}{}_{\tilde{\nu}_1 \dots \tilde{\nu}_n}, \quad (4.8)$$

which is compatible with the spatial metric  $\gamma_{\mu\nu}$ . The extrinsic curvature is defined as the quantity

$$K_{\mu\nu} := -\gamma_{\mu}^{\alpha}\gamma_{\nu}^{\beta}\nabla_{(\alpha}n_{\beta)}. \quad (4.9)$$

The historically most notable first-order in time formulation is given by the so called ADM equations [46]. Nowadays other formulations better suited for numerical simulations have been developed allowing long-term stable evolutions. The most wide spread evolution formalisms as of today are the BSSN formulation [47, 48], Z4-like formulations [49–51] and the Generalized Harmonic Gauge (GHG) formulation [52]. The Einstein field equations also give rise to constraint equations to be satisfied on every spatial hypersurface, for which several formulations exist as well. Most of the standard formulations recast the constraints into elliptic equations, e.g. by the conformal transverse traceless (CTT) or the conformal thin-sandwich (CTS) decomposition [53]. For the CTS equations it is possible to show uniqueness under certain conditions [54–56] which is by itself a favorable property when the equations are applied in a numerical scheme. In practice however the system is often extended to the extended conformal thin-sandwich (XCTS) equations [46, 57] to fix the value and time derivative of the trace of the extrinsic curvature. For the XCTS system uniqueness of the solutions is no longer guaranteed [55, 56, 58], but it is easier to construct solution well suited as initial data for numerical evolutions. Besides the constraints on the metric there are also constraints on the matter variables, which follow for example from the necessity that the energy momentum tensor must always be divergence free. The constraints on the matter variables will be discussed in Sec. 4.2.1 for the case of a relativistic perfect fluid.

### 4.1.2. The Extended Conformal Thin-Sandwich Equations

The XCTS equations are the formulation of choice for the initial data generated in this work. For the results of this work a slight modification of the equations is solved

#### 4. Initial Data for General Relativistic Neutron Star Binary Simulations

using the HypRelax method. For the construction of the XCTS equations the spatial metric is decomposed into a conformal factor  $\psi$  and a spatial conformal metric  $\bar{\gamma}_{ij}$  as  $\gamma_{ij} = \psi^4 \bar{\gamma}_{ij}$ . For conformal quantities (denoted by a bar) the conformal spatial metric  $\bar{\gamma}^{ij}$  lowers and raises indices and for quantities without bar the physical spatial metric  $\gamma^{ij}$  is used. In the XCTS framework the constraint equations take the form

$$\bar{D}^j \bar{D}_j \psi = \frac{\psi}{8} \bar{R} - \psi^5 \left( 2\pi\rho - \frac{K^2}{12} + \frac{1}{8} A_{ij} A^{ij} \right), \quad (4.10)$$

$$\begin{aligned} \bar{D}^j \bar{D}_j \beta^i &= -\frac{1}{3} \bar{D}^i \bar{D}_j \beta^j - \bar{R}^i_j \beta^j + 16\pi\alpha\psi^4 J^i \\ &+ (\bar{D}^i \beta^j + \bar{D}^j \beta^i - \frac{2}{3} \bar{\gamma}^{ij} \bar{D}_k \beta^k) \\ &\cdot \bar{D}_j \ln(\alpha\psi^{-6}) \end{aligned} \quad (4.11)$$

$$\begin{aligned} &- \alpha\psi^{-6} \bar{D}_j (\alpha^{-1} \psi^6 \partial_t \bar{\gamma}^{ij}) + \frac{4}{3} \alpha \bar{D}^i K, \\ \bar{D}^j \bar{D}_j (\alpha\psi) &= \alpha\psi^5 \left( \frac{7}{8} A_{ij} A^{ij} + \frac{5}{12} K^2 + 2\pi(\rho + 2J) \right) \\ &- \psi^5 (\partial_t - \beta^j \bar{D}_j) K + \frac{1}{8} \alpha\psi \bar{R}. \end{aligned} \quad (4.12)$$

Here  $\bar{D}_i$  is the covariant derivative compatible with the conformal metric  $\bar{\gamma}_{ij}$ ,  $\bar{R}_{ij}$  is the Ricci tensor of  $\bar{\gamma}_{ij}$  and  $\bar{R}$  is the corresponding Ricci scalar. The tensor  $A_{ij}$  is the tracefree part of the extrinsic curvature  $K_{ij}$  and  $K$  is the trace of  $K_{ij}$ .  $A_{ij}$  can be expressed as  $A_{ij} = -\psi^4 / (2\alpha) (\partial_t \bar{\gamma}_{ij} - (\bar{L}\beta)_{ij})$  with  $(\bar{L}\beta)_{ij} = \bar{D}_i \beta_j + \bar{D}_j \beta_i - \frac{2}{3} \bar{\gamma}_{ij} \bar{D}_k \beta^k$ . The matter source terms are defined as the following contractions of the energy-momentum tensor  $T_{\alpha\beta}$ :  $\rho = T_{\alpha\beta} n^\alpha n^\beta$ ,  $J^i = -T_{\alpha\beta} \gamma^{i\alpha} n^\beta$  and  $J = \gamma^{\alpha\beta} T_{\alpha\beta}$ . In the XCTS equations  $\bar{\gamma}_{ij}$ ,  $\partial_t \bar{\gamma}_{ij}$ ,  $K$  and  $\partial_t K$  are given functions, depending on the type of initial data one wants to construct.

In Eq. (4.12) the product  $\alpha\psi$  is taken as one variable. For the computations in this work this equation is rewritten with the help of Eq. (4.10) as

$$\begin{aligned} \bar{D}^j \bar{D}_j \alpha &= -\frac{2}{\psi} (\bar{D}^j \alpha) (\bar{D}_j \psi) - \psi^4 (\partial_t - \beta^j \bar{D}_j) K \\ &+ \alpha\psi^4 \left( A_{ij} A^{ij} + \frac{K^2}{3} + 4\pi(\rho + J) \right), \end{aligned} \quad (4.13)$$

## 4.2. Numerical Solution of the Hydrodynamical Constraint Equations

solving directly for  $\alpha$ . The embedding of the XCTS equations within the hyperbolic relaxation method is discussed in detail in [1].

At the domain boundary it is imposed that the solution falls off like the Schwarzschild solution, i.e.  $\psi = \frac{a}{r} + 1$  and  $\alpha = \frac{b}{r} + 1$ . This ansatz gives rise to the following Robin boundary conditions

$$\partial_s \psi|_{\partial\Omega} = \frac{1 - \psi}{r}, \quad \partial_s \alpha|_{\partial\Omega} = \frac{1 - \alpha}{r}. \quad (4.14)$$

For the shift likewise a radial falloff is imposed by the Robin condition

$$\partial_s \beta^i|_{\partial\Omega} = -\frac{\beta^i}{r}. \quad (4.15)$$

As an initial guess always the flat space solution is used, i.e.  $\psi = 1$ ,  $\alpha = 1$ ,  $\beta^i = 0$ . Of course an initial guess, that is a good approximation to the solution is always the preferred start for the relaxation, since it will take less time to relax to the solution or might not be necessary to relax at all. However the simple initial guess has been found to work well and demonstrates in a nice way the high robustness of the hyperbolic relaxation method exhibited in the numerical experiments.

## 4.2. Numerical Solution of the Hydrodynamical Constraint Equations

### 4.2.1. Review and Critique of the Current Construction Methods for Binary Neutron Star Initial Data

In numerical simulations neutron stars are usually modeled by perfect fluids, i.e. the energy momentum tensor is given by

$$T_{\alpha\beta} = (\epsilon + p)u_\alpha u_\beta + pg_{\alpha\beta}, \quad (4.16)$$

#### 4. Initial Data for General Relativistic Neutron Star Binary Simulations

where  $\epsilon$  is the proper energy density,  $p$  the fluid pressure and  $u^\alpha$  the fluid four-velocity. For the discussion of the fluid properties one often considers two special observers. The Lagrangian observer is moving with the four-velocity of the fluid  $u^\mu$ , whereas the Eulerian observer is moving with the coordinates and hence has the four-velocity  $n^\mu$ .

This chapter will introduce some improvements and advances to the methods used for the construction of equilibrium initial data for binary neutron star simulations. All modern codes for binary neutron star initial data [15, 59, 60] use in principle only variations of the formalism developed by Tichy [61, 62], building on prior work for irrotational [63–66] and spinning binaries [67, 68] and later being extended to incorporate also elliptical orbits [15, 69]. For the review in this chapter I will therefore follow mostly along the lines of [61] and [15] and use the notation therein.

Besides the metric variables which can be determined solving the XCTS equations outlined in the previous section, there are also constraint equations for the matter variables that must be solved for the interior of the stars. The first set of equations follows from energy-momentum conservation,  $\nabla_\mu T^{\mu\nu} = 0$ . The part relevant for the construction of initial data is obtained by projecting onto the hypersurface orthogonal to the world line of the Lagrangian observer. Using the projector

$$P_\mu^\alpha := \delta_\mu^\alpha + u^\alpha u_\mu \quad (4.17)$$

one obtains, inserting the energy-momentum tensor for a perfect fluid (4.16), the relativistic Euler equations

$$0 = P_\mu^\alpha \nabla_\mu T^{\mu\nu} = (\epsilon + p)(u^\mu \nabla_\mu u^\alpha) + P_\mu^\alpha \nabla^\mu p. \quad (4.18)$$

The constraint following from the projection  $u_\nu \nabla_\mu T^{\mu\nu} = 0$  becomes only relevant in an actual evolution of the data. Additionally the baryonic mass must be conserved, which is ensured by the continuity equation

$$0 = \nabla_\mu (\rho u^\mu), \quad (4.19)$$



## 4.2. Numerical Solution of the Hydrodynamical Constraint Equations

where  $\rho$  is the baryonic mass density.

To close the system of equations it is necessary to include a thermal and a caloric equation of state. For neutron stars the caloric equation is usually fixed by assuming that the fluid is approximately barotropic, since the temperature is much lower than the Fermi temperature,  $E_F = \frac{\hbar^2}{2m} \left( \frac{3\pi^2 N}{V} \right)^{2/3} \gg k_B T$ , and thus the chemical potential  $\mu = E_0 + E_F + \mathcal{O}((k_B T/E_F)^2)$  depends on the baryonic density  $N/V$  only. In this case it is sufficient to specify the thermal equation of state, e.g. by specifying  $p(\rho)$ . The thermodynamic quantities can then be expressed in terms of the specific enthalpy

$$h := \frac{\epsilon + p}{\rho}. \quad (4.20)$$

Introducing the enthalpy current  $\tilde{u}_\nu := h u_\nu$ , the Euler equations in this case are conveniently written as

$$0 = \tilde{u}^\mu \nabla_{[\mu} \tilde{u}_{\nu]}. \quad (4.21)$$

For the construction of initial data for an equilibrium configuration time derivatives of the metric and the matter variables have to be chosen in an appropriate way. Usually one assumes the existence of an approximate Killing vector  $\xi$ . Approximate in this context means that the defining equation for a Killing field  $\xi$ :

$$\mathcal{L}_\xi g_{\mu\nu} = 0, \quad (4.22)$$

is satisfied momentarily on the initial data hypersurface. For the Killing vector the common choice (see e.g. [15]) is given by

$$\xi_{1,2}^\mu = (\partial_t)^\mu + \Omega \left( (x - x_{F1,2}) (\partial_y)^\mu - y (\partial_x)^\mu \right), \quad (4.23)$$

where  $\Omega$  is the rotational frequency parameter and  $x_{F1,2} = x_{\text{cm}} + e(x_{C1,2} - x_{\text{cm}})$  are the  $x$ -coordinates of the centers of the circular orbits momentarily inscribed by the motion of each star. The  $x_{C1,2}$  are the positions of the stars centers and  $e$  and  $x_{\text{cm}}$  are parameters describing the ellipticity and the position of the center of mass respectively. Here the choice has been made that the neutron stars initially move in

#### 4. Initial Data for General Relativistic Neutron Star Binary Simulations

the xy-plane and the stars centers are initially located on the x-axis. For a helical Killing vector,  $e = 0$ , both stars inscribe motions on a circle and thus their orbit is approximately circular. For  $e \neq 0$  each star has a different Killing vector and the resulting orbit is approximately elliptical (helliptical Killing vector).

The enthalpy current  $\tilde{u}^\mu$  is then decomposed into a part corotating with  $\xi^\mu$  and an internal motion described by the spatial vector  $V^\mu$ , yielding the expression

$$\tilde{u}^\mu = \tilde{U}(\xi^\mu + V^\mu), \quad (4.24)$$

where the scalar  $\tilde{U} = -\tilde{u}^\mu n_\mu / \alpha$  is the time component of the enthalpy current as measured by the Eulerian observer. Another possibility [59] is to split  $u^\mu$  into a part parallel to the timelike normal to the hypersurface plus a remainder as it is usually done for general relativistic hydrodynamics formulations [70].

To solve the equations (4.18) and (4.19) it is necessary to make choices for the temporal derivatives of the matter variables. The time derivative of the mass density is fixed by assuming [61]

$$\mathcal{L}_\xi \left( \frac{\rho \tilde{U}}{h} \right) = 0 \quad (4.25)$$

momentarily on the initial data hypersurface. To impose time derivatives on the enthalpy current it is split into a rotational and an irrotational part. An irrotational fluid is characterized by a vanishing kinematic vorticity tensor [64, 71]

$$\omega_{\alpha\beta} := \frac{1}{2} P_\alpha^\mu P_\beta^\nu (\nabla_\mu u_\nu - \nabla_\nu u_\mu) = 0, \quad (4.26)$$

where  $P_\alpha^\mu$  is the projection operator (4.17). For a barotropic fluid this implies that also the vorticity tensor vanishes:  $\nabla_{[\mu} \tilde{u}_{\nu]} = 0$ . The interpretation of Eq. (4.26) is, that for the Lagrangian observer the movement of the fluid must appear irrotational. Introducing  ${}^{(3)}\tilde{u}_i = \gamma_i^\mu \tilde{u}_\mu$  it can be shown [64] that Eq. (4.26) is equivalent to

$$D_i {}^{(3)}\tilde{u}_j - D_j {}^{(3)}\tilde{u}_i = 0 \quad (4.27)$$

## 4.2. Numerical Solution of the Hydrodynamical Constraint Equations

for a barotropic perfect fluid. The irrotational part can thus be described by the gradient of a scalar function  $\phi$ :

$${}^{(3)}\tilde{u}^i_{\text{irr}} = D^i\phi, \quad (4.28)$$

and the decomposition into rotational and irrotational part can be written as

$$\tilde{u}^\mu = \nabla^\mu\phi + w^\mu, \quad (4.29)$$

where the time component of  $\nabla^\mu\phi$  is determined through the normalization  $\tilde{u}^\mu\tilde{u}_\mu = -h^2$ . The rotational part will remain in the same rotational movement with respect to the “far away masses” which define the inertial frame, because the influence of viscosity that would tidally lock the two neutron stars is negligibly small. Hence the rotational part is not stationary in the corotating frame but in the inertial frame. The term “inertial frame” is really only well defined at spatial infinity as the non-rotating frame, i.e.  $\beta^i = 0$ . Therefore for the rest of this work the terminology irrotational frame or “fixed stars” frame is used to distinguish it from the already established notion of inertial frames. It was now the great insight of Tichy [61] that in this setup the two parts of the enthalpy current are momentarily Lie dragged by the vectors  $\xi$  and  $\bar{\xi}$  respectively:

$$\gamma_i^\nu \mathcal{L}_\xi(\nabla_\nu\phi) = 0, \quad \gamma_i^\nu \mathcal{L}_{\bar{\xi}}(w_\nu) = 0, \quad (4.30)$$

where  $\bar{\xi}^\mu = \nabla^\mu\phi/\tilde{U}$ . The Lie derivative for  $w_\nu$  can be interpreted in the following way. It is assumed that the other star perturbs the kinematic vorticity in a negligible way and hence  $\nabla_\nu\phi$  is not rotating with respect to the far away masses. Observers moving with the irrotational velocity are therefore to a good approximation at rest in the “fixed stars” frame. Thus it becomes clear that  $\gamma_i^\nu \mathcal{L}_{\bar{\xi}}(w_\nu) = 0$  indeed describes the stationarity of  $w_\nu$  in the “fixed stars” frame.

For a clean separation of rotational and irrotational part we require the rotational part  $w^i$  to be divergence-free:

$$D_i w^i = 0. \quad (4.31)$$

#### 4. Initial Data for General Relativistic Neutron Star Binary Simulations

A solution to this equation is given in the Eulerian frame by

$$w^i = \sum_{j,k} f \left( |x^l - x_C^l|, \sum_l \omega^l x^l \right) \frac{1}{\sqrt{\gamma}} [ijk] \omega^j (x^k - x_C^k), \quad (4.32)$$

where  $[ijk]$  is the antisymmetric symbol,  $\omega^i$  and  $x_C^i$  are constants and  $f$  is an arbitrary function of two arguments. Furthermore linear superpositions of solutions of this type are solutions as well. This solution is a generalization of the solution proposed by Tichy in [61]. In subsequent works [15, 62] however Tichy uses  $w^i$  which are missing the factor  $\sqrt{\gamma}^{-1}$  and thus are no longer divergence free. However this choice yields initial data with smaller expansion and shear and for this reason has been adopted subsequently also by other groups [59, 60]. However dropping the factor  $\sqrt{\gamma}^{-1}$  essentially breaks the clear distinction between purely irrotational parts and purely rotational ones. Since this clear distinction is the primary motivation for the Lie derivatives chosen in (4.30) it should be maintained if possible. If minimizing the expansion is of concern one could choose  $\mathcal{L}_u \rho = 0$ , which is the necessary and sufficient condition for the expansion to vanish. This choice however is in contradiction to Eq. (4.25) and thus the initial data in the current formalism is not expansion free by construction. Indeed it should not be surprising that conservation of  $\frac{\rho \tilde{U}}{h}$  in a corotating frame might not be a perfect assumption, since the rotational part  $w^i$  and consequently also  $\tilde{U}$  is not conserved in that frame. For future investigations I therefore propose to insist on  $\mathcal{L}_u \rho = 0$  which after a straight forward calculation leads to the new choice:

$$\mathcal{L}_\xi \left( \frac{\rho \tilde{U}}{h} \right) = \left( \frac{\rho^{(3)} \tilde{u}_i^{(3)} \tilde{u}^i}{h^2 \tilde{U}^2} {}^{(3)}\tilde{u}^j \partial_j h + \frac{\rho^{(3)} \tilde{u}_i}{h \tilde{U}} \partial_t {}^{(3)}\tilde{u}^i - \xi^i \partial_i \left( \frac{\rho \tilde{U}}{h} \right) + \frac{{}^{(3)}\tilde{u}^i}{h} \partial_i \rho \right), \quad (4.33)$$

where the time derivatives  $\partial_t {}^{(3)}\tilde{u}^i$  are determined through Eqs. (4.30). This particular choice however is not investigated any further in the course of this work, but it appears promising to investigate whether this choice also reduces the shear of the fluid and whether it yields initial data closer to an equilibrium configuration. As will be shown in section 4.2.2  $w^i$  cannot be chosen as in Eq. (4.32) for other reasons.

## 4.2. Numerical Solution of the Hydrodynamical Constraint Equations

Having introduced all the required time derivatives and the split of the enthalpy current, the internal motion of the stars fluid is given by

$$V^i = \frac{D^i \phi + w^i}{\tilde{U}} - (\beta^i + \xi^i) \quad (4.34)$$

and the Euler equations and the continuity equation can be written in the form [61]:

$$0 = -D_i C + {}^{(3)}\mathcal{L}_{w/\tilde{U}} w_i, \quad (4.35)$$

$$0 = D_i \left( \frac{\rho \alpha}{h} \tilde{U} V^i \right) = D_i \left( \frac{\rho \alpha}{h} (D^i \phi + w^i - \tilde{U}(\beta^i + \xi^i)) \right), \quad (4.36)$$

where  $C$  is given by

$$C = -\frac{h^2}{\tilde{U}} - V^k D_k \phi. \quad (4.37)$$

The specific enthalpy is then expressed in terms of the unknowns  $C$  and  $\phi$  and given quantities in the following way:

$$h = \sqrt{L^2 - (D_i \phi + w_i)(D^i \phi + w^i)}, \quad (4.38)$$

with

$$L = -\frac{C - (\beta^i + \xi^i) D_i \phi}{2\alpha} + \sqrt{\left( \frac{C - (\beta^i + \xi^i) D_i \phi}{2\alpha} \right)^2 + w^i (D_i \phi + w_i)}.$$

At last the scalar  $\tilde{U}$  is obtained from the normalization of the four-velocity,  $u^\mu u_\mu = -1$ , yielding

$$\tilde{U} = \frac{\sqrt{h^2 + (D_i \phi + w_i)(D^i \phi + w^i)}}{\alpha}. \quad (4.39)$$

The Euler equation (4.35) has now turned into a set of ordinary differential equations that can be integrated by specifying the value of  $C$  at an arbitrary point. In practice however the Lie derivative in Eq. (4.35) is always neglected, because that term is of order  $\mathcal{O}(w)^2$  and the spin (and thus the rotational velocity piece) is assumed to be small. In this case  $C$  is constant throughout the star. The value of  $C$  is fixed for example by evaluating Eq. (4.37) at the center of the star, when the central specific enthalpy is given. Another possibility is to tune  $C$  such that the mass of the star has a given value. The continuity equation is often assumed to be an elliptic equation

#### 4. Initial Data for General Relativistic Neutron Star Binary Simulations

in divergence form for the *velocity potential*  $\phi$ . Observing however that  $h, \rho(h), \tilde{U}$  also depend on  $D_i\phi$  it becomes clear that derivatives of these quantities give rise to terms in the principal part as well. Because of the nonlinear nature of these terms it is not simple (and maybe not even possible) to prove the definiteness of the principal part (2.55) and thus it is in fact not clear whether this equation is elliptic or not. In the rest of this work however it will be assumed that equation (4.36) is elliptic. As another complication it must be noted that the equation is not elliptic on the surface of the star, where  $\rho = 0$  and as a consequence two eigenvalues of the principal part matrix vanish. This can be cured by dividing the equation with  $\rho$  which of course leaves solutions to the equation unchanged. In this case the principal part has two finite non-zero eigenvalues and one unbound eigenvalue going to infinity on the stellar surface. This type of elliptic equations is called *non-uniformly elliptic* and some theorems on uniqueness and existence of their solutions can be found in [39]. These theorems usually demand some special properties from the boundary conditions and thus I will shortly review the commonly used boundary condition. Taking the limit  $\rho \rightarrow +0$  of the continuity equation (4.36) yields  $w^\mu \nabla_\mu \rho = 0$ , i.e. at the stellar surface the fluid is expansion free. Together with the choice (4.25) this requires

$$0 = \tilde{U}V^i D_i \rho = (D^i \phi + w^i - \tilde{U}(\beta^i + \xi^i))D_i \rho. \quad (4.40)$$

Here  $D_i \rho$  yields a vector that is orthogonal to the surface of the neutron star. Thus on the surface of the star the “internal” flow  $V^i$  of the star must be tangential to the stellar surface. Eq. (4.40) is usually viewed as a Robin boundary condition on the velocity potential  $\phi$ . This view however is problematic since the equation is derived from the elliptic itself and thus does not impose anything new; instead the equation is a regularity condition that has to hold on the boundary. Further problems become evident recalling that  $\rho$  itself depends on derivatives of  $\phi$ . Due to the nonlinear dependence of  $\rho$  on  $D_i\phi$  there might be more than one solution for  $D_i\phi$ . Furthermore the derivatives  $D_i\rho$  lead to second derivatives of  $\phi$  and thus the equation does not fall into the class of Robin boundary condition. The question

how to choose a good boundary condition on the stellar surface thus remains open. It must be noted however that imposing Eq. (4.40) like a Robin boundary condition still leads to stable numerical schemes and sensible initial data. The process of imposing the boundary conditions also has to deal with the fact that the domain of the problem is variable since the size of the star is not known beforehand. This issue is handled by fitting the coordinates [72–74] to the domain in every iteration step [62] which however is numerically expensive. From the above observations however it appears possible that the system of equations (4.35) and (4.36) does not have a unique solution and thus different implementations could lead to differing solutions.

Related to the problem of boundary conditions is the fact that the system of equations (4.35)+(4.36) depends on derivatives of the velocity potential  $\phi$ , but not on  $\phi$  itself. Thus the solution to  $\phi$  is in any case undetermined up to an additive constant which could be fixed by imposing a Dirichlet condition. It is however possible that the solutions are non-unique even beyond this additive constant. The general assumption that the regularity condition is sufficient for uniqueness seems to come historically from an argument in [75], where the authors consider a similar equation in one dimension. A rigorous proof however seems to be still missing.

The regularity condition (4.40) will be problematic in the case where  $D_i\rho = 0$  at the stellar surface, which happens for example for polytropes with polytropic index  $n > 1$  (See Eq. (4.56)). In that case it might be better to consider the same condition as in [66], where the derivative on  $\rho$  is replaced by a derivative in  $h$ :

$$0 = \tilde{U}V^i D_i\rho = (D^i\phi + w^i - \tilde{U}(\beta^i + \xi^i))D_i h. \quad (4.41)$$

Since  $\rho$  is a function of  $h$ , Eq. (4.40) is fulfilled whenever Eq. (4.41) is satisfied. As a side remark it is interesting to observe, that if we assume that the star is expansion free,  $\mathcal{L}_u\rho = 0$ , throughout the star, the necessity for the regularity condition will actually vanish.

#### 4. Initial Data for General Relativistic Neutron Star Binary Simulations

The review of the current construction methods is concluded with a remark on the used algorithm. In prior works the metric and matter equations are always solved iterating sequentially, i.e. first the constraint equations for the metric are solved with static matter terms, followed by solving the matter constraint with static metric terms and so forth. This sequential approach can be problematic if there exists a “metastable” approximate solution, i.e. in a configuration that does not admit solutions there might be an approximate solution that barely changes in every iteration step. Because one part of the equations is held fixed the other part cannot move away from the metastable state and thus the approximation seems to converge. In this work the hyperbolic relaxation method is used solving all the constraint equations concurrently. With this method it has been found that the head-on collision case briefly discussed in [69] does actually not admit solutions in the constant three-velocity approximation.

The review above revealed some problems and difficulties in the currently used initial data construction formalism, therefore improvements and potential fixes are investigated in the following sections. It must be noted however that the current state is already successfully applied in a multitude of simulations.

#### 4.2.2. Constraints from the Euler Equations on the Rotational Part

In Sec. 4.2.1 it has been discussed that the Euler equations (4.35) are only solved in an approximate manner, since the spatial Lie derivative is neglected. The following investigations will be dedicated to the first computations solving the Euler equations exactly.

To start with, one has to ask the question under which conditions the equations actually do possess a solution. Inspecting the equations one observes that there



## 4.2. Numerical Solution of the Hydrodynamical Constraint Equations

can only be a solution if  ${}^{(3)}\mathcal{L}_{w/\tilde{U}}w_i$  can be expressed as the gradient of a scalar, i.e.  ${}^{(3)}\mathcal{L}_{w/\tilde{U}}w_i$  must be curl-free:

$$0 \stackrel{!}{=} D_i {}^{(3)}\mathcal{L}_{w/\tilde{U}}w_j - D_j {}^{(3)}\mathcal{L}_{w/\tilde{U}}w_i. \quad (4.42)$$

This gives rise to constraints on the possible spin velocities  $w^i$  which have been completely neglected in the past. Indeed one could have wondered why the three Euler equations only fix the single variable  $C$ . It is exactly the constraints on components of  $w^i$  that were missing in the calculation. Evaluating Eq. (4.42) yields the expression

$$\begin{aligned} 0 = & D_i \left( \frac{1}{\tilde{U}} \right) (w^k D_k w_j - w^k D_j w_k) - D_j \left( \frac{1}{\tilde{U}} \right) (w^k D_k w_i - w^k D_i w_k) \\ & + \frac{1}{\tilde{U}} (D_i (w^k D_k w_j) - D_j (w^k D_k w_i)). \end{aligned} \quad (4.43)$$

The expression for  $\tilde{U}$  depends on a multitude of variable and it appears unlikely that a completely general solution for arbitrary  $\tilde{U}$  can be found. Instead it is more promising to find solution for which the factors containing  $w^i$  vanish. A natural ansatz is to choose solutions that satisfy

$$0 = w^k D_k w_i - w^k D_i w_k = 2w^k D_{[i} w_{k]} = w^k \epsilon_{jki} \epsilon^{jmn} D_m w_n = \epsilon_{jki} w^k (\text{curl } w)^j, \quad (4.44)$$

for which the first two terms in Eq. (4.43) obviously cancel. It follows easily that this condition is also sufficient for the last term to vanish. After using Eq. (4.44) to replace  $w^k D_k w_i$  by  $w^k D_i w_k$  and expanding the derivatives the result follows from an easy calculation.

It is interesting to observe that Eq. (4.44) has the same structure as Eq. (4.21), i.e. for the rotational spatial part of the enthalpy current the structure of the enthalpy current four-vector reemerges. The meaning of Eq. (4.44) is that the curl of  $w^i$  is in the same direction as the field  $w^i$  itself:

$$\epsilon^{jmn} D_m w_n = \lambda w^j, \quad (4.45)$$

#### 4. Initial Data for General Relativistic Neutron Star Binary Simulations

where  $\lambda$  is an arbitrary function which is called *abnormality* of  $w^i$  in mathematical contexts [76]. Additional to this equation  $w^i$  must also be divergence-free, Eq. (4.31). Divergence-free fields obeying (4.45) appear in the context of fluid dynamics and magnetohydrodynamics and are known as Beltrami fields or force free magnetic fields respectively. These equations still admit a variety of possible solutions, but they do not admit solutions with a planar or axisymmetric flow. Instead typical solutions describe flows moving on a helix-like curve. From this fact it is immediately clear that Tichys choice (4.32) is incompatible with the Euler equations. In fact Tichys choice is quite the opposite of what is required. In flat space Eq. (4.32) becomes a complex lamellar field, i.e. the field is orthogonal to its own curl.

Some general properties of and basic examples for Beltrami fields are discussed in [76]. Historically notable solutions to Eq. (4.45) for constant  $\lambda$  are the Trkal-Berker solution [77] and the Chandrasekhar-Kendall functions [78]. These solutions however are maybe not the best approximation to the rotational velocity field. To understand why, the following criteria for a physically reasonable solution are assumed.

1. There is some notion of a spin axis and the solution is approximately axisymmetric around this spin axis.
2. There is little differential rotation inside the star and the star is rotating approximately uniformly.

The Trkal-Berker solution changes the direction of rotation periodically with distance from the rotation axis, so it is not rotating uniformly and there is a lot of differential rotation, which excludes this solution. The Chandrasekhar-Kendall functions are a wide class of solutions, but typically they fall off towards zero with growing distance from the rotation axis and thus the star is not rotating uniformly, which also excludes this class of solutions.

## 4.2. Numerical Solution of the Hydrodynamical Constraint Equations

General relativistic approaches to force free magnetic fields also exist [79–82], but for the investigations in this work I will restrict to results derived for a flat spacetime, for which  $w^i$  can be expressed analytically and which is sufficient for a first study of the effects. To construct solutions satisfying above criteria one can make the ansatz:

$$w^i = (-\omega(y - y_C), \omega(x - x_C), w^3), \quad (4.46)$$

which describes a rotation around an axis in  $z$ -direction through the point  $(x_C, y_C, 0)$  with an angular frequency  $\omega$ . The toroidal component of the enthalpy current has the magnitude

$\sqrt{(w^1)^2 + (w^2)^2} = \omega\sqrt{(x - x_C)^2 + (y - y_C)^2}$ , which grows linearly with distance from the spin-axis and thus describes a uniformly rotating enthalpy flow. The poloidal component  $w^3$  is still undetermined, but it is already clear that it is not identically zero, since planar flow is forbidden. Inserting the ansatz (4.46) in Eq. (4.45) and Eq. (4.31) yields three first order differential equations from which it is easily found that for spin in  $z$ -direction the ansatz (4.46) admits only the following solutions:

$$w^i = \omega \left( y_C - y, x - x_C, \pm 2\sqrt{c^2 - \frac{(x - x_C)^2 + (y - y_C)^2}{2}} \right), \quad (4.47)$$

where  $c$  is a constant and the  $\lambda$  in Eq. (4.45) is given by  $\lambda = \pm(c^2 - ((x - x_C)^2 + (y - y_C)^2)/2)^{-1/2}$ . This solution has some remarkable properties:

1. There is a maximum distance from the rotation axis,  $(x - x_C)^2 + (y - y_C)^2 \leq 2c^2 = d_{\max}^2$ , which is determined by the constant  $c$ . In other words, if  $R$  is the radius of the star,  $c$  must be chosen  $c > R/\sqrt{2}$ .
2. The poloidal component is monotonically decreasing with distance from the rotation axis. This means that the helix that is curved by the flow lines is winding up/down faster in the center than at the surface. At the maximum distance the poloidal velocity component is exactly zero and the flow lines become planar. At the center the poloidal component is the only non-vanishing

#### 4. Initial Data for General Relativistic Neutron Star Binary Simulations

one and its value is  $w^3 = 2\omega c$ . Thus for given angular frequency  $\omega$  there is a lower bound on this axial current that is determined by the stars radius  $R$ :  $|w^3|_{d=0} > \sqrt{2}\omega R$ , which is even bigger than the angular velocity at the stellar surface. The consequences of the helix motion and the axial current in particular are not entirely clear, but there might be an impact on jet generation and the magnetic field configuration in pulsars like the famous Hulse-Taylor binary (PSR 1913+16) [9, 10]. It will be interesting to investigate the effect in future numerical simulations.

3. There are two branches of solutions with opposite chirality. In one case the axial current is aligned with the spin, in the other case the axial current is exactly anti-aligned.

The choice of the constant  $c$  is only constrained through the radius of the neutron star, which alas is not known in advance. For the construction of the initial data it will however be safe to set  $c$  larger than some estimated maximum size of the star, e.g. larger than 20 km. It is however desirable to constraint  $c$  further, eventually by finding the solution with minimal shear.

Having discussed the properties of the solution one has to keep in mind that these only hold for the purely rotational part of the enthalpy current. The gradient part will actually counteract most of the axial current as will be seen later in the investigation of the full numerical solution. Whether the new form for  $w^i$  actually contributes to the formation of jets must be investigated through full numerical simulations. Relativistic jet formation through purely hydrodynamic processes is nothing new and several models for it exist [70, 83]. It is therefore not too far-fetched to assume that also this new form for  $w^i$  might actually contribute to jet formation. It is clear however that jets cannot be consistent with an equilibrium situation. Eventually even more important could be the impact on the magnetic fields. Even if the axial current is counteracted by the gradient part, the result could be a convective flow that acts as a dynamo for the magnetic field.

## 4.2. Numerical Solution of the Hydrodynamical Constraint Equations

The solution to Eq. (4.45) for arbitrary spin is given by:

$$w^i = \epsilon^{ijk} \omega_j (x_k - x_{Ck}) \pm 2\omega^i \sqrt{c^2 - \frac{\delta_{ij}(x^i - x_C^i)(x^j - x_C^j)}{2} + \frac{\delta_{ij}(\omega^j(x^i - x_C^i))^2}{2\delta_{kl}\omega^l\omega^k}}, \quad (4.48)$$

where  $\omega^i$  is a spin vector, in which the angular frequency  $\omega$  and the spin direction have been subsumed, and the  $x_i$  are the spatial coordinates. Here the spin vector is chosen such that the first term coincides with the choice of Tichy. Alas the generalization to curved space is not straight forward, but could eventually be found numerically following the formalisms in [81, 82]. As a first approximation  $w_{\text{curved}}^i = \frac{1}{\sqrt{\gamma}} w_{\text{flat}}^i$  at least yields a divergence-free  $w^i$ , but it is not exactly orthogonal to its curl. For the numerical applications in this work  $w_{\text{curved}}^i$  will be used as the most accurate analytical expression at hand.

In the following I will shortly discuss some possible variations to the ansatz (4.46). In the ansatz above uniform rotation has been defined by the toroidal components of the rotational part of the enthalpy current increasing proportionally to the distance from the rotation axis. Uniform rotation might be better defined by in terms of the actual three-velocity field, i.e.

$$\sqrt{(w^1)^2 + (w^2)^2} = \sqrt{(\tilde{U}v_{\text{rot}}^1)^2 + (\tilde{U}v_{\text{rot}}^2)^2} = \omega\tilde{U}\sqrt{x^2 + y^2} \quad (4.49)$$

where  $v_{\text{rot}}^i := w^i/(\tilde{U})$  indicates the purely rotational component of the three-velocity field  $v^i$ . In this case however the solution is harder to find and in particular will depend on the specific enthalpy  $h$  and thus has to be computed anew in every iteration step. Another variation might be found by choosing the abnormality  $\lambda$  of Eq. (4.45) as a function of the specific enthalpy  $h$ . By taking the divergence of Eq. (4.45) it is easily found that in this case  $w^i$  is orthogonal to  $D_i h$ , i.e. the rotational enthalpy flow moves on surface of constant  $h$ . In particular the rotational velocity on the surface will be tangential to the stellar surface, which would be the expected behaviour. It must be noted however that the internal motion described by  $V^i$  is automatically tangential to the surface by virtue of the regularity condition (4.41). Since for the solution (4.47) the absolute value of  $\lambda$  is increasing towards

#### 4. Initial Data for General Relativistic Neutron Star Binary Simulations

the surface one can infer that this should also be true here. Thus a possible choice might be  $\lambda(h) = \pm 1/h$ . Yet another variant can be motivated by the differential rotation found in stars like the sun. At the equator they show a higher rotational frequency than near the poles. Transferring this naively to Eq. (4.48) would lead to a smaller axial current at the poles, which might be a positive outcome. However, the rotational frequency in stars does not vanish at the poles, so at least following this simple heuristics the axial part of  $w^i$  does not vanish at the surface.

Since solutions for isolated neutron stars do not require this special type of solutions one has to ask why these constraints should occur for binary neutron stars. Tracing back its origin in the derivation one arrives at the choice of the time derivatives of the fluid, i.e. Eqs. (4.30), as the root cause. In isolated neutron stars the gradient part and the divergence-free part are typically Lie dragged by the same vector, which is not the case here. The spin direction of the neutron stars does not change due to their inertia, but the stars force each other to move on an orbit which is described by the Lie derivative with respect to  $\xi^\mu$ . As such it should be the tidal forces between the neutron stars which can be seen as the cause of the helix-like fluid motion. However even at infinite separation, where the stars should be behaving like isolated objects, the formalism still only allows Beltrami fields as solutions, which is a first hint that there is a deeper lying problem. Concluding this section it is noteworthy that instead of enforcing the Lie derivative for the divergence-free part in Eq. (4.30) and deriving a solution for  $w^i$ , the Lie derivative could also be changed such that a given choice for  $w^i$  is compatible with the Euler equations. However, since the choices for the Lie derivatives in Eqs. (4.30) appear natural and reasonable there is no indication that they should be changed at this point.

### 4.2.3. Exact Integration of the Euler Equations

Up to now the necessity to solve the Euler equations was ignored since it has been assumed that the spin of the neutron stars is small and thus also the divergence-free part of the enthalpy current  $w^i$  must be small. As has been shown in the previous section however there is a non negligible axial component in  $w^i$  which can be chosen very large (by choosing a large  $c$  in Eq. (4.47)) without changing the angular frequency. Thus for the choices of  $w^i$  discussed in the previous section it is no longer implied that small spin corresponds to small  $w^i$ . This is an additional motivation to solve the Euler equations (4.35) in a numerically exact manner.

To solve the Euler equations the Lie derivative is reformulated

$${}^{(3)}\mathcal{L}_{w/\tilde{U}}w_i = \frac{w^j}{\tilde{U}}D_jw_i + w_jD_i\left(\frac{w^j}{\tilde{U}}\right) \quad (4.50)$$

$$= \frac{w^j}{\tilde{U}}D_jw_i + D_i\left(\frac{w_jw^j}{\tilde{U}}\right) - \frac{w^j}{\tilde{U}}D_iw_j, \quad (4.51)$$

and since  $w^i$  is chosen as a Beltrami field, Eq. (4.44), the Lie derivative simplifies to

$${}^{(3)}\mathcal{L}_{w/\tilde{U}}w_i = D_i\left(\frac{w_jw^j}{\tilde{U}}\right),$$

and the Euler equations (4.35) become

$$0 = D_i(-C_w) = D_i\left(\frac{h^2}{\tilde{U}} + V^kD_k\phi + \frac{w_jw^j}{\tilde{U}}\right), \quad (4.52)$$

where  $C_w$  is now the new (and exact) constant of integration

$$C_w = -\left(\frac{h^2}{\tilde{U}} + V^kD_k\phi + \frac{w_jw^j}{\tilde{U}}\right). \quad (4.53)$$

The specific enthalpy is now expressed in terms of  $C_w$  by

$$h = \sqrt{L_w^2 - (D_i\phi + w_i)(D^i\phi + w^i)}, \quad (4.54)$$

with

$$L_w = -\frac{C_w - (\beta^i + \xi^i)D_i\phi}{2\alpha} + \sqrt{\left(\frac{C_w - (\beta^i + \xi^i)D_i\phi}{2\alpha}\right)^2 + w^iD_i\phi}. \quad (4.55)$$

The equation for  $\tilde{U}$  remains in the form (4.39).

#### 4.2.4. Extension of the Continuity Equation to Vacuum

To solve the problem of imposing the regularity condition (4.41) on the stellar surface usually the coordinates are fitted such that the stellar surface coincides with the domain boundary of a spectral element. This process is computationally expensive and thus alternative approaches are worth investigating.

The idea pursued in this work is to extend the solution of the velocity potential  $\phi$  to the vacuum region, instead of stopping at the stellar surface. Since all of the analytical expressions appearing in the continuity equation (4.36) can be easily extended to regions with specific enthalpy smaller than one, there seems to be no immediate reason to not extend the solution. The only question is whether the equation of state (EOS), relating mass density  $\rho$  and specific enthalpy  $h$ , can also be extended. For a polytropic equation of state we have

$$\rho = \kappa^{-n} \left( \frac{h-1}{n+1} \right)^n, \quad (4.56)$$

with polytropic constant  $\kappa$  and polytropic index  $n = \frac{1}{\Gamma-1}$ , where  $\Gamma$  is the adiabatic index. This equation can be easily extended to  $h < 1$  for all integers  $n \in \mathbb{N}$ . For non-integer  $n > 1$  the continuation can not be directly extended, but it is possible to set  $\rho = 0$  in the  $h < 1$  region. For  $0 < n < 1$  the derivative  $\partial\rho/\partial h$  is undefined at the stellar surface and thus we are unavoidably left with a function  $\rho(h)$  that is not continuously differentiable at the domain boundary. Many realistic equations of state for neutron stars can be approximated with a  $n < 1$  polytrope, which would then pose a problem for the continuous continuation to vacuum. However  $n < 1$  holds only in the interior of the star, but not for the crust where the actual transition to vacuum happens. There is general agreement that the crust is well described by the Sly EOS [84] which is approximated by  $n > 1$  polytropes [85]. Thus for the continuation to vacuum the case  $n < 1$  can be ignored in all physically meaningful situations. A similar discussion holds for other types of analytically given EOS and tabulated EOS can be extended through extrapolation.



## 4.2. Numerical Solution of the Hydrodynamical Constraint Equations

For a first discussion let us restrict to the simple case  $n = 1$ , for which the density  $\rho$  can be easily extended to vacuum. It is then a natural ansatz to solve the exact same equation in the interior region ( $h > 1$ ) and the vacuum region ( $h < 1$ ). The first problem occurring with this ansatz is that  $\rho$  becomes negative, thus the equation is no longer strongly elliptic (Eq. (2.10)) and therefore the hyperbolic relaxation method can not converge to a steady state. This can be fixed by multiplying the equation with  $(-1)$  in the vacuum region, which of course leaves the solutions to the equation unaffected. Usually elliptic operators lead to solutions that are as smoothed out as possible, but at the surface the operator is non-elliptic and loses a lot of its smoothing properties, hence slowing down extremely the convergence to the solution. Consequently the solution will barely adapt to fulfill the regularity condition (4.41) and the interior and the exterior solution will practically relax independently from each other.

The observation that the interior solution relaxes practically independently from the vacuum region seems to suggest that we can choose any “good” elliptic equation in the vacuum region, without affecting the interior solution. The vacuum elliptic equation will be “good” if it smoothes out the solution and if it is compatible with the regularity condition (4.41). To smooth out the solution in fact every uniformly elliptic equation with smooth coefficients will suffice, so the main problem is to satisfy the regularity condition. The next ansatz is thus to extend elliptic equation for the continuity equation (4.36) with a simple Laplacian equation:

$$0 = D_i A^i = \begin{cases} D_i \left( \frac{\rho\alpha}{\rho_c h} (D^i \phi + w^i - \tilde{U}(\beta^i + \xi^i)) \right) & \text{if } h \geq 1 \\ D_i D^i \phi & \text{if } h < 1 \end{cases}, \quad (4.57)$$

where  $A^i$  plays the same role as in the discussion of the HypRelaxDiv method, see e.g. Eq. (2.54). Note that the equation for  $h \geq 0$  has been scaled with  $\rho_c$ , the central mass density of the respective neutron star, to yield a principal part of the elliptic equation with eigenvalues  $\lesssim 1$ .

#### 4. Initial Data for General Relativistic Neutron Star Binary Simulations

This equation alone however is not sufficient to obtain solutions that fulfill the regularity conditions (4.41) if hyperbolic relaxation is used. First, the outer (physically irrelevant) boundary conditions must be chosen such that they actually permit such a solution. Second, the parameters determining the Killing vector  $\xi^\mu$  change in every relaxation step. Since the principal part of the elliptic equation (almost) vanishes close to the boundary the relaxation becomes slow close to the stellar surface and therefore the solution cannot adapt fast enough to the changes of the Killing vector, which is determined by the solution in the center of the neutron star. These problems can be leveraged after making the following observation. For an irrotational star the internal velocity field  $V^i$  describes a circular flow around the center of the star [86]. Therefore  $D^i\phi$  must be such that in the center of the star

$$D^i\phi \approx \tilde{U}(\beta^i + \xi^i) - w^i, \quad (4.58)$$

i.e.  $V^i$  approximately vanishes in the center of the star. Since the three velocity is almost constant throughout the star [69] it is natural to split off this constant velocity part  $D_i\phi_0$ , which is given by

$$D_i\phi_0 = (\tilde{U}(\beta_i + \xi_i) - w_i)|_{x=x_C} = \text{const.}, \quad (4.59)$$

where  $\phi_0$  is a scalar. The velocity potential is then split into

$$\phi = x^i D_i\phi_0 + \sigma, \quad (4.60)$$

where  $\sigma$  is the potential of the residual velocity which then becomes the new potential that has to be solved for. This split is the most important part in fulfilling the regularity condition, since without it it was not possible to find appropriate boundary conditions that admit solution that satisfy the regularity conditions.

Since the parameters, like the constant from the Euler equation  $C_w$ , the approximate Killing vector  $\xi^\mu$  or the choice of the rotational enthalpy current part  $w^i$ , can differ for both stars the transition between the (extended) numerical domains of the stars will be smooth only on special cases. Eq. (4.57) is therefore solved on two separated

## 4.2. Numerical Solution of the Hydrodynamical Constraint Equations

domains which both have an outer boundary on the  $yz$ -plane, see Fig. 4.1. For the metric equations however the domain will remain connected across the  $yz$ -plane. Since  $\sigma$  is a residual quantity it should fluctuate around zero and hence its boundary condition is set to

$$\sigma = 0, \quad (4.61)$$

along the  $yz$ -plane. For the outer shell boundaries the conditions must be compatible with the condition imposed on the  $yz$ -plane. A compatible Dirichlet condition could be found by simply applying the same condition (4.61). A compatible Neumann condition is given by:

$$\delta^{ij} s_i \partial_j \sigma = 0, \quad (4.62)$$

where  $s_i$  is the normal vector to domain boundary. This is also the condition that is used to obtain all the results that presented in Sec. 4.3. It has to be remarked that even with the introduction of the split (4.60) with the first naive ansatz discussed in this section, extending the continuity equation with the interior expression, it was not possible to obtain solutions that perfectly satisfied the regularity condition (4.41). In particular for the ‘‘helix’’ choice of the rotational velocity piece (4.48) solutions with this ansatz would describe a situation in which the fluid leaves the star at the poles.

Since the solution will start relaxing from a simple initial guess the expression for  $w^i$  (Eq. (4.48)) (multiplied with  $\frac{1}{\sqrt{\gamma}}$ ) must also be changed which is already clear from the fact that there is a maximum radius for which it is defined. The modified expression is

$$w^i = \frac{1}{\sqrt{\gamma}} \epsilon^{ijk} \omega_j (x_k - x_{Ck}) \pm 2 \frac{1}{\sqrt{\gamma}} \omega^i \sqrt{c^2 - \frac{f_c |x_j - x_{Cj}|^2}{2} + \frac{\delta_{ij} (\omega^j (x^i - x_C^i))^2}{2 \delta_{kl} \omega^l \omega^k}} \quad (4.63)$$

where  $f_c$  is a function falling off to zero given by

$$f_c = \begin{cases} 1 & \text{if } |x^i - x_C^i| \leq c \\ \exp(-16(c - |x^i - x_C^i|)^2 / c^2) & \text{if } |x^i - x_C^i| > c. \end{cases} \quad (4.64)$$

## 4. Initial Data for General Relativistic Neutron Star Binary Simulations

The falloff in  $f_c$  sets in at a distance  $c$  from the center of the star and hence  $c$  must now be chosen larger than the stars radius. Since the exact radius is not known a priori, it must be estimated in advance. Typically neutron stars have radii between fifteen and ten kilometers [87], so choosing  $c$  larger then 15 km should work in most applications. However, since this is a coordinate length it is possible to construct coordinates such that the neutron star exceeds this radius.

## 4.3. Numerical Results

### 4.3.1. Implementation Details

To solve for the initial data Eqs. (4.10), (4.11), (4.13) and (4.57) are solved concurrently using hyperbolic relaxation, where for the specific enthalpy  $h$  Eqs. (4.54) and (4.63) are used. At the outer boundary Robin boundary conditions are specified for the metric variables as given in (4.14) and (4.15).

Some adjustments have to be made in comparison to the standard implementation of an evolution project in `bamps`. These adjustments, some of which have already been stated in text, are collected in the following list.

1. After every full Runge-Kutta step the data is interpolated to the centers of the stars to determine the necessary parameters. The parameter  $C_w$  is determined for each star by evaluating Eq. (4.53) and the parameters  $x_{\text{cm}}$  and  $\Omega$  are chosen such that the derivative of the specific enthalpy, Eq. (4.54), along the  $x$ -axis is zero at the stars centers. To compute the parameters a root finder estimates the minimum of  $|D_3 h|$  at  $x_{1,2}$  in the intervals  $0 < \Omega < 1/|x_{1,2} - x_{c1,2}|$  and  $x_1 < x_{\text{cm}} < x_2$ , where the notation of Eq. (4.23) has been used.

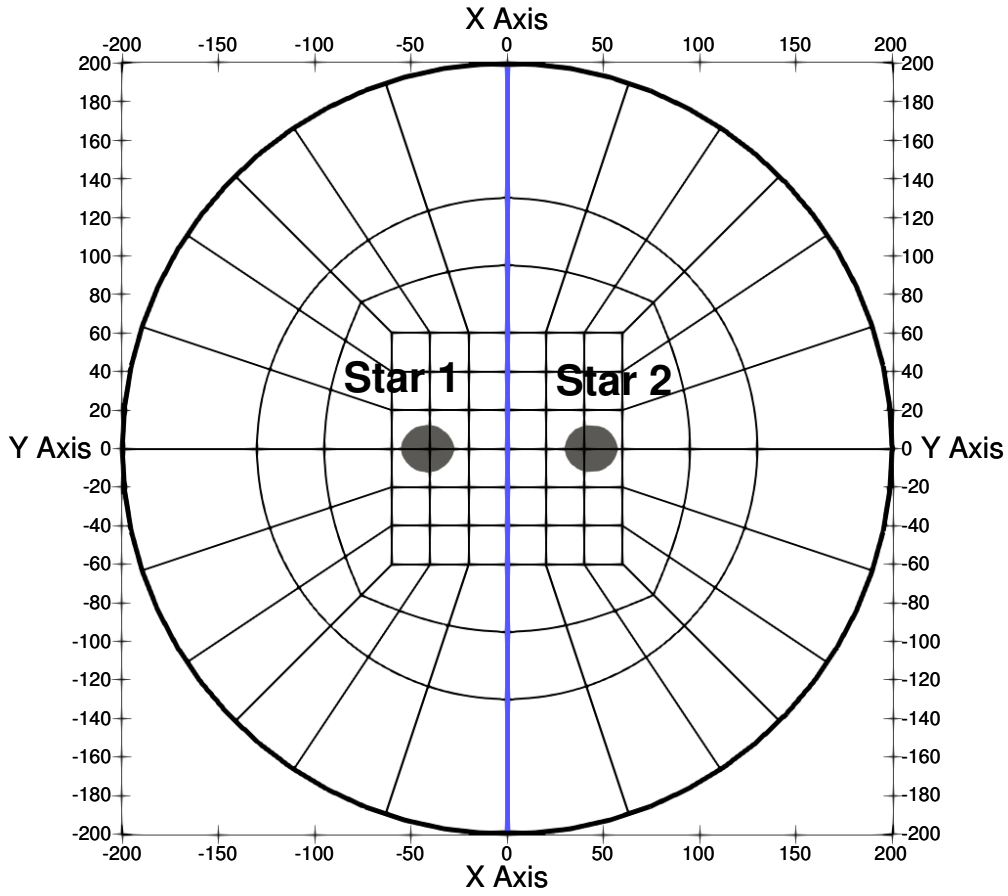


Figure 4.1.: Grid structure of bamps. The figure shows a cut through the  $xz$ -plane ( $z = 0$ ). The numerical domain is divided into subpatches and their borders are visualized in the figure. Thick lines denote the outer boundaries for the numerical domain. For the solution of the matter system the domain is decomposed into two domains and the additional domain boundary is indicated by the thick blue line along the  $y$ -axis. The dark gray spots indicate the position of the neutron stars.

#### 4. Initial Data for General Relativistic Neutron Star Binary Simulations

2. For the matter equations the subpatch boundary communication is switched off along the  $yz$ -plane, which separates the numerical domains of the individual stars. This is done to avoid Gibbs' phenomenon which would otherwise occur due to the sudden jump in the divergence-free part of the enthalpy current  $w^i$ , the value of  $C_w$  (Eq. (4.53)) and the approximate Killing vector  $\xi^\nu$ . Instead the boundary condition (4.61) is enforced on the  $yz$ -plane which requires boundaries of subpatches everywhere on the  $yz$ -plane (cmp. Fig. 4.1). On the outer boundary (4.62) is imposed for compatibility.
3. The spin frequency and the values of the central specific enthalpy are increased slowly to their final values. This is a well known technique called continuation method, see e.g. [88]. To be precise the parameters are linearly increased over a time span ten times as long as the slowest characteristic variable needs to travel once through the whole grid. In all relaxations considered in this work the diameter of the numerical grid is 400, so the number of iteration steps for this initial phase is  $t_{\text{continuation}} = 4000/\Delta t$ .
4. Initially the metric is solved with the energy-momentum tensor given in the constant three-velocity approximation [69], to generate a sufficiently good initial guess for the metric. Only after that the equations are solved completely consistently.

For irrotational neutron star binaries the problem is symmetric under reflection on the orbital plane, which is exploited to reduce the numerical costs by 50 % solving only in the upper half sphere.

For the following computations a polytropic EOS, Eq. (4.56), is used with the following parameters which have been used before in numerical tests [15, 69]

$$\kappa = 123.6489 \quad n = 1.$$

The choice of  $\kappa$  basically fixes the length scale of the problem. In this case the choice is made such that all length units are in kilometers if masses are given in solar masses.

### 4.3.2. Initial Data through Hyperbolic Relaxation

This work studies initial data that is solved with the hyperbolic relaxation method. Since the continuity equation (4.36) is expressed in divergence form and its principal part is solution dependent, it is naturally solved with the HypRelax for elliptic equations in divergence form discussed in Sec. 2.2. The described relaxation method on its own is not stable enough to start from a trivial initial guess. Therefore the initial guess for the metric variables is constructed in the constant three-velocity approximation following the scheme of [69]. In contrast to the method of Ref. [69] the results of this work are not obtained by starting with superposed (boosted) TOV solutions, but instead starting with a flat metric  $\psi = 1$ ,  $\alpha = 1$ ,  $\beta^i = 0$ , as discussed at the end of Sec. 4.1.2. The metric constraints are solved taking the energy-momentum tensor in the constant three-velocity approximation as input. At the same time the Eqs. (4.36) and (4.35) are solved for the matter variables with the metric variables as input. After this scheme has found an approximate solution all equations are solved simultaneously, now taking the correct energy-momentum tensor computed from the solution of the matter variables. As has been discussed in the previous section this method of concurrent solution of the constraints has the advantage of avoiding “metastable” solutions.

The constant three-velocity approximation is used as a first test for the solver. Initial data is constructed for an equal mass neutron star binary with a specific enthalpy of  $h = 1.01$  in each of their centers and a separation of 80. For the equation of state a polytrope, Eq. (4.56), is chosen with  $\kappa = 123.6489$  and  $n = 1$ . The stars’ centers are located at the  $x$ -axis and their velocities are parallel to the  $y$ -axis. The initial

#### 4. Initial Data for General Relativistic Neutron Star Binary Simulations

data is constructed for irrotational stars on a quasicircular orbit. In Fig. 4.2 results are presented for the conformal factor, lapse, the  $y$ -component of the shift and the residual of the conformal factor equation.

##### 4.3.3. Fulfillment of the Regularity Condition

It will be verified that the continuation to the vacuum indeed yields data for the velocity potential that satisfies the regularity condition (4.41). This can be done by visually investigating the direction of the  $V^i$  field which should be tangential to the star surface. For this test a rotating binary with rotational velocity piece given by the “old” equation (4.32) is used. The factor is chosen by  $f = 1$  and the spin parameter is chosen as  $\omega^i = (0, 0, 0.005)$ , i.e. the spin axis is aligned with the spin axis. The second stars spin is anti-aligned with the same magnitude. The neutron stars are chosen to have equal mass, given through a central enthalpy of  $h_C = 1.16$ , moving on a quasi-circular orbit. The results are shown in Fig. (4.3) confirming that the regularity condition is satisfied.

##### 4.3.4. Convergence of the Solution

To discuss the convergence of solution with increasing resolution the convergence of the Chebyshev coefficients against the coefficients of a high resolution solution is investigated. Fig. 4.4 shows the convergence behavior of the lowest Chebyshev mode  $C(0,0,0)$  against its value at a resolution of 21 collocation points for the solution of the velocity potential for a binary with non-spinning neutron stars. Because the solution for the metric variables is not smooth at the stellar surface the convergence is not perfectly exponential. In particular in subpatches containing the stellar surface the method converges only in an averaged sense. In tests with a single neutron star in spherical symmetry (Tolmann-Oppenheimer-Volkoff star) the same



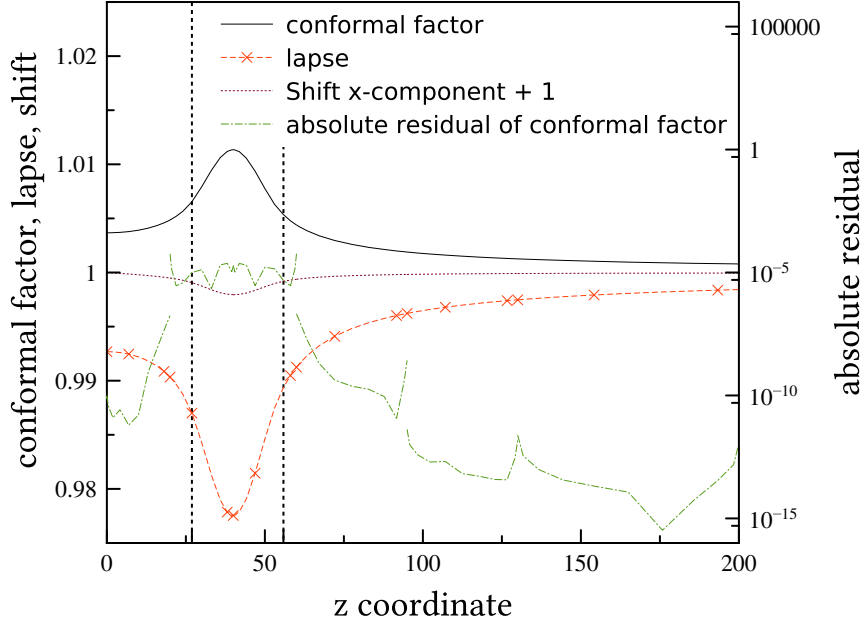


Figure 4.2.: Steady state at a resolution of 11 collocation points per subpatch for the initial data of a binary neutron star system in the constant three-velocity approximation. The figure shows the data along the positive  $x$ -axis. The values on the negative axis are symmetric (anti-symmetric for the shift component  $\beta^y$ ). Solid line: conformal factor. Orange dashed line with markers: lapse. Purple dotted line:  $y$ -component of the shift, shown here with an offset of one for clarity. Green dash-dotted line: absolute value of the residual for the conformal factor, as given by the right-hand side of Eq. (4.10). Vertical dashed line: location of the stellar surface.

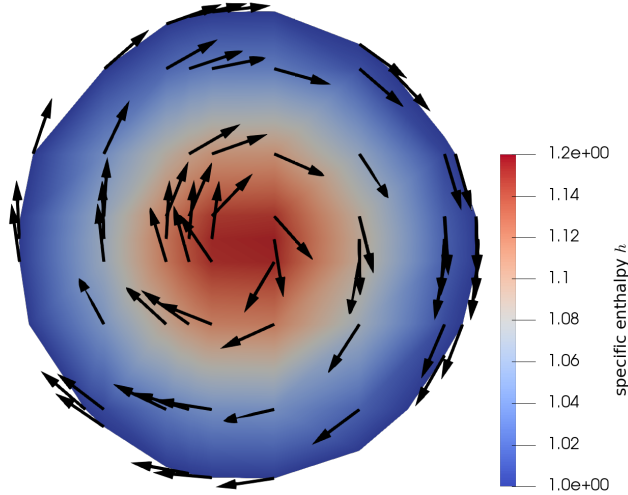


Figure 4.3.: Internal velocity field  $V^i$  on a section through the  $xy$ -plane. The spin axis is orthogonal to the  $xy$ -plane and the spin parameter  $\omega^i = (0, 0, 0.005)$ . Black arrows represent the direction of  $V^i$ . The color shows the profile of the specific enthalpy  $h$ .

behaviour is known and empirically it has been found that the upper limit for the error converges linearly, whereas the lower limit seems to decrease exponentially. Only with surface fitted coordinates was it possible to obtain a clean (but slow) exponential convergence [1]. Although this may be a disadvantage for studies of initial data per se, the situation changes if the goal is evolution of the data. Since in an actual evolution of this data surface-fitted coordinates are normally not retained, the high accuracy of initial data with surface-fitted coordinates will be lost relatively quickly anyway. On the other hand, methods like [74] require expensive iterations to determine the surface fitting coordinates as part of the solution process.

#### 4.3.5. Influence of the New Rotational Velocity Choice

The effects of the “helix” rotational velocity proposed in Eq. (4.63) are now discussed comparatively to the “planar” choice (4.32). For this comparison the spins are chosen to be anti-aligned and orthogonal to the orbital plane. The specific choice for the

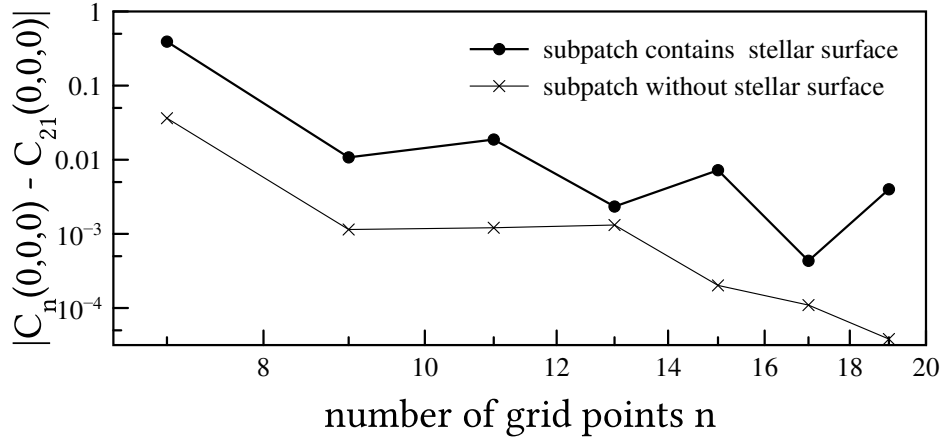


Figure 4.4.: Convergence of the lowest Chebyshev coefficient  $C(0,0,0)$  of the velocity potential for non-spinning stars for two representative subpatches **Dots:** subpatch containing parts of the neutron star surface. **Crosses:** subpatch without neutron star surface. The system is relaxed for different numbers of collocation points. The plot shows the absolute value of the difference between the Chebyshev coefficient at the highest resolution (21 collocation points) and its value for  $n$  collocation points per subpatch. The central cube grid was divided into eight subpatches in each dimension.

#### 4. Initial Data for General Relativistic Neutron Star Binary Simulations

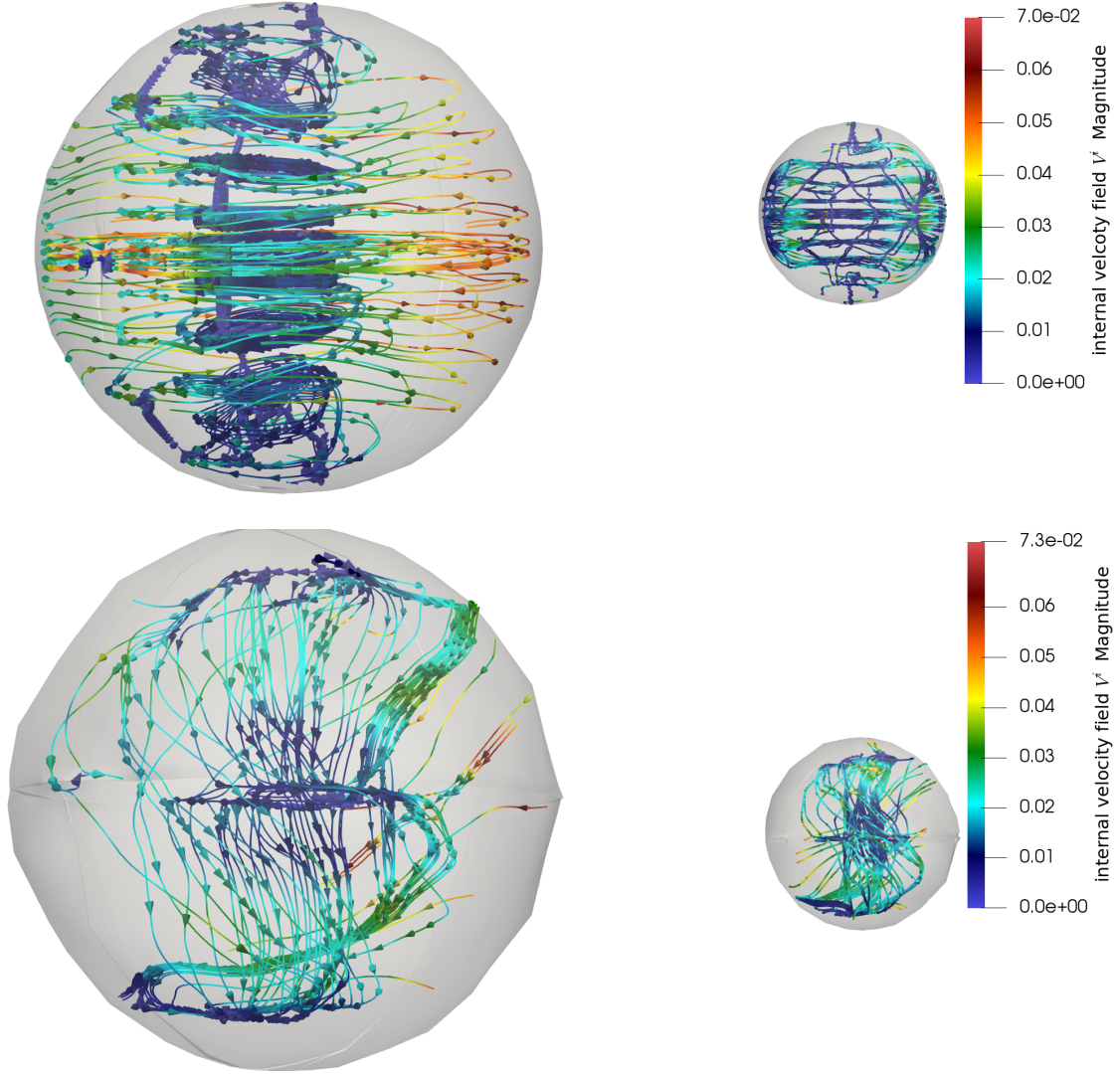


Figure 4.5.: Internal velocity field  $V^i$  for two neutron stars moving in the  $xy$ -plane. The spins are anti-aligned with spin parameters  $\omega_1^i = (0, 0, 0.005)$  and  $\omega_2^i = (0, 0, -0.005)$ . **Upper figure:** planar flow rotational current, Eq. (4.32). **Lower figure:** helix flow rotational current, Eq. (4.63). Both stars have the same mass. The second star in the background appears smaller due to the perspective. Arrows indicate the direction of the flow. The color shows the magnitude of  $V^i$  computed according to  $\text{Magnitude}(V^i) = V^i V^j \delta_{ij}$ . The opaque spheres indicate the stellar surfaces.

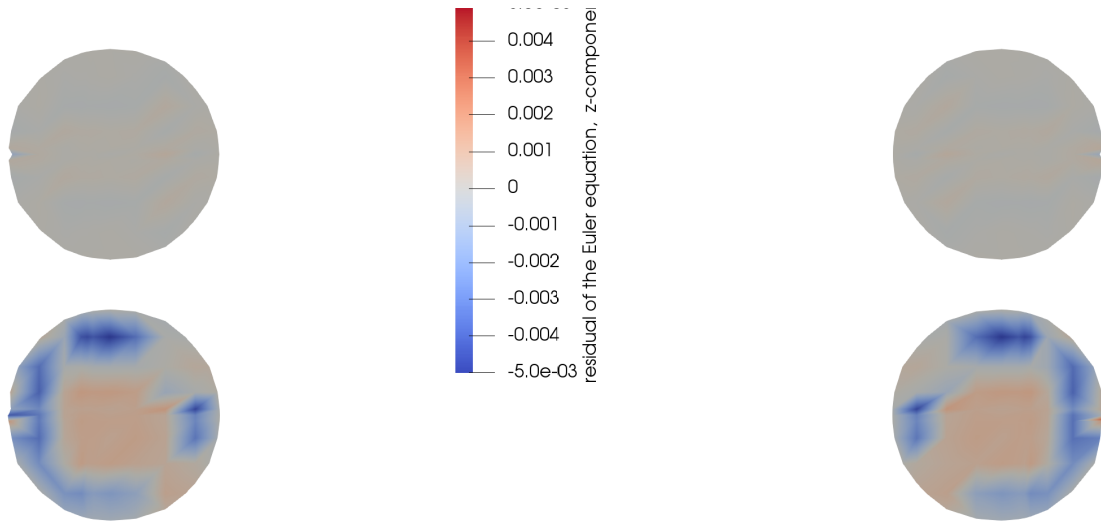


Figure 4.6.: Residuals of the Euler equation on a section through the orbital plane showing both neutron stars. Shown is the z-component, which is in the direction of the spin axis. **Upper row:** planar flow rotational current, Eq. (4.32). **Lower row:** helix flow rotational current, Eq. (4.63). The error magnitude in the planar case are almost not perceivable compared to the helix case.

#### 4. Initial Data for General Relativistic Neutron Star Binary Simulations

spin parameter is

$$\omega_1^i = (0, 0, 0.005) \quad \omega_2^i = (0, 0, -0.005). \quad (4.65)$$

For the constant  $c$  a value of  $\sqrt{2} \cdot 10$  is chosen, which is sufficiently large for the parameters assumed here. In both cases Eq. (4.53) is used to integrate the Euler equations, but note that with the choice (4.32) the Euler equations are not curl free and hence there is no chance of converging to completely solved equations.

In Fig. 4.5 the stream lines of the internal velocity field  $V^i$  are shown for both choices of  $w^i$ . For the generation of the stream lines the *Stream Tracer* filter of the visualization program `Paraview 5.4.0` [89] is used which employs a fifth order Runge-Kutta integrator with adaptive step size control. The calculations were carried out on a grid with nine collocation points in every dimension in every subpatch and the central cube of the `bamps` grid (Fig. 4.1) was divided into eight subpatches in every dimension. The stream lines reveal that for the planar  $w^i$  the resulting flow of  $V^i$  is also approximately planar. The helix  $w^i$  likewise leaves its imprint in  $V^i$ , which exhibits a clear helix like form, in the perspective projection of Fig. 4.5 appearing like an S-shape. From the figure it is visible that there are three distinct regions of small internal velocity; one in the center and one at each of the two poles. For the planar case in contrast the low velocity region is found everywhere along the spin axis.

Fig. 4.6 shows the residual of the Euler equations (4.35). Shown is the  $z$ -component of the equations, where differences between the two choices for  $w^i$  are clearly visible. For the other components the residuals look almost identical. Fig. 4.6 shows that the residual is actually worse using the new choice (4.63), but keep in mind, that with the old choice the Euler equations can actually not be integrated and thus they can not converge. The errors for the “helix” choice stem mostly from the boundary region which indicates that for this choice the solution for the velocity potential  $\phi$  close to the boundary is more demanding for the elliptic solver in this case and more

resolution would be required to see the “helix” choice overtaking the “planar” one. In the “helix” case there are also some stream lines that end at the stellar surface which indicates that the regularity condition is actually not perfectly maintained for this solution, which is another confirmation that this solution is more demanding for the solver.

Having now investigated the influence of the new choice of the rotational velocity piece, it will be interesting to investigate the effects in a numerical evolution. There is however a conceptual problem with the formalism, that should be visible when the data is evolved. The derivative of the velocity potential  $\phi$  cancels the axial current at the initial data hypersurface. The time derivatives of  $\nabla_\mu\phi$  and  $w_\mu$  however are chosen such that the axial current and the canceling part from  $\nabla_\mu\phi$  are stationary in different frames. The rotational axis of the rotational part would keep its orientation with respect to the irrotational frame, whereas the orientation of the canceling current would rotate in this frame instead keeping its orientation in the corotating frame. This has the consequence that if the data would be evolved the two parts would no longer cancel and there would be some mass leaving the neutron star soon after. One might consider this then as a hydrodynamical ejecta mechanism, but this situation is then still unsatisfactory, because the initial data hypersurface should not represent a special situation where the star stopped ejecting material for a brief moment. Discarding the idea of ejecta there is a need for alternatives, which could for example be provided by another choice of  $w^i$ , with vanishing axial current at the stellar surface. It is however not clear whether such a solution could be constructed in a physically meaningful way.

The second alternative are changes in the time derivatives of  $\nabla_\mu\phi$  and  $w_\mu$ . From the result that they have to cancel partially it seems obvious that the velocity parts should be split in another way. In the rationale for his choice of time derivatives, Eq. (4.30), Tichy assumed that  $\nabla^\mu\phi$  is parallel to the movement of the stars center. With the axial current being canceled by  $\nabla^\mu\phi$  this is certainly no longer true.

#### 4. Initial Data for General Relativistic Neutron Star Binary Simulations

The principal idea of the rotational frame being stationary in the irrotational frame, however, seems still reasonable, but could be refined by actually not choosing the rotational enthalpy current to be stationary in the “fixed stars” frame, but instead making this choice for the rotational part of the actual four-velocity, i.e.

$$\gamma_i^\nu \mathcal{L}_{\nabla\phi/\tilde{U}} \frac{w_\nu}{h} = 0, \quad (4.66)$$

which will differ from (4.30), because the  $h$  is not stationary in the same frame. There is however yet something else that possibly spoils the Lie derivatives. As will be shown next, the current formalism does actually not split the velocity in an irrotational and purely rotational part, which might in the end be the true reason for this oddity of the solution.

## 4.4. Sketch of an Improved Approach to Initial Data for Neutron Star Binaries with Spin

### 4.4.1. Identification of the Problems in the Previous Approach

The findings of Sec. 4.3.5 suggest that there might be an inconsistency in the separation of the irrotational and rotational part. One possible problem is the fact that the Lie derivatives in (4.30) are applied on the enthalpy current instead of the four-velocities. Since by making the choice (4.25) the specific enthalpy is neither stationary in the corotating nor in the irrotational frame, this means that neither will the irrotational velocity be stationary in the corotating frame nor will the rotational velocity piece be stationary in the irrotational frame.

Another problem becomes apparent noticing that the irrotational velocity  $\frac{\nabla^\mu\phi}{h}$  is not normalized to  $-1$ , but the time component is instead chosen such that the total



velocity is normalized to  $-1$ . The normalization to  $-1$  however is a crucial ingredient to show the equivalence of Eq. (4.26) and (4.27) in the irrotational case [64]. Since the normalization of the irrotational velocity piece changes for spinning neutron stars, Eq. (4.27) can in this case no longer be used to define the irrotational part and consequently  $\frac{\nabla^\mu \phi}{h}$  will also contain rotational parts.

#### 4.4.2. Split Into Irrotational and Rotational Part

Since it is now clear that the formalism of Tichy does in fact not perfectly separate the irrotational and rotational part of the fluid, a refined version of the existing approach must be found. As a starting point the ansatz is to split the four-velocity into its irrotational and its rotational part:

$$u^\mu = t(u_{\text{irr}}^\mu + u_{\text{rot}}^\mu) \quad (4.67)$$

where  $u_{\text{irr}}^\mu$  is normalized such that  $u_{\text{irr}}^\mu u_{\text{irr}\mu} = -1$ . The scalar  $t$  is fixed by the normalization constraint  $u^\mu u_\mu = -1$ , which reduces to  $t = 1$  in the purely irrotational case  $u_{\text{rot}}^\mu = 0$ . One can then define the projection operator onto the frame of the irrotational observer

$$P_{\text{irr}\mu}^\nu = \delta_\mu^\nu + u_{\text{irr}}^\nu u_{\text{irr}\mu}. \quad (4.68)$$

The irrotational part must then have vanishing kinematic vorticity (cmp. Eq. (4.26))

$$0 = \frac{1}{2} P_{\text{irr}\alpha}^\mu P_{\text{irr}\beta}^\nu (\nabla_\mu u_{\text{irr}\nu} - \nabla_\nu u_{\text{irr}\mu}) \quad (4.69)$$

$$= \frac{1}{2} (\nabla_\alpha u_{\text{irr}\beta} - \nabla_\beta u_{\text{irr}\alpha} + u_{\text{irr}\alpha} u_{\text{irr}}^\nu \nabla_\nu u_{\text{irr}\beta} - u_{\text{irr}\beta} u_{\text{irr}}^\nu \nabla_\nu u_{\text{irr}\alpha}). \quad (4.70)$$

For the purely irrotational case this has been further reduced using the Euler equations (4.21). For spinning neutron stars however one should not assume that the irrotational part alone also satisfies the Euler equation. The Euler equations hold for the total four-velocity, but not for arbitrarily split off components. Besides the problem that the irrotational part was not normalized to  $-1$ , this seems to be a

#### 4. Initial Data for General Relativistic Neutron Star Binary Simulations

further possible problem in the previous formalism, where this has always implicitly been assumed. Although this is actually a free choice, it might be physically not the best one.

Instead let us proceed assuming there is a non-zero scalar  $X$  such that

$$0 = u_{\text{irr}}^\mu \nabla_\mu (X u_{\text{irr}\nu}) + \nabla_\nu X \quad (4.71)$$

$$= X u_{\text{irr}}^\mu \nabla_\mu u_{\text{irr}\nu} + P_{\text{irr}\nu}^\mu \nabla_\mu X. \quad (4.72)$$

Then Eq. (4.70) can be reformulated to

$$0 = \nabla_\alpha (X u_{\text{irr}\beta}) - \nabla_\beta (X u_{\text{irr}\alpha}). \quad (4.73)$$

In the irrotational case the new variable  $X$  should coincide with the specific enthalpy  $h$  not only on the spatial slice, but also their Lie derivatives should agree.

A solution to Eq. (4.73) is given by

$$u_{\text{irr}i} = \frac{1}{X} D_i \sigma, \quad (4.74)$$

where  $\sigma$  is now the new velocity potential. It is trivial to show that this solution indeed fulfills the spatial projection of (4.73)

$$0 = D_i (X u_{\text{irr}j}) - D_j (X u_{\text{irr}i}). \quad (4.75)$$

The projection on  $n^\alpha n^\beta$  is also trivially satisfied. The constraint that also the projection on  $n^\alpha \gamma_i^\beta$  should vanish, fixes the choice of the time derivative of  $X u_{\text{irr}\mu}$ .

The necessary supplementary requirement for irrotation is then:

$$\gamma_i^\mu \mathcal{L}_n X u_{\text{irr}\mu} = D_i (n_\mu X u_{\text{irr}}^\mu) = -D_i (\alpha X u_{\text{irr}}^t) = 0. \quad (4.76)$$

For example making the specific choice

$$\gamma_i^\mu \mathcal{L}_\xi (X u_{\text{irr}\mu}) = 0 \quad (4.77)$$

#### 4.4. Sketch of an Improved Approach to Initial Data for Neutron Star Binaries with Spin

can be shown to satisfy the irrotation conditions in a complete analogy to the calculation given in [64], with the Euler equations replaced by (4.71) and the fluid four-velocity  $u^\mu$  replaced by  $u_{\text{irr}}^\mu$ . Furthermore after introducing the split

$$u_{\text{irr}}^\mu = u_{\text{irr}}^t (\xi^\mu + V_{\text{irr}}^\mu) \quad (4.78)$$

the following relations are also derived analogously

$$u_{\text{irr}}^t := -\frac{u_{\text{irr}}^\mu n_\mu}{\alpha} = \frac{\sqrt{1 + X^{-2} D_i \sigma D^i \sigma}}{\alpha}, \quad (4.79)$$

$$V_{\text{irr}}^i = \frac{D^i \sigma}{u_{\text{irr}}^t X} - \xi^i - \beta^i, \quad (4.80)$$

$$X = \sqrt{L_{\text{irr}}^2 - D^i \sigma D_i \sigma}, \quad (4.81)$$

$$L_{\text{irr}} = \frac{(\beta^i + \xi^i) D_i \sigma - C_{\text{irr}}}{\alpha}, \quad (4.82)$$

$$C_{\text{irr}} = -\frac{X}{u_{\text{irr}}^t} - V_{\text{irr}}^j D_j \sigma = \text{const.} \quad (4.83)$$

Equations (4.79) and (4.80) hold in the general case, whereas the last three equations hold for the specific choice (4.77). The solution for  $X$  is given by (4.81) in terms of  $D_i \sigma$ ,  $C_{\text{irr}}$  and given quantities.  $\sigma$  must be computed by solving the continuity equation and  $C_{\text{irr}}$  is a yet undetermined constant that must be chosen such that the Euler equations are satisfied.

The rotational part can be expressed as

$$u_{\text{rot}}^\mu = \frac{w^\mu}{X}, \quad (4.84)$$

where again  $w^\mu$  is chosen to be spatial,  $w^\mu n_\mu = 0$ , and divergence free,  $D_i w^i = 0$ .

The four-velocity can now be written as

$$u^\mu = \frac{t}{X} (\nabla^\mu \sigma + w^\mu) = t \left( u_{\text{irr}}^t (\xi^\mu + V_{\text{irr}}^\mu) + \frac{w^\mu}{X} \right). \quad (4.85)$$

Inserting (4.85) in the Euler equations (4.21) using (4.73) yields

$$0 = h u^\mu (\nabla_\mu (h u_\nu) - \nabla_\nu (h u_\mu)) \quad (4.86)$$

$$= \frac{hX}{t} (\delta_\nu^\mu + u^\mu u_\nu) \nabla_\mu \frac{ht}{X} + \frac{h^2 t}{X} u^\mu (\nabla_\mu w_\nu - \nabla_\nu w_\mu) \quad | \cdot \frac{\gamma_i^\nu}{h^2} \quad (4.87)$$

$$0 = \gamma_i^\nu (\delta_\nu^\mu + u^\mu u_\nu) \nabla_\mu \ln \left( \frac{ht}{X} \right) + \frac{t}{X} u^\mu \gamma_i^\nu (\nabla_\mu w_\nu - \nabla_\nu w_\mu). \quad (4.88)$$

#### 4. Initial Data for General Relativistic Neutron Star Binary Simulations

The second term can be expressed as

$$\frac{t}{X} u^\mu \gamma_i^\nu (\nabla_\mu w_\nu - \nabla_\nu w_\mu) = \frac{t}{X} X u_{\text{irr}}^\mu \gamma_i^\nu (\nabla_\mu w_\nu - \nabla_\nu w_\mu) + \frac{t}{X} w^\mu \gamma_i^\nu (\nabla_\mu w_\nu - \nabla_\nu w_\mu) \quad (4.89)$$

$$\begin{aligned} &= t u_{\text{irr}}^t \gamma_i^\nu \mathcal{L}_{u_{\text{irr}}/u_{\text{irr}}^t} w_\nu - t u_{\text{irr}}^t \gamma_i^\nu \left( w_\mu \nabla_\nu \frac{u_{\text{irr}}^\mu}{u_{\text{irr}}^t} + \frac{u_{\text{irr}}^\mu}{u_{\text{irr}}^t} \nabla_\nu w_\mu \right) \\ &\quad + \frac{t}{X} w^j (D_j w_i - D_i w_j) \end{aligned} \quad (4.90)$$

$$\begin{aligned} &= t u_{\text{irr}}^t \gamma_i^\nu \mathcal{L}_{u_{\text{irr}}/u_{\text{irr}}^t} w_\nu - t u_{\text{irr}}^t D_i \frac{u_{\text{irr}}^\mu}{u_{\text{irr}}^t} w_\mu \\ &\quad + \frac{t}{X} w^j (D_j w_i - D_i w_j) \end{aligned} \quad (4.91)$$

Interestingly the last term is the same as in the expression for the defining equation of a Beltrami field (4.44).

#### 4.4.3. Choice of the Time Derivatives

Investigating Eq. (4.91) it is tempting and seems natural to choose the following time derivative for  $w^i$ :

$$\gamma_i^\mu \mathcal{L}_{u_{\text{irr}}/u_{\text{irr}}^t} (X u_{\text{rot}\mu}) = \gamma_i^\mu \mathcal{L}_{\xi+V_{\text{irr}}} w_\mu = 0. \quad (4.92)$$

It is however not clear how to motivate this choice physically. Why should the field  $X$ , that is used to define the irrotational part, appear in the time derivative of the rotational part? A more physically motivated choice would actually be stationarity of the rotational part in the irrotational frame:

$$\gamma_i^\mu \mathcal{L}_{u_{\text{irr}}/u_{\text{irr}}^t} u_{\text{rot}\mu} = \gamma_i^\mu \mathcal{L}_{\xi+V_{\text{irr}}} \frac{w_\mu}{X} = 0. \quad (4.93)$$

Enforcing both (4.92) and (4.93) would require

$$\mathcal{L}_{u_{\text{irr}}/u_{\text{irr}}^t} X = 0, \quad (4.94)$$

#### 4.4. Sketch of an Improved Approach to Initial Data for Neutron Star Binaries with Spin

which also does not have a direct physical justification. In the irrotational case however, where  $X = h$ , this choice corresponds then to an expansion free fluid. Eventually more justified might be the case where  $X$  is stationary in the corotating frame, i.e. in the frame in which also  $u_{\text{irr}}$  is stationary. After all Eq. (4.71) should hold at least for an infinitesimal time span, which should be fulfilled in this case. This choice, expressed by

$$\mathcal{L}_\xi X = 0, \quad (4.95)$$

together with (4.93) results in

$$\gamma_i^\mu \mathcal{L}_{u_{\text{irr}}/u_{\text{irr}}^t}(X u_{\text{rot}\mu}) = \gamma_i^\mu u_{\text{rot}\mu} \mathcal{L}_{\xi+V_{\text{irr}}} X = \frac{w_i}{X} V_{\text{irr}}^j D_j X. \quad (4.96)$$

The second term of Eq. (4.88) is now completely expressed in terms of variables given on the spatial slice, except for the new velocity potential  $\sigma$  and  $C_{\text{irr}}$ . The first term of (4.88) still contains a time derivative, which is fixed by the choosing the time derivative of  $h$ . Note that  $t$  is given completely in terms of  $u_{\text{irr}}$  and  $u_{\text{rot}}$  and thus its time derivative is determined by the time derivative of these quantities. The Euler equations are then expressed completely by quantities on the spatial slice and can be integrated for  $h$ , given that the expression is actually curl free. It is not yet clear whether the constraints on  $w^i$  that were present in Tichys formalism actually remain or whether the choice of  $w^i$  is now absorbed for example in the value of  $C_{\text{irr}}$ . Another question is, under which requirements on the Lie derivatives a rotational part with planar flow is permissive. If it turns out that a planar flow is still prohibitive, then the irrotational part should at least turn out such that the axial velocity in the center of the helix decreases with distance from the stars center and eventually vanishing on the boundary. Otherwise the irrotational part still has to cancel parts of the rotational part and the choices that were proposed for the Lie derivatives (4.77) and (4.93) would be still problematic for the same reasons discussed at the end of Sec. 4.3.5.

The last missing piece to complete the formalism for initial data construction is to actually solve for the velocity potential  $\sigma$ . This quantity will be obtained by

#### 4. Initial Data for General Relativistic Neutron Star Binary Simulations

inserting all expressions in the the continuity equation (4.19) which should yield a presumably elliptic equation for  $\sigma$ . To close the discussion the formalism is investigated in the irrotational case. Setting  $w^\mu = 0$  and  $t = 1$  Eq. (4.88) becomes

$$0 = D_i \ln \frac{h}{X} + {}^{(3)}u_i u^\mu \nabla_\mu \ln \frac{h}{X}. \quad (4.97)$$

Clearly the equations are solved if  $h$  and  $X$  and their time derivatives coincide. In this case the solution for  $h$  is given for example by (4.81). Next it is also interesting to investigate the case where the time derivatives do not coincide. Let us take as an example

$$\mathcal{L}_\xi X = 0 \quad \mathcal{L}_u h = 0, \quad (4.98)$$

i.e. the fluid is expansion free. In this case the Euler equations become

$$0 = D_i \ln \frac{h}{X} - {}^{(3)}u_i u^\mu \nabla_\mu \ln X \quad (4.99)$$

$$= D_i \ln \frac{h}{X} - X (D_i \sigma) V_{\text{irr}}^j D_j \ln X = D_i \ln \frac{h}{X} - (D_i \sigma) V_{\text{irr}}^j D_j X. \quad (4.100)$$

The equations can then still be solved for  $h$  if  $V^j D_j X = \text{const.}$ . It seems unlikely that (4.81) provides such a solution, however Eq. (4.81) has been obtained under the assumption (4.77) and the Euler equations actually do not directly depend on it. Hence it is also possible to choose  $X$  and the Lie derivative for  $X u_{\text{irr}\mu}$  follows from (4.76). Concluding, it actually seems possible to construct purely irrotational solutions where  $X$  and  $h$  do not coincide. How physically reasonable the resulting time derivatives are however, remains another question.

## 5. Conclusion

A first result of this thesis is that hyperbolic relaxation can be formulated not only for simple problems like the Poisson equations, but also for non-trivial equations. The HypRelax method has been successfully applied to the extended conformal-thin-sandwich equations and after developing a variation, the HypRelaxDiv method, also to the continuity equation for a neutron star binary.

Beyond the intrinsic interest in a new method, we have to ask whether hyperbolic relaxation, after some significant further development that is beyond the scope of this thesis, might become an interesting alternative to the highly developed standard methods. For example, Jacobi relaxation is a fundamental building block of many advanced methods, but it is essentially never used on its own because of its slow convergence (for long wavelengths). However, multigrid methods with parabolic relaxation as smoother (for short wave lengths) are highly efficient, reducing the computational complexity from  $\mathcal{O}(n^2)$  to  $\mathcal{O}(n \log(n))$ . The solver could also profit from adaptive-mesh refinement techniques which are often present in modern evolution codes. It remains to be seen how efficient hyperbolic relaxation can be, with and without acceleration methods.

Applying the HypRelaxDiv formalism to the continuity equation an approach avoiding the necessity of surface-fitted coordinates has been explored. To achieve this the equation for the velocity potential has been extended to vacuum by the Poisson equation. Since the relaxation at the surface of the star is very slow it has been

## 5. Conclusion

found difficult to satisfy the regularity conditions on the stellar surface, because certain parts like the Killing vector change on a very short time scale the velocity potential  $\phi$  cannot adapt to. It was possible to achieve regularity satisfying solutions by introducing a splitting of the constant part of the irrotational enthalpy current. The bottom line is however that this relaxation scheme is not optimal for this type of equation. Either direct solvers should be used or the method should in some way be accelerated near the stellar surface.

For the matter equations the Euler equations have been solved for a binary neutron star system with spinning stars solving the Euler equations without any simplifications. This has revealed that previous choices for the rotational enthalpy current were actually incompatible with the Euler equations. It was shown that the rotational part of the enthalpy current cannot be a planar flow, but instead must be divergence-free Beltrami field, in which case the Euler equations can be easily integrated using an analytic formula. A rotational part that is divergence-free Beltrami field has been derived for a rigidly rotating neutron star, which as a new feature exhibits an additional component along the direction of the spin axis. This new finding might have consequences in evolutions of the data in particular for the magnetic field of these neutron stars.

These findings however also revealed a conceptual problem in the formalism. The irrotational part has to cancel the new axial component of the rotational velocity piece. The time derivatives of the irrotational and rotational part however are chosen such that the cancellation is not conserved when the data is evolved. This indicates that the choice of the time derivatives is actually flawed. Furthermore it has been shown that the current formalism does actually not separate irrotational and rotational velocity piece correctly. A new rigorous split into irrotational and rotational velocity piece has been proposed and the solution of the Euler equations has been discussed in this new split has been discussed. For an application to neutron star initial data the approach must be completed by writing down the



equations for the continuity equation in this new formalism, which remains a task for the future. Whether this formalism also resolves the described problem with the axial current and whether this formalism would also allow planar rotational velocity pieces remains yet to be investigated.



## 6. Bibliography

- [1] Hannes R. Rüter et al. “Hyperbolic Relaxation Method for Elliptic Equations”. In: (2017). Accepted. (To be published in Phys. Rev. D). arXiv: 1708.07358 [gr-qc].
- [2] Albert Einstein. “Die Grundlage der allgemeinen Relativitätstheorie”. In: *Ann. Phys.* 354 (1916), pp. 769–822. URL: <https://doi.org/10.1002/andp.19163540702>.
- [3] Albert Einstein. “The Foundation of the General Theory of Relativity”. In: *Einstein Papers Project (English translation supplement)* 6 (1916). translation from H. A. Lorentz et al., pp. 146–200. URL: <https://einsteinpapers.press.princeton.edu/vol6-trans/158>.
- [4] H. Pfister and K. H. Braun. “Induction of correct centrifugal force in a rotating mass shell”. In: *Class. Quantum Grav.* 2 (1985), p. 909. DOI: 10.1088/0264-9381/2/6/015.
- [5] Karl Schwarzschild. “Über das Gravitationsfeld eines Massenpunktes nach der Einsteinschen Theorie”. In: *Sitzungsber. Dtsch. Akad. Wiss. Berlin, Kl. Math. Phys. Tech.* (1916), pp. 189–196.
- [6] Albert Einstein. “Die Feldgleichungen der Gravitation”. In: *Preuss. Akad. Wiss. Berlin, Sitzungsber.* (1915), pp. 844–847.
- [7] B. P. Abbott et al. “Observation of Gravitational Waves from a Binary Black Hole Merger”. In: *Phys. Rev. Lett.* 116.6 (2016), p. 061102. arXiv: 1602.03837 [gr-qc].

## 6. Bibliography

- [8] A. Einstein. “Über Gravitationswellen”. In: *Sitzungsberichte der Königlich Preußischen Akademie der Wissenschaften (Berlin)*, Seite 154-167. (1918).
- [9] Joel M. Weisberg, Joseph H. Taylor, and Lee A. Fowler. “Gravitational Waves from an Orbiting Pulsar”. In: *Scientific American* 245.4 (1981), pp. 74–83. ISSN: 00368733, 19467087. URL: <http://www.jstor.org/stable/24964580>.
- [10] J.M. Weisberg and J.H. Taylor. “The Relativistic Binary Pulsar B1913+16: Thirty Years of Observations and Analysis”. In: *ASP Conference Series* 328 (2005), p. 25. eprint: [astro-ph/0407149](https://arxiv.org/abs/astro-ph/0407149).
- [11] B. P. Abbott et al. “GW170817: Observation of Gravitational Waves from a Binary Neutron Star Inspiral”. In: *Phys. Rev. Lett.* 119.16 (2017), p. 161101. arXiv: 1710.05832 [gr-qc].
- [12] Frank Löffler et al. “The Einstein Toolkit: A Community Computational Infrastructure for Relativistic Astrophysics”. In: *Class. Quant. Grav.* 29 (2012), p. 115001. arXiv: 1111.3344 [gr-qc].
- [13] SpEC - Spectral Einstein Code, <http://www.black-holes.org/SpEC.html>.
- [14] B. Brügmann. “Bifunctional adaptive mesh (BAM) for 3d numerical relativity”. In: *Proceedings of The 18th Texas Symposium on Relativistic Astrophysics*. Ed. by A. Olinto, J. Frieman, and D. Schramm. Singapore: World Scientific, 1998.
- [15] Tim Dietrich et al. “Binary Neutron Stars with Generic Spin, Eccentricity, Mass ratio, and Compactness - Quasi-equilibrium Sequences and First Evolutions”. In: *Phys. Rev.* D92.12 (2015), p. 124007. arXiv: 1507.07100 [gr-qc].
- [16] David Hilditch, Andreas Weyhausen, and Bernd Brügmann. “Pseudospectral method for gravitational wave collapse”. In: *Phys. Rev.* D93.6 (2016), p. 063006. DOI: 10.1103/PhysRevD.93.063006. arXiv: 1504.04732 [gr-qc].
- [17] Marcus Bugner. “Discontinuous Galerkin Methods for General Relativistic Hydrodynamics”. PhD thesis. Germany: University of Jena, 7/2017.

- [18] Yousef Saad. *Iterative Methods for Sparse Linear Systems*. 2nd. Philadelphia, USA: SIAM Press, 2003. ISBN: ISBN 0-89871-534-2.
- [19] Yousef Saad and Henk van der Vorst. “Iterative solution of linear systems in the 20th century”. In: *J. Comp. App. Math.* 123 (2000), pp. 1–33.
- [20] William H. Press et al. *Numerical Recipes 3rd Edition: The Art of Scientific Computing*. 3rd ed. New York, NY, USA: Cambridge University Press, 2007. ISBN: 0521880688, 9780521880688.
- [21] Ling Hsiao and Tai-Ping Liu. “Convergence to nonlinear diffusion waves for solutions of a system of hyperbolic conservation laws with damping”. In: *Communications in Mathematical Physics* 143.3 (1992), pp. 599–605. DOI: 10.1007/BF02099268. URL: <http://dx.doi.org/10.1007/BF02099268>.
- [22] Kenji Nishihara. “Asymptotic Behavior of Solutions of Quasilinear Hyperbolic Equations with Linear Damping”. In: *Journal of Differential Equations* 137.2 (1997), pp. 384–395. ISSN: 0022-0396. DOI: <http://dx.doi.org/10.1006/jdeq.1997.3268>.
- [23] Jens Wirth. “Diffusion phenomena for partially dissipative hyperbolic systems”. In: *Journal of Mathematical Analysis and Applications* 414.2 (2014), pp. 666–677. ISSN: 0022-247X. DOI: 10.1016/j.jmaa.2014.01.034.
- [24] Ryosuke Hirai et al. “Hyperbolic self-gravity solver for large scale hydrodynamical simulations”. In: *Phys. Rev. D* 93 (8 Apr. 2016), p. 083006. DOI: 10.1103/PhysRevD.93.083006. URL: <https://link.aps.org/doi/10.1103/PhysRevD.93.083006>.
- [25] A. Ilyin, Y. Rykov, and S. Zelik. “Hyperbolic relaxation of the 2D Navier-Stokes equations in a bounded domain”. In: (2017). eprint: [arXiv:1707.00121](https://arxiv.org/abs/1707.00121).
- [26] Miguel Alcubierre et al. “Gauge conditions for long-term numerical black hole evolutions without excision”. In: *Phys. Rev. D* 67 (2003), p. 084023. eprint: [gr-qc/0206072](https://arxiv.org/abs/gr-qc/0206072).

## 6. Bibliography

- [27] J. Balakrishna et al. “Coordinate conditions in three-dimensional numerical relativity”. In: *Class. Quantum Grav.* 13 (1996), pp. L135–142.
- [28] Bertil Gustafsson, Heinz-Otto Kreiss, and Joseph Oliger. *Time dependent problems and difference methods*. New York: Wiley, 1995.
- [29] Olivier Sarbach and Manuel Tiglio. “Continuum and Discrete Initial-Boundary Value Problems and Einstein’s Field Equations”. In: *Living Reviews in Relativity* 15.9 (2012). arXiv: 1203.6443 [gr-qc]. URL: <http://www.livingreviews.org/lrr-2012-9>.
- [30] David Hilditch. “An Introduction to Well-posedness and Free-evolution”. In: *Int. J. Mod. Phys. A* 28 (2013), p. 1340015. DOI: 10.1142/S0217751X13400150. arXiv: 1309.2012 [gr-qc].
- [31] Bernd Brüggemann. “A pseudospectral matrix method for time-dependent tensor fields on a spherical shell”. In: *J. Comput. Phys.* 235 (2013), pp. 216–240. arXiv: 1104.3408 [physics.comp-ph].
- [32] Sergio Dain. “Elliptic systems”. In: *Lect. Notes Phys.* 692 (2006), pp. 117–139. eprint: gr-qc/0411081.
- [33] Heinz-Otto Kreiss, Omar E. Ortiz, and Oscar A. Reula. “Stability of Quasi-linear Hyperbolic Dissipative Systems”. In: *Journal of Differential Equations* 142.1 (1998), pp. 78–96. ISSN: 0022-0396. DOI: 10.1006/jdeq.1997.3341. URL: <http://dx.doi.org/10.1006/jdeq.1997.3341>.
- [34] Heinz-Otto Kreiss and Jens Lorenz. “Stability for time-dependent differential equations”. In: *Acta Numerica* 7 (1998), pp. 203–285. DOI: 10.1017/S096249290000283X.
- [35] J. S. Hesthaven. “Spectral penalty methods”. In: *Appl. Numer. Math.* 33 (2000), pp. 23–41.
- [36] Jan S. Hesthaven, Sigal Gottlieb, and David Gottlieb. *Spectral Methods for Time-Dependent Problems*. Cambridge: Cambridge University Press, 2007.

- [37] Nicholas W. Taylor, Lawrence E. Kidder, and Saul A. Teukolsky. “Spectral methods for the wave equation in second-order form”. In: *Phys.Rev.* D82 (2010), p. 024037. DOI: 10.1103/PhysRevD.82.024037. arXiv: 1005.2922 [gr-qc].
- [38] Carsten Gundlach and Jose M. Martín-García. “Hyperbolicity of second-order in space systems of evolution equations”. In: *Class. Quantum Grav.* 23 (2006), S387–S404. eprint: gr-qc/0506037.
- [39] David Gilbard and Neil S. Trudinger. *Elliptic Partial Differential Equations*. Berlin Heidelberg New York: Springer-Verlag, 2001.
- [40] C. Ronchi, R. Iacono, and P.S. Paolucci. “The “Cubed Sphere”: A New Method for the Solution of Partial Differential Equations in Spherical Geometry”. In: *J. Comput. Phys.* 124.1 (1996), pp. 93–114.
- [41] John P. Boyd. *Chebyshev and Fourier Spectral Methods (Second Edition, Revised)*. New York: Dover Publications, 2001. ISBN: 0-486-41183-4.
- [42] William H. Press et al. *Numerical Recipes: The Art of Scientific Computing*. 3rd ed. New York, NY: Cambridge University Press, 2007.
- [43] R. Barrett et al. *Templates for the Solution of Linear Systems: Building Blocks for Iterative Methods*. <http://www.netlib.org/templates/>: SIAM, 1993.
- [44] Xiyang I.A. Yang and Rajat Mittal. “Acceleration of the Jacobi iterative method by factors exceeding 100 using scheduled relaxation”. In: *Journal of Computational Physics* 274 (2014), pp. 695–708. ISSN: 0021-9991. DOI: <https://doi.org/10.1016/j.jcp.2014.06.010>. URL: <http://www.sciencedirect.com/science/article/pii/S0021999114004173>.
- [45] J.E. Adsuara et al. “Scheduled Relaxation Jacobi method: Improvements and applications”. In: *Journal of Computational Physics* 321 (2016), pp. 369–413. ISSN: 0021-9991. DOI: <https://doi.org/10.1016/j.jcp.2016.05.053>. URL: <http://www.sciencedirect.com/science/article/pii/S002199911630198X>.

## 6. Bibliography

- [46] Thomas W. Baumgarte and Stuart L. Shapiro. *Numerical Relativity: Solving Einstein's Equations on the Computer*. Cambridge: Cambridge University Press, 2010. ISBN: 978-0521514071.
- [47] M. Shibata and T. Nakamura. “Evolution of three-dimensional gravitational waves: Harmonic slicing case”. In: *Phys. Rev. D* 52 (1995), pp. 5428–5444.
- [48] T. W. Baumgarte and S. L. Shapiro. “On the Numerical integration of Einstein's field equations”. In: *Phys. Rev. D* 59 (1998), p. 024007. eprint: [gr-qc/9810065](#).
- [49] C. Bona et al. “General-covariant evolution formalism for numerical relativity”. In: *Phys. Rev. D* 67 (2003), p. 104005. eprint: [gr-qc/0302083](#).
- [50] C. Bona and C. Palenzuela. “Dynamical shift conditions for the Z4 and BSSN hyperbolic formalisms”. In: *Phys. Rev. D* 69 (2004), p. 104003. eprint: [gr-qc/0401019](#).
- [51] Sebastiano Bernuzzi and David Hilditch. “Constraint violation in free evolution schemes: comparing BSSNOK with a conformal decomposition of Z4”. In: *Phys. Rev. D* 81 (2010), p. 084003. DOI: [10.1103/PhysRevD.81.084003](#). arXiv: [0912.2920 \[gr-qc\]](#).
- [52] Lee Lindblom et al. “A New Generalized Harmonic Evolution System”. In: *Class. Quant. Grav.* 23 (2006), S447–S462. eprint: [gr-qc/0512093](#).
- [53] Gregory B. Cook. “Initial Data for Numerical Relativity”. In: *Living Rev. Relativity* 3 (2000), p. 5. URL: <http://www.livingreviews.org/lrr-2000-5>.
- [54] James W. York. “Conformal ‘thin-sandwich’ data for the initial-value problem of general relativity”. In: *Phys. Rev. Lett.* 82 (1999), pp. 1350–1353. DOI: [10.1103/PhysRevLett.82.1350](#). arXiv: [gr-qc/9810051](#).



- [55] Thomas W. Baumgarte, Niall O Murchadha, and Harald P. Pfeiffer. “The Einstein constraints: uniqueness and non-uniqueness in the conformal thin sandwich approach”. In: *Phys. Rev. D* 75 (2007), p. 044009. DOI: 10.1103/PhysRevD.75.044009. arXiv: gr-qc/0610120.
- [56] Isabel Cordero-Carrión et al. “Improved constrained scheme for the Einstein equations: An approach to the uniqueness issue”. In: *Phys. Rev. D* 79.2 (Jan. 2009), p. 024017. DOI: 10.1103/PhysRevD.79.024017. arXiv: 0809.2325 [gr-qc].
- [57] Wolfgang Tichy. “The initial value problem as it relates to numerical relativity”. In: *Reports on Progress in Physics* 80.2 (2017), p. 026901. URL: <http://stacks.iop.org/0034-4885/80/i=2/a=026901>.
- [58] Harald P. Pfeiffer and James W. York. “Uniqueness and Nonuniqueness in the Einstein Constraints”. In: *Phys. Rev. Lett.* 95 (9 Aug. 2005), p. 091101. DOI: 10.1103/PhysRevLett.95.091101. URL: <https://link.aps.org/doi/10.1103/PhysRevLett.95.091101>.
- [59] Nick Tacik et al. “Binary Neutron Stars with Arbitrary Spins in Numerical Relativity”. In: *Phys. Rev. D* 92.12 (2015), p. 124012. arXiv: 1508.06986 [gr-qc].
- [60] Antonios Tsokaros, Kōji Uryū, and Luciano Rezzolla. “A new code for quasi-equilibrium initial data of binary neutron stars: corotating, irrotational and slowly spinning systems”. In: *Phys. Rev. D* 91.10 (2015), p. 104030. DOI: 10.1103/PhysRevD.91.104030. arXiv: 1502.05674 [gr-qc].
- [61] Wolfgang Tichy. “Initial data for binary neutron stars with arbitrary spins”. In: *Phys. Rev. D* 84 (2011), p. 024041. DOI: 10.1103/PhysRevD.84.024041. arXiv: 1107.1440 [gr-qc].
- [62] Wolfgang Tichy. “Constructing quasi-equilibrium initial data for binary neutron stars with arbitrary spins”. In: *Phys. Rev. D* 86 (2012), p. 064024. arXiv: 1209.5336 [gr-qc].

## 6. Bibliography

- [63] S. Bonazzola, E. Gourgoulhon, and J.-A. Marck. “Relativistic formalism to compute quasiequilibrium configurations of nonsynchronized neutron star binaries”. In: *Phys. Rev. D* 56 (1997), pp. 7740–7749.
- [64] Masaru Shibata. “A relativistic formalism for computation of irrotational binary stars in quasi equilibrium states”. In: *Phys. Rev. D* 58 (1998), p. 024012. DOI: 10.1103/PhysRevD.58.024012. arXiv: gr-qc/9803085.
- [65] E. Gourgoulhon et al. “Quasiequilibrium sequences of synchronized and irrotational binary neutron stars in general relativity: Method and tests”. In: *Phys. Rev. D* 63 (2001), p. 064029.
- [66] Koji Uryū et al. “Non-conformally flat initial data for binary compact objects”. In: *Phys. Rev. D* 80 (2009), p. 124004. DOI: 10.1103/PhysRevD.80.124004. arXiv: 0908.0579 [gr-qc].
- [67] Pedro Marronetti and Stuart L. Shapiro. “Relativistic models for binary neutron stars with arbitrary spins”. In: *Phys. Rev. D* 68 (2003), p. 104024. DOI: 10.1103/PhysRevD.68.104024. arXiv: gr-qc/0306075.
- [68] Thomas W. Baumgarte and Stuart L. Shapiro. “A Formalism for the construction of binary neutron stars with arbitrary circulation”. In: *Phys. Rev. D* 80 (2009), p. 064009. DOI: 10.1103/PhysRevD.80.064009. arXiv: 0909.0952 [gr-qc].
- [69] Niclas Moldenhauer et al. “Initial data for binary neutron stars with adjustable eccentricity”. In: *Phys. Rev. D* 90.8 (2014), p. 084043. DOI: 10.1103/PhysRevD.90.084043. arXiv: 1408.4136 [gr-qc].
- [70] Luciano Rezzolla and Olindo Zanotti. *Relativistic Hydrodynamics*. Oxford: Oxford University Press, 2013.
- [71] Stephen W. Hawking and George F. R. Ellis. *The Large Scale Structure of Space-Time*. Cambridge (UK): Cambridge University Press, 1973. ISBN: 0-521-20016-4 (hardcover), 0-521-09906-4 (paperback).

- [72] S. Bonazzola, E. Gourgoulhon, and J.-A. Marck. “Numerical approach for high precision 3-D relativistic star models”. In: *Phys. Rev. D.* 58 (1998), p. 104020. arXiv: astro-ph/9803086 [astro-ph].
- [73] Marcus Ansorg. “Multi-Domain Spectral Method for Initial Data of Arbitrary Binaries in General Relativity”. In: *Classical Quantum Gravity* 24 (2007), S1–S14. DOI: 10.1088/0264-9381/24/12/S01. arXiv: gr-qc/0612081 [gr-qc].
- [74] Wolfgang Tichy. “A new numerical method to construct binary neutron star initial data”. In: *Classical Quantum Gravity* 26 (2009), p. 175018. DOI: 10.1088/0264-9381/26/17/175018. arXiv: 0908.0620 [gr-qc].
- [75] M. Ansorg, A. Kleinwächter, and R. Meinel. “Highly accurate calculation of rotating neutron stars: Detailed description of the numerical methods”. In: *Astron. Astrophys.* 405 (2003), p. 711. eprint: astro-ph/0301173.
- [76] A. W. Marris. “Vector fields of solenoidal vector-line rotation”. In: *Archive for Rational Mechanics and Analysis* 27 (1967), pp. 195–232.
- [77] Ratip Berker. “Integration des equations du mouvement d’un fluide visqueux incompressible”. In: *Handbuch der Physik VIII/2 Strömungsmechanik 2* (1963), pp. 1–384.
- [78] S. Chandrasekhar and P. C. Kendall. “On Force-Free Magnetic Fields”. In: *Astrophysical Journal* 126 (1957), pp. 457–460.
- [79] Toshio Uchida. “Theory of force-free electromagnetic fields. I. General theory”. In: *Phys. Rev. E* 56 (2 Aug. 1997), pp. 2181–2197. DOI: 10.1103/PhysRevE.56.2181. URL: <https://link.aps.org/doi/10.1103/PhysRevE.56.2181>.
- [80] Toshio Uchida. “Theory of force-free electromagnetic fields. II. Configuration with symmetry”. In: *Phys. Rev. E* 56 (2 Aug. 1997), pp. 2198–2212. DOI: 10.1103/PhysRevE.56.2198. URL: <https://link.aps.org/doi/10.1103/PhysRevE.56.2198>.

## 6. Bibliography

- [81] Samuel E. Gralla and Ted Jacobson. “Spacetime approach to force-free magnetospheres”. In: *Monthly Notices of the Royal Astronomical Society* 445.3 (2014), pp. 2500–2534. DOI: 10.1093/mnras/stu1690. eprint: /oup/backfile/content\_public/journal/mnras/445/3/10.1093/mnras/stu1690/2/stu1690.pdf. URL: <http://dx.doi.org/10.1093/mnras/stu1690>.
- [82] Geoffrey Compère, Samuel E. Gralla, and Alexandru Lupsasca. “Force-free foliations”. In: *Phys. Rev. D* 94 (12 Dec. 2016), p. 124012. DOI: 10.1103/PhysRevD.94.124012. URL: <https://link.aps.org/doi/10.1103/PhysRevD.94.124012>.
- [83] Miguel A. Aloy and Luciano Rezzolla. “A powerful hydrodynamic booster for relativistic jets”. In: *Astrophys. J.* 640 (2006), pp. L115–L118. arXiv: astro-ph/0602437.
- [84] F. Douchin and P. Haensel. “A unified equation of state of dense matter and neutron star structure”. In: *Astron. Astrophys.* 380 (2001), p. 151. DOI: 10.1051/0004-6361:20011402. arXiv: astro-ph/0111092 [astro-ph].
- [85] Jocelyn S. Read et al. “Constraints on a phenomenologically parameterized neutron-star equation of state”. In: *Phys. Rev. D* 79 (2009), p. 124032. DOI: 10.1103/PhysRevD.79.124032. arXiv: 0812.2163 [astro-ph].
- [86] Eric Gourgoulhon et al. “Quasiequilibrium sequences of synchronized and irrotational binary neutron stars in general relativity: Method and tests”. In: *Phys. Rev. D* 63 (2001), p. 064029. eprint: gr-qc/0007028.
- [87] Andreas Bauswein et al. “Neutron-star Radius Constraints from GW170817 and Future Detections”. In: *The Astrophysical Journal* 850.2 (Nov. 2017), p. L34. DOI: 10.3847/2041-8213/aa9994. URL: <https://doi.org/10.3847/2041-8213/aa9994>.
- [88] Achi Brandt. “Multi-level Adaptive Solutions to Boundary-Value Problems”. In: *Math. Comp.* 31 (1977), pp. 333–390.

- [89] Sandia National Laboratories, Los Alamos National Laboratory, and Kitware Inc. Paraview. URL: <https://www.paraview.org/>.



# A. Ehrenwörtliche Erklärung

Ich erkläre hiermit ehrenwörtlich, dass ich die vorliegende Arbeit selbständig, ohne unzulässige Hilfe Dritter und ohne Benutzung anderer als der angegebenen Hilfsmittel und Literatur angefertigt habe. Die aus anderen Quellen direkt oder indirekt übernommenen Daten und Konzepte sind unter Angabe der Quelle gekennzeichnet. Die nachstehend aufgeführten Personen haben mich bei der Auswahl und Auswertung unentgeltlich unterstützt.

- Dr. Marcus Bugner
- Dr. David Hilditch
- Dr. Bernd Brüggemann

Weitere Personen waren an der inhaltlich-materiellen Erstellung der vorliegenden Arbeit nicht beteiligt. Insbesondere habe ich hierfür nicht die entgeltliche Hilfe von Vermittlungs- bzw. Beratungsdiensten (Promotionsberater oder andere Personen) in Anspruch genommen. Niemand hat von mir unmittelbar oder mittelbar geldwerte Leistungen für Arbeiten erhalten, die im Zusammenhang mit dem Inhalt der vorgelegten Dissertation stehen.

Die Arbeit wurde bisher weder im In- noch im Ausland in gleicher oder ähnlicher Form einer anderen Prüfungsbehörde vorgelegt.

Die geltende Promotionsordnung der Physikalisch-Astronomischen Fakultät ist mir bekannt.

Ich versichere ehrenwörtlich, dass ich nach bestem Wissen die reine Wahrheit gesagt und nichts verschwiegen habe.

Jena, 29. Juli 2019

---

Hannes Rüter